VALORIZATION OF ŞIRNAK ASPHALTITE AND BIOMASS

A THESIS SUBMITTED TO
THE GRADUATE SCHOOL OF NATURAL AND APPLIED SCIENCES
OF
MIDDLE EAST TECHNICAL UNIVERSITY

BY

VEYSI HELVACI

IN PARTIAL FULFILLMENT OF THE REQUIREMENTS
FOR
THE DEGREE OF MASTER OF SCIENCE
IN
CHEMICAL ENGINEERING

SEPTEMBER 2019

Approval of the thesis:

VALORIZATION OF ŞIRNAK ASPHALTITE AND BIOMASS

submitted by **VEYSI HELVACI** in partial fulfillment of the requirements for the degree of **Master of Science in Chemical Engineering Department, Middle East Technical University** by,

Prof. Dr. Halil Kalıpçılar
Dean, Graduate School of **Natural and Applied Sciences**

Prof. Dr. Pınar Çalık
Head of Department, **Chemical Engineering**

Prof. Dr. Deniz Üner
Supervisor, **Chemical Engineering, METU**

Prof. Dr. Mahmut Parlaktuna
Co-Supervisor, **Petroleum and Natural Gas Eng Dept, METU**

Examining Committee Members:

Assoc. Prof. Dr. Çağlar Sınayuç
Petroleum and Natural Gas Engineering Department, METU

Prof. Dr. Deniz Üner
Chemical Engineering, METU

Prof. Dr. Mahmut Parlaktuna
Petroleum and Natural Gas Engineering Department, METU

Assist. Prof. Dr. Harun Koku
Chemical Engineering Department, METU

Assist. Prof. Dr. Başar Çağlar
Department of Energy Systems Engineering, Yaşar University

Date: 05.09.2019

I hereby declare that all information in this document has been obtained and presented in accordance with academic rules and ethical conduct. I also declare that, as required by these rules and conduct, I have fully cited and referenced all material and results that are not original to this work.

Name, Surname: Veysi Helvacı

Signature:

ABSTRACT

VALORIZATION OF ŞIRNAK ASPHALTITE AND BIOMASS

Helvacı, Veysi
Master of Science, Chemical Engineering
Supervisor: Prof. Dr. Deniz Üner
Co-Supervisor: Prof. Dr. Mahmut Parlaktuna

September 2019, 105 pages

In this study, the hydrogenation and pyrolysis behavior of Şırnak asphaltite, and the synergetic effect of increasing amount of liquid product obtained from steam distillation of Şırnak asphaltite and biomass and dry reforming were studied. For that purpose, Şırnak asphaltite samples were hydrogenated and pyrolyzed and the products are analyzed. For synergetic effect investigation, steam distillation of Şırnak asphaltite with and without the presence of pepper plant biomass was performed. Results show that hydrogenation of Şırnak asphaltite results in collection of important portions of alkanes in coal structure as liquid product and synergetic effect was observed in steam distillation of Şırnak asphaltite and pepper plant biomass. The tar component of the pyrolysis of biomass consisted mostly of aromatic compounds. In order to explore the valorization of tar from biomass, CO_2 reforming was selected. As a model compound, benzene was selected to represent aromatics. Dry reforming of benzene was investigated in the presence of perovskite oxides. Results show that CO_2 can be used as a feedstock for valorization of biomass derived tar.

Keywords: Asphaltite, Biomass, Pyrolysis, Steam Distillation, Dry Reforming

ÖZ

ŞIRNAK ASFALTİTİ VE BİYOKÜTLENİN DEĞERLENDİRİLMESİ

Helvacı, Veysi
Yüksek Lisans, Kimya Mühendisliği
Tez Danışmanı: Prof. Dr. Deniz Üner
Ortak Tez Danışmanı: Prof. Dr. Mahmut Parlaktuna

Eylül 2019, 105 sayfa

Bu çalışmada Şırnak Asfaltiti'nin hidrojenleme ve piroliz işlemlerindeki davranışı, asfaltit ve biyokütlenin buhar distilasyonu metoduyla işlenmesinin sıvı ürün artışına etkisi ve katran kuru reformlama çalışılmıştır. Bu amaçla asfaltit örnekleri hidrojenlenmiş ve pirolize uğratılmış, çıkan ürünler analiz edilmiştir. Sinerjik etki araştırmalarında, asfaltitin biyokütle varlığında ve yokluğunda, buhar distilasyonundaki etkisi gözlemlenmiştir. Sonuçlar göstermektedir ki hidrojenleme sonucunda elde edilen sıvı örneklerde yapıdaki alkanların önemli bölümü toplanabilmiştir ve buhar distilasyonunda sinerjik bir etki gözlemlenmiştir. Biyokütle pirolizinden ortaya çıkan katranın çoğunun aromatik bileşiklerden oluştuğu belirlendiğinden katranların değerlendirilmesi için CO_2 reformlamadan faydalanıldı. Aromatik bileşikleri benzen ile temsil edildi. Benzen kuru reformlaması perovskit oksitlerin varlığında test edildi. Sonuçlar CO_2'nin biyokütleden elde edilen katran bileşiklerinin değerlendirilmesi için kullanılabileceğini göstermektedir.

Anahtar Kelimeler: Asfaltit, Biyokütle, Piroliz, Buhar Distilasyonu, Kuru Reformlama

To My Lovely Wife Zeynep and My Dear Family…

ACKNOWLEDGEMENTS

For her endless support and guidance since we met, I would like to thank Prof. Dr. Deniz Üner, not only for her guidance in my M.Sc. studies, for her contributions in NMR experiments, but also her guidance and wisdom for everything life has brought. I would like to thank Prof. Dr. Mahmut Parlaktuna for his helps and guidance in research phase of my M.Sc. Study. I would like to thank Assist. Prof. Dr. Başar Çağlar for teaching me a lot about performing a research, his helps in dry reforming experiments, catalyst synthesis, and his friendship and support.

I would like to thank my family. My father for teaching me how to be a good engineer and encouraging me for M.Sc. studies, my mother for teaching me how to be a good person and my dear brother Muzaffer for making me believe in myself. For their endless support, I would like to thank Sadık Bahaettin Akdağ and Ali Pırlantı whom and will be the older brothers for me.

I would like to specially thank Atalay Çalışan for his help through my experiments and patiently teaching me practical aspects of laboratory works and his friendship. I also thank other Cactus group members, Deniz Kaya, Mustafa Yasin Aslan, Ezgi Yavuzyılmaz, Orhun Kahraman, together with Emre Hatipoğlu, Arzu Arslan, Seda Sivri for their support and friendship. For their contributions, I would like to thank Dr. Jun Xu for solid state NMR experiments, Ecem Ünal for her helps in liquid NMR in Figure 26, Prof. Dr. Ali İhsan Arol for his helps in asphaltite sample preparation and METU PAL Staff for Detailed Hydrocarbon Analysis. I would like to thank Tuartek A.Ş. family for their helps, especially Ali Güneyli and Doruk Yılmaz for all of their helps when I need them.

Without my wife's love and continuous support throughout my M.Sc. studies, I know I would have already given up. I cannot thank her enough for everything she did. She made everything better and more meaningful for me.

TABLE OF CONTENTS

CHAPTERS

LIST OF TABLES

TABLES

LIST OF FIGURES

FIGURES

LIST OF ABBREVIATIONS

ABBREVIATIONS

AMU	Atomic Mass Unit
BM	Biomass
DHA	Detailed Hydrocarbon Analysis
DMSO	Dimethyl sulfoxide
DrTGA	Derivative Thermogravimetric Analysis
NMR	Nuclear Magnetic Resonance
PAA	Peroxy Acetic Acid
SCCM	Standard cm^3/min
ŞA	Şırnak Asphaltite
TCE	Trichloroethylene
TGA	Thermogravimetric Analysis

CHAPTER 1

INTRODUCTION

1.1. Background on Coal and Asphaltite

Coal is the first fossil fuel humankind used as an energy source. It is well distributed all around the world and it is still the cheapest fossil fuel. Coal is firstly used fossil fuel and it is still the second primary energy source. Energy distribution by fuel as can be seen in Figure 1.

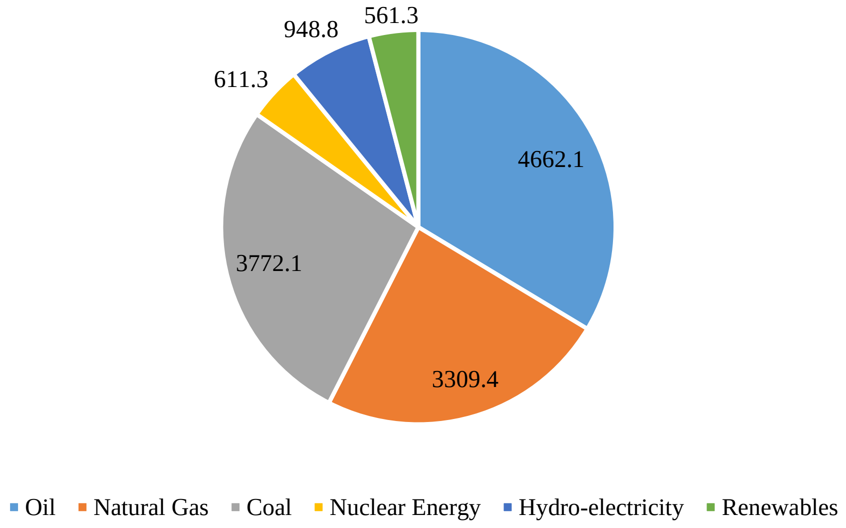

**million tonnes of Petroleum Equivalent

Figure 1: World Energy Production by Fuel ("Statistical Review of World Energy: Energy economics: Home", 2019)

Coal is categorized mainly by its carbon/energy content and moisture content. High rank coals have high energy, low moisture and low sulfur content while lower rank coals have low energy, high moisture and high sulfur content.

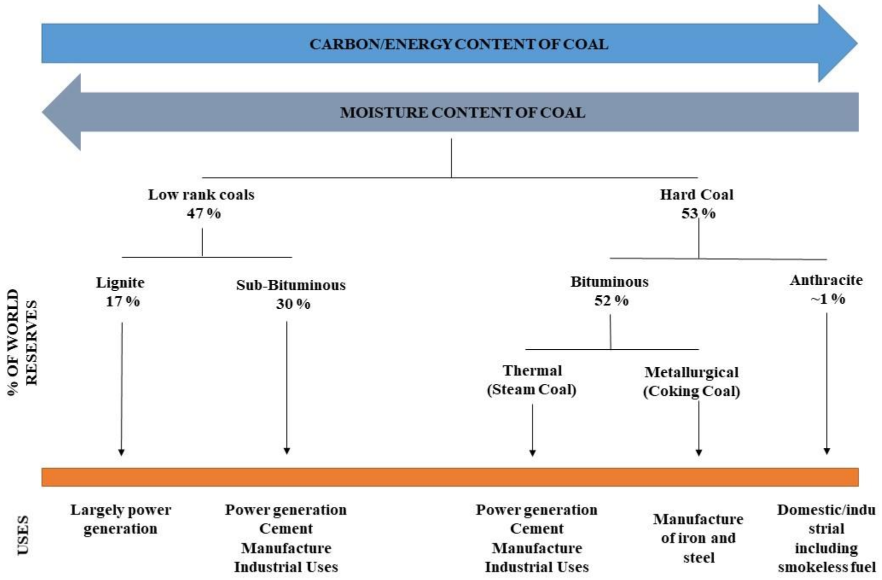

Figure 2: Coal Classification by Carbon/Energy and Moisture Content (Adopted from World Coal Association (n.d.))

Coal and asphaltite molecules have large, heavy and complicated structure. Coal molecules have high amount of sulfur and nitrogen content together with tetrahedral structures. The complex structure of coal makes it hard to build a stable process. In addition to their complex structure, chemical composition of coals from same reserve can also change due to heterogenic nature of the coal. A model coal molecule can be seen in Figure 3.

Coal has mainly 2 types of sulfur compounds, which are inorganic sulfur and organic sulfur. Inorganic sulfur compounds are mainly pyrite (FeS_2). Organic forms of sulfur in coal are mainly 3 groups, which are mercaptanes, thiopenes and sulfides.

Although asphaltite is a form of petroleum, due to its physical state, it is mostly used as an alternative to coal. Starting from 2009, Şırnak asphaltite is mainly used in Şırnak Silopi Thermal Power Station. This station has 405 MW capacity ("Silopi Electric", 2019). However, Turkish asphaltite has high sulfur, both organic and inorganic, which limits domestic use. Local rules have forbidden utilization of domestic coal or similar solid fossil fuels with sulphur content higher than 2% for environmental purposes (Isinmadan Kaynaklanan Hava Kirliliğinin Kontrolü Yönetmeliği, 2009).

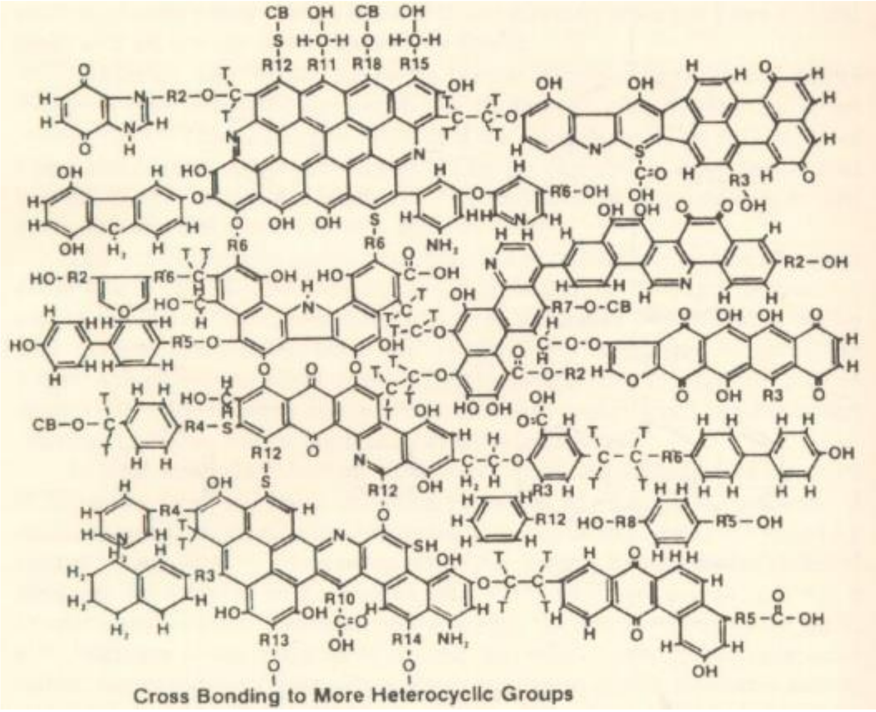

Figure 3: Example of Coal Structure (S, Kasper (1981))

For desulfurization of coal, processes used are divided into 2 main groups, which are physical desulfurization methods and chemical desulfurization methods. Physical desulfurization methods are used for removal of pyritic sulfur. Coal washing, flotation and oil agglomeration and physical desulfurization methods. Chemical desulfurization methods are used for removal of all types of sulfur compounds in coal structure, inorganic and organic sulfurs. Leaching, extraction, oxidative methods, hydrothermal methods, hydrogenation and electrochemical methods are chemical coal desulfurization methods. Types of organic sulfur compounds in coal can be found in Table 1.

Table 1: Organic Sulfur Compounds in Solid Fossil Fuels (Kanca, A. (2013))

Sulfur Compounds	Structure
Mercaptane (Thiol)	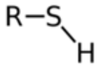
Thiophene	
Sulfide	R-S-R

Since direct combustion of coal results in toxic sulfur compounds to be released, environmentally friendly ways of coal utilization should be used. Liquefaction, gasification and desulfurization can be used to reduce sulfur emissions from coal utilization. Although desulfurization processes are widely used for petroleum products, it is hard to desulfurize solid fossil fuels due to their heterogenic structure. For this purpose, high sulfur content fossil fuels can also be blended with biomass. Mixing not only reduces overall sulfur ratio of the processed sample, but also a possible synergetic effect between solid fuel and biomass can increase utilization rate of both solid fuels.

1.2. Coal reserves

Coal reserves are distributed all around the world. As it can be seen from Table 2, Turkey has nearly 1% of the World’s total coal reserves, while the biggest reserves are held by USA, Russia, China and Australia.

Table 2: Coal Reserve Distribution across Countries (("Statistical Review of World Energy: Energy economics: Home", 2019)

Country	Total Reserve (million tons)
USA	250.219
Russia	160.364
Australia	147.435
China	138.819
Turkey	11.526
Total	1.054.782

With the current reserves, among petroleum and natural gas, coal and its derivatives are expected to have the highest reserve life.

Turkey has total of 314 million tons of asphaltite reserves, mainly distributed in Şırnak and Silopi regions. Although not appropriate for domestic use, due to its high volatility and mild energy content, asphaltite can be processed easier than coal and used as an important energy source.

1.3. Background on Biomass

All organic matter obtained from plants, animals and humans are biomass. Biomass is considered as renewable energy source. Biomass samples can be utilized by direct combustion, can be processed to produce biofuels or syngas which can be further utilized by Fischer-Tropsch synthesis to produce synthetic fuels.

1.4. Motivation

High sulfur containing coals lead to high amount of SO_2 and NO_2 emissions in direct combustion. The SO_2 resulting in this process can lead to corrosion and air pollution. The motivation of this study is utilization of coal reserves in environmentally friendly and economically way.

To increase overall process efficiency to obtain valuable products, biomass and asphaltite can benefit from co-processing. The synergetic affect rises mainly since sulfur compounds in asphaltite can decrease the difficulty of activating lignocellulose. Also, CO_2 formed from biomass combustion is accepted to be a part of carbon cycle, hence has minimum effect in climate change, which overall reduces asphaltite’s effects. Steam distillation is chosen as co-processing method since biomass and asphaltite has significant amount of water unless dried and small amount of hydrogen can be produced from water inside biomass by minerals in asphaltite, which also increases overall process efficiency. Since motivation is to increase the value of Şırnak asphaltite and biomass, keeping sulfur inside the process residue is desired.

1.5. Objectives

The aim of this M.Sc. study is valorization of Şırnak asphaltite in an environmentally friendly way, and investigate the synergetic effect investigation of co-processing of biomass and Şırnak asphaltite while charactering the products obtained and improving process efficiency by dry reforming.

CHAPTER 2

LITERATURE SURVEY

2.1. Desulfurization

Removal of sulfur from fossil fuel structure has high importance to reduce the environmental effects of fuel utilization (Demirbas & Balat, 2004). For fossil fuels, petroleum desulfurization methods are being widely used to regulate petroleum used for Euro 5 and Euro 6 standards, to reduce petroleum sulfur content below 10 ppm (ICCT, 2016).

The industrial approach for desulfurization of petroleum products is hydrodesulfurization (Srivastava, 2012). For hydrodesulfurization processes mostly used catalysts are Ni-Mo/Al_2O_3 and Co-Mo/Al_2O_3 in their sulfide forms. These catalysts can also be used for hydrocracking reactions. The difference is their operating temperature. Hydrodesulfurization processes are carried out at 35-150 bar pressure and temperature between 330-410 °C. Hydrocracking reactions are being carried out at 100-200 bar pressure and temperature between 350-385 °C. (Speight, 2000), (Srivastava, 2012).

Ni-Mo/Al_2O_3 and Co-Mo/Al_2O_3 catalysts are called bifunctional catalysts. Ni-Mo and Co-Mo sites of the catalyst is called metallic site and alumina site is called acidic site. (Jukic, 2016), (Uner, 2017).

Coal desulfurization methods are divided into 2 main parts, which are physical and chemical desulfurization methods.

2.1.1. Physical Desulfurization of Coal

Physical desulfurization of coal aims to minimize inorganic sulfur compounds (mainly pyrite) from coal structure. Physical desulfurization of coal involves, flotation, oil agglomeration, gravimetric and magnetic methods are feasible for the physical operations (Longwell, Rubin, & Wilson, 1995), (Demirbas & Balat, 2004). However, previously studied methods in the literature have shown that, physical desulfurization methods applied on Şırnak asphaltite has failed to reduce the sulfur content of the asphaltite below the limit of Şırnak Municipality, which is 2% by weight (Demir, 2009).

2.1.2. Chemical Desulfurization of Coal

Chemical desulfurization methods can be used to remove organic and inorganic sulfur contents from coal structure. One of the most effective and common methods of chemical coal desulfurization method is hydrogenation. This method can be applied by the help of a solvent or in a flow system under atmopheric pressure. 66% of desulfurization can be obtained by direct hydrogenation (Zhang, Du, Zhang, & Xu, 2014) . In the study of Zhang et al., 2014, It was observed that, increasing hydrogen flow rate increases the desulfurization rate. It was seen in their study that aliphatic sulfur, a form of organic sulfur compounds, are removed under the temperature of 250-450°C and pyritic and aromatic thiophenic sulfur were removed under the temperature of 450-650ºC. However, since these experiments were conducted under differential reactors, liquid products were not obtained due to the small sample size.

Hydrogenation is the most common method that is used for the coal liquefaction activities. “Lurgi-Rhurgas”, “Consolidation Coal’s Stirred Fluid Bed Process” and “Nedol” processes are used for the coal liquefaction processes. (Holmes, Cochran, Edwards, Joy, & Lantz, 1977), (NEDO, 2006). NEDOL process is based on hydrogenation of coal dissolved in a solvent. After hydrogenation, coal oil and solvent is separated.

Hydrodesulfurization can also be applied by using suitable solvents. For example $NaBH_4$ solution can lead to 40.8 % desulfurization under atmospheric pressure and 30°C (Li, et al., 2010). Also, at 600°C, if KOH or NaOH catalyts is used, 83% of the sulfur content can be eliminated (Liu, et al., 2005). Moreover, in a study that is performed on Çayırhan lignite, it was observed that sulfur content was decreased by

90% at 150 bars and temperature below 520°C with the presence of MoS_2 catalyst (Garcia, Moinelo, Lafferty, & Snape, 1991). The other catalyst that is used for the catalytic hydrodesulfurization method is $P(C_4H_9)_3$. Under the atmospheric pressure and temperature of 250°C, it was observed that sufur content was diminished 90% (Verkade, Mohan, & Angelici, 1995).

Another method for chemical desulfurization of coal is extraction. It can be performed either at the atmospheric pressure or at the supercritical conditions. For extraction, different type of solvents can be used. According to the literature, 75% of desulfurization can be achived by using nitric acid-water solution (Alam, Moghaddam, & Omidkhah, 2009), (Mesroghli, Yperman, Jorjani, Carleer, & Noaparast, 2015). In the study of Mesroghli, they reduced the coal sulfur ratio by 63% by dissolving the microwave treated coal in peroxy acetic acid in Iranian Tabas coal. Lompa-Krzymien, (1982) used copper ions and obtained 100% desufurization. Nevertheles, regaining of copper was not explained in this study. Other solvents used for this method are sodium hypochlorite and potassium permanganate. Unfortunately, their yields are very low (Kawatra & Eisele, 2001).

On the other hand, supercritical extraction is a very efficient method for the removal of organic sulfur. CO_2, water and methanol can be used as a mixture or separately. In the literature it was observed that 82 % desulfurization was achieved by supercritical extraction (Kawatra & Eisele, 2001).

Besides the hydrogenation and extraction methods, oxidesulfurization is another method for the removal of pyritic and organic sulfur compounds by the help of water and oxygen in a more effective and economical way (Demirbas & Balat, 2004), (Luo, Kang, Zhu, & Dai, 2014). By this method, sulfur compounds ind the solid fossil fuels are oxidized under the oxygen gas at a high pressure. By this way, non-combustible sulfur compounds can be obtained. These compound can be removed by using a suitable solvent such as water. Since oxidized sulfur compounds carried in the solvent show acidic properties, basic compounds can be added to the solvent and by this way it can be neutralized. It was expressed that these basic compunds does not harm the wall of the reactor and also increases the yield of the desulfurization operation (Demirbas, 2006).

For the removal of pyritic and organic sulfur compounds, different types of oxidized materials are being used. Some of them are H_2O_2 solution (Gürü and Alıcılar, 2001), (Borah, Baruah, & Gogoi, 2005), permanganate solution (Gürü, 2004), the fluorination, dimethyl oxirane and sodium hypochlorite.

The C-S bond should be broken for the removal of organic sulfur from the solid fuel. By this way, while sulfur is being removed, carbon amount will not decrease and calorific value will be preserved. It is expected that after oxidization of sulfur compounds, they will be converted into sulfate which enables them to be solved in a solvent. Mayer process uses iron ions for the oxidizing agent, but this method is not effective for the removel of organic sulfur compounds (Borah, Baruah, & Gogoi, 2005). It was seen that after oxidation at 150 °C using sulfuric acid with iron ions, organic sulfur was converted into sulphon ($R - S (=O)_2 - R$) and sulfoxide ($R - S = O - R$). In the study using iron (Fe + 3) based salts, it was observed that thiophene was slowly oxidized from the organic sulfur compounds (Lalvani, Pata, & Coughlin, 1983).

Air is also used as an oxidizer in the literature. It is seen that 44% of the organic sulfur compounds in coal extracted from Illinois USA are removed under 150-200 °C and 35-70 bar air pressure. Also, coals from the Meghalaya region of India showed 10.9% of the organic sulfur compounds are removed under atmospheric pressure and at 150 °C (Friedman, Lacount, Warzinski, 1977), (Borah & Baruah, 2001).

Another important oxidizing agent for the oxidesulfurization is potassium permanganate. It was observed that 87% sulfur was removed by using this compound (Attia, Weiven, 1987). Yet, after oxidation operation, strong acid treatment was needed for the removal of remaining potassium permanganate. Another compound is hydrogen peroxide. It has been found that 9.24% by mass of organic sulfur compounds are removed within one day after India's Meghalaya coal has been treated with hydrogen peroxide (Borah, Baruah, & Haque, 2002). It was observed that 28.14% of the organic sulfur compounds and 31.12% of the organic sulfur compounds were removed in 24 hours for the Pd^{+2} ions and 4 hours for the Sb^{+3} ions, respectively, as a result of oxidesulfurization using metal ions together with hydrogen peroxide. Studies were also available which were used peroxyacetic acid for the oxidizing agent (Borah, Baruah, & Gogoi, 2005), (Palmer & Hippo, 1991). In these studies, it was determined that 16% of the organic sulfur compounds are eliminated and the desulphurization rate is 23-32% when the Pd^{+2} ion is added.

Sulfur content in the lignite were removed by oxydesulfurization method under 10 bar oxygen pressure and 0.1 M of sodium carbonate that is obtaibed from the Gediz region. By this way it was observed that sodium carbonate solution is a good canditate for the extraction method (Yaman & Küçükbayrak, 1996). Another study for this lignite showed that ammonia solution increses the yield of oxidesulfurization method. In another study, it was observed that 12.5% of the organic sulfur in the lignite coal extracted from the Central Anatolia region was removed by mass of 20% sodium hydroxide (NaOH) solution at 345 K for 8 hours (Kara & Ceylan, 1988). In the study that is conducted by $FeCl_3$ solution, it was observed that process temperature and particle size is very important. In the same study, it was observed that increasing the concentration of $FeCl_3$ solution and decreasing the acidicity has a positive effect of removing pritic sulfur compounds (Boncukcuoğlu, Kocakerim, & Erşahan, 1994). There are also ultrasound supported deep oxidesulfurization studies present in the literature (Mei, Mei, & Yen, 2003).

Various processes used for coal processing are summarized in Table 3 with values of temperature, pressure, process time, solvent and desulfurisation percent. Information not available on this table is left blank.

Table 3: Coal Processing Literature Survey

Reference	Coal Type	Process	Time	Catalyst	Temp.	Pressure	Solvent	Sulfur Removal (%)			
								Pyrite	Organic	Sulfatic	Total
Li et al. (2010)	Yanzhou and Yanshan Coal	Hydrodesulfurization	1 min	-	30 °C	Atmospheric	NaBH$_4$ – Water Solution	59	15	100	40.8
Moghaddam and Omidkhah (2009)	Tabas Mezino Coal	Leaching	90 min	KOH and NaOH	90 °C	Atmospheric	HNO$_3$ – Water Solution	-	-	-	75.36
Liu et al. (2005)	Yima and Yanzhou Coal	Pyrolysis/Hydrogenation and washing	30 min	-	600 °C	Atmospheric	-	-	-	-	81.4
Lompa-Krzymien (1982)	Prince Coal	Solvent extraction and washing	24 – 48 hours	-	150-200 °C	Atmospheric	Copper Solution	-	-	-	100
Mesroghli et al. (2015)	Tabas Coal	Microwave treatment and peroxyacetic acid treatment	90 min	-	55 °C	Atmospheric	PAA	85-98	48	100	63
Ghauri et al. (2013)	Galler Coal	Oxidesulfurization	-	MoS$_2$		300 bars	-	75	30-72	100	-
Garcia and Moinelo (1991)	Çayırhan lignite	Pyrolysis, hydropyrolysis and catalytic hydropyrolysis	-	PBu$_3$	520 °C	150 bars	-	-	-	-	90
Verkade (1997)	-	Hydrogenation	48 saat		250 °C	Atmospheric	-	-	-	-	90
Kawatra and Eisele (2001)		Supercritical extraction		NaClO	Supercritical	Supercritical	CO$_2$, water, methanol	-	-	-	82
Kawatra and Eisele (2001)	Illinois Coal	Extraction	1 Hour	Co-Mo	25 °C			15-25	26-49.5	-	-
Wang et al. (2007)	-	Catalytic supercritical extraction	-		Supercritical	Supercritical	Water	-	-	-	73

2.2. Catalytic Tar Reforming

Tar is a complex organic molecule that generally forms as a result of thermal decomposition or partial combustion of organic molecules. Thermal processing of biomass feedstock mainly produces alcohols, aldehydes, ketones, carboxylic acids and other oxygen rich organic molecules (Evans & Milne, 1987). These molecules convert into secondary tar products depending on processing temperatures (Brage, Yu, Chen, & Sjöström, 2000), (Adegoroye, 2004).

Organic pollutants heavier than benzene is accepted as tar. Although benzene is not included in this definition, it generally has the highest weight ratio among organic pollutants of biomass products and needs to be removed (Torres, Pansare, & Goodwin, 2007).

Catalytic tar removal is performed at similar temperatures of gasification reaction temperatures, together with other gasification products (El-Rub, Bramer, & Brem, 2004). Oxygen or water can also be added to the gas mixture. Tar molecules are converted into smaller hydrocarbons, such as CO, CH_4 and H_2, through steam reforming, dry reforming or hydrocracking reactions.

If benzene is selected as model compound, these reactions can be demonstrated as follows:

Steam Reforming

$C_6H_6 + 6H_2O \rightarrow 6CO + 9H_2$

$C_6H_6 + 12H_2O \rightarrow 6CO_2 + 15H_2$

Dry Reforming

$C_6H_6 + 6CO_2 \rightarrow 12CO + 3H_2$

$C_6H_6 + 9CO_2 \rightarrow 15CO + 3H_2O$

Hydrocracking

$C_6H_6 + 9H_2 \rightarrow 6CH_4$

Boudouard Reaction

$2CO \rightarrow CO_2 + C_{(S)}$

Cracking

$C_6H_6 \rightarrow 3H_2 + 6C_{(S)}$

Tar removal through hydrocracking reactions is preferred when the product methane is combusted to produce energy. However, if the product gas will be used to produce methane or ammonia, hydrocracking is not preferred.

All catalytic reactions to remove tar result in producing coke as a side product, which deposit on catalyst surface and reduce activity. While cracking and Boudouard reactions produce coke, water-gas shift reaction can also occur to increase produced hydrogen gas amount.

Following specifications are desired in catalysts used in catalytic tar removal:

1. Effectively produce desired gases in mild temperature range (600-800 °C),
2. High resistance against sulfur poisoning,
3. Low selectivity of cracking and Boudouard reactions.

Although nickel is known to have high activity in decomposition of carbon and WGS, sintering and coke deposition are problem in nickel catalysts. To overcome those problems, perovskite loading can help (Jung, et al., 2015).

For above reasons, $Ni/LaCoO_3$ is selected[1] and referenced against standard Ni/Al_2O_3 catalyst. Catalyst performance is tested on model benzene molecule.

2.3. Co-Processing of Asphaltite and Biomass

Co-Processing of coal and biomass can increase product yield and decrease pollutant content (Singh & Zondlo, 2017). Synergetic Effect of Co-Processing is defined as increased efficiency of singular processes increase due to mixing of reactants. While high H/C content of biomass can increase coal decomposition, minerals and inorganics

---

[1] $Ni/LaCoO_3$ is synthesized and characterized by Asst. Prof. Dr. Başar Çağlar.

inside coal can increase decomposition of biomass (Krerkkaiwan, Fushimi, Tsutsumi, & Kuchonthara, 2013).

In literature, asphaltite co-processing is only studied with lignite (Ballice & Sağlam, 2003). In the work of Ballice & Sağlam, main focus is the analysis of co-pyrolysis gas product analysis using GC.

In synergetic effect investigation, coal to biomass ratio, temperature range and material preparation are important parameters. Hemicellulose, cellulose and lignin are important constitutes of biomass to be cracked in processing. Hemicellulose decomposes around 310°C, cellulose decomposes around 365°C while lignin decomposes in wide range between 400°C and 800°C (Agarwal & Lattimer, 2014).

Characterization methods used for synergetic effect investigation varies. SEM, TGA, GC, GC-MS are widely used characterization methods (Agarwal & Lattimer, 2014), (Wang, 2017), (Zhang, Xu, Zhao, & Liu, 2007), (Collot, Zhuo,Dugwell & Kandiyoti, 2000).

Non-dried, dried and water leached samples are investigated in its effect of co-processing of coal and biomass. It is found out that, although water leached and dried samples result in highest process efficiency, decomposition temperature significantly increases (Agarwal & Lattimer, 2014).

Due to above reasons, to investigate the synergetic effect between Şırnak asphaltite and pepper plant biomass, steam distillation was selected to eliminate the necessity of drying of reactants, reaction temperature is selected as 450°C and analysis methods are selected as TGA and NMR.

CHAPTER 3

MATERIALS AND METHODS

The overall experimental algorithm is outlined in Figure 4.

Figure 4: The Algorithm of Experimental Strategy

3.1. Şırnak Asphaltite Preparation

For Şırnak asphaltite preparation, size reduction was performed. Aim of the size reduction of Şırnak asphaltite was to get <150 mesh (0.084 milimeters) Şırnak asphaltite samples. Particle size is selected based on previous experiments with these particles. It is decided that, <150 mesh particle size is the optimum particle size considering heat and mass transfer limitations. These samples were needed for hydrogenation and pyrolysis experiments. 150 mesh particle size was selected for lower mass transfer limitations of the reactant gases. Size reduction experiments were carried out at Ore Dressing Laboratory in METU Mining Engineering Department. Raw Şırnak asphaltite rocks were obtained from TKİ Şırnak. About 4-5 kg of raw material was processed. Materials had waited for a long time. Hence these asphaltites should be considered "dead asphaltite", meaning it has lost significant number of volatiles in waiting period.

3.1.1. Experimental Procedure

Size reduction of the particles has 4 different steps which are, crushing with hammer, jaw crusher, rolling crusher and grinding. Asphaltite rocks are first crushed using hammer into smaller rocks. Then jaw crushing is used to reduce particle size to 1-2 centimeters. Only 1 run for each sample was enough.

Rolling crusher is used to reduce sample size below 1 mm. At first, the distance between rolling disks was near maximum. After each run, crushed sample is obtained, sieved, and <1mm particles are separated and >1 mm particles are again fed to rolling crusher while the distance between disks was shortened. These 2 steps are done 5-6 times until small amount of >1 mm parts were left, which were discarded. After rolling crusher, samples were sieved to find out the percentage of <150 mesh particles.

For grinding part, a grinder cylinder is taken and filled up to half with 125 of 18.97 mm and 90 of 25.35 mm stainless steel balls. For each run of grinding, 1 kg of asphaltite is fed to grinder. After the process ended all the samples were sieved and <150 mesh and >150 mesh particles are separated by using Retsch AS 200-digit sieve shaker.

3.1.2. Grinding Calibration Curve

To get a calibration curve for grinding, <150 mesh particles after rolling crusher is found. For that purpose, 2 different experiments are carried out.

For first 2 experiments, a full shovel is weighed, then the samples are sieved. These experiments are named Exp. 1.1 and 1.2. For second set nearly 100 gram of sample is fed to sieve and undersize vessel together. All the experimental results can be seen in Table 4.

Table 4: <150 Mesh Particle Size After Rolling Process

Exp 1.1	Empty (g)	Full	Percentage of <150 mesh
Undersize Vessel	254.53	257.64	0.13
Shovel	159.53	184.23	
Exp 1.2	Empty (g)	Full	Percentage of <150 mesh
Undersize Vessel	254.53	260.01	0.24
Shovel	159.53	182.19	
Exp 2.1	Empty (g)	Full	Percentage of <150 mesh
Undersize Vessel	254.34	265.23	0.11
Sieve and Undersize Vessel	515.73	615.43	
Exp 2.2	Empty (g)	Full	Percentage of <150 mesh
Undersize Vessel	254.46	264.10	0.10
Sieve and Undersize Vessel	515.70	615.91	

Result obtained from Exp. 1.2 is accepted to be an outlier and average <150 mesh particle size after grinding was accepted to be around 10%. For grinding time calibration, <150 mesh particles after 15-minute, 45-minute and 60-minute grinding is found. Calibration data tables and graph can be found in Table 5,

Table 6 and Figure 5: Asphaltite Grinding Calibration Curve.

Table 5: Grinding Calibration Runs

t=15 min	Empty (g)	Full (g)	Net Weight (g)
Undersize Vessel	254.10	295.41	41.31
Sieve and Undersize Vessel	515.55	615.60	100.05
t=45 min			
Undersize Vessel	254.00	326.77	72.77
Sieve and Undersize Vessel	515.39	615.46	100.07
t=60 min			
Undersize Vessel	254.06	332.32	78.26
Sieve and Undersize Vessel	515.16	615.56	100.40

Table 6: <150 mesh Particle Size Percentage for Different Grinding Times

T (minute)	<150 Mesh Particle Size Percentage
0	10%
15	41.29%
45	72.72%
60	77.95%

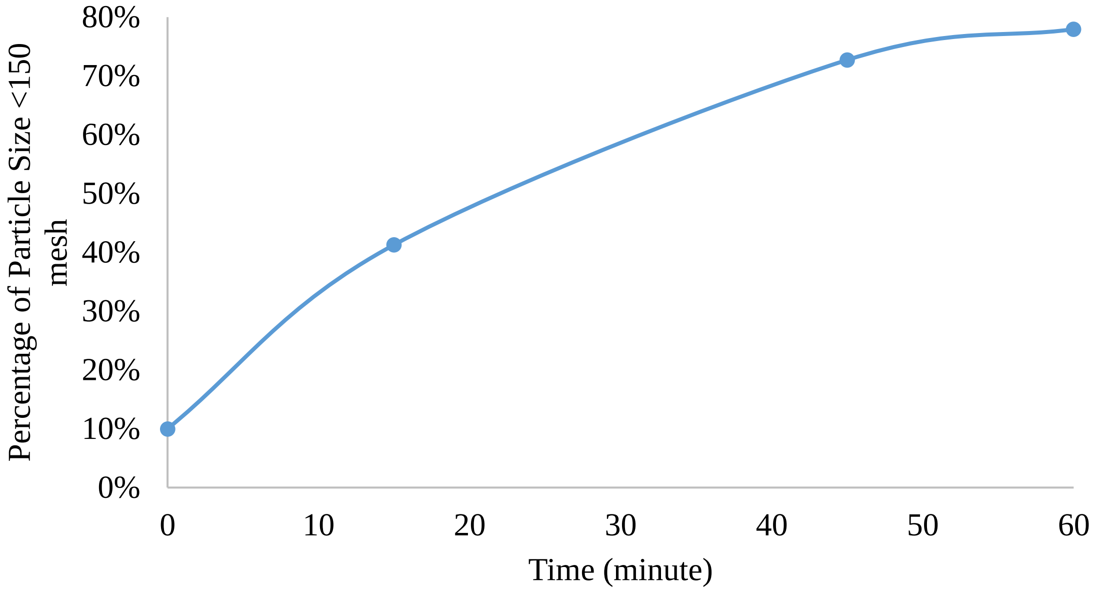

Figure 5: Asphaltite Grinding Calibration Curve for <150 Mesh Particle Percentage

Using this calibration curve, grinding time is selected as 1 hour. Extending 1-hour grinding time may seem to increase required particle size percentage, however increasing this process time may result in pressing of particles instead of crushing them. Grinding calibration curve is obtained to effectively reduce time of grinding process for later particle size preparation works.

3.1.3. Last Sieving

After all the crushing process is over, final sieving is done. For this part around 200 gr sample is sieved for 5 minutes with 60 amplitude. In this process just 150 mesh sieves are used. Hence the distribution over and below 150 mesh particle size is not obtained. Also, the sieving process is kept short, hence there are probably some <150 mesh particles still in >150 mesh particles.

3.2. Biomass Preparation

Biomass used in experiments are >150 mesh waste pepper plant particles. Waste pepper plants are obtained from Tarımsal Araştırma Merkezi (TAGEM). After cleaning soil on the biomass, biomass crushed using a household blender. Crushed biomass samples are dried in room conditions for 5 days. Dried samples are again crushed using household blender. Samples are sieved and >150 mesh waste pepper plant samples are obtained.

3.3. Asphaltite Sampling

No sampling methods were used for asphaltite. To ensure the homogeneity of asphaltite samples, the samples are well mixed and verified using elemental analysis. Results show that there is no significant difference in asphaltite elemental distribution.

3.4. Pyrolysis and Hydrogenation of Asphaltite

Hydrogenation and pyrolysis experiments are carried out for Şırnak asphaltite. Total gas flow for those experiments is 100 sccm (standard cm^3/min). Pyrolysis is performed under nitrogen flow, hydrogenation experiments are performed under 10% hydrogen and balance nitrogen and oxidation experiments are performed under dry air atmosphere. In each experiment, 25 grams of the sample is processed. Reactor is heated from room temp to 550°C with 10°C per min ramp. A sweep reactor is used for those experiments. Drawing of sweep reactor can be found in Figure 7. Flowchart of the experimental setup can be found in Figure 6. Inlet gas is regulated by a gas manifold. Outlet stream is first sent to condenser to collect liquid product. Stream leaving condenser enters PbAc solution. PbAc solution helps removal of H_2S. PbAc solution was planned to be used for overall sulfur balance, however due to losses, it could not be performed. Change of PbAc solution throughout the experiment can be seen in Figure 8. Gas stream then enters mass spectrometer for detailed analysis. After it is released from the hood.

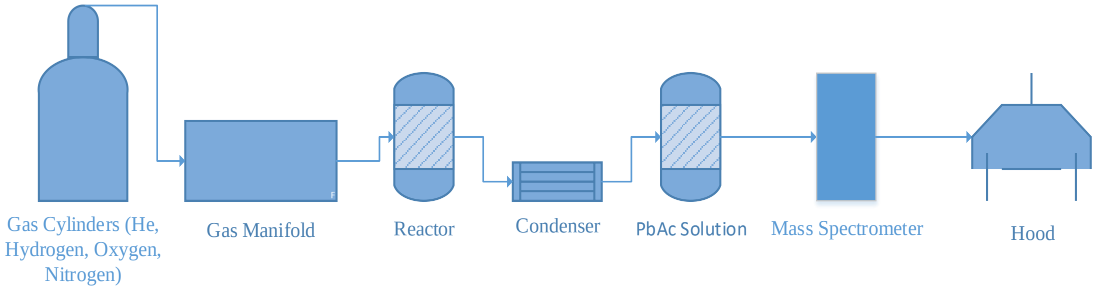

Figure 6: Schematic Drawing of Şırnak Asphaltite Pyrolysis and Hydrogenation Experimental Setup

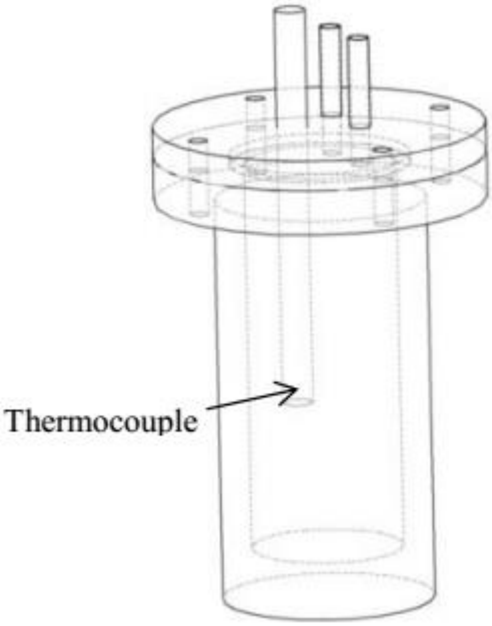

Figure 7: Sweep Reactor Drawing

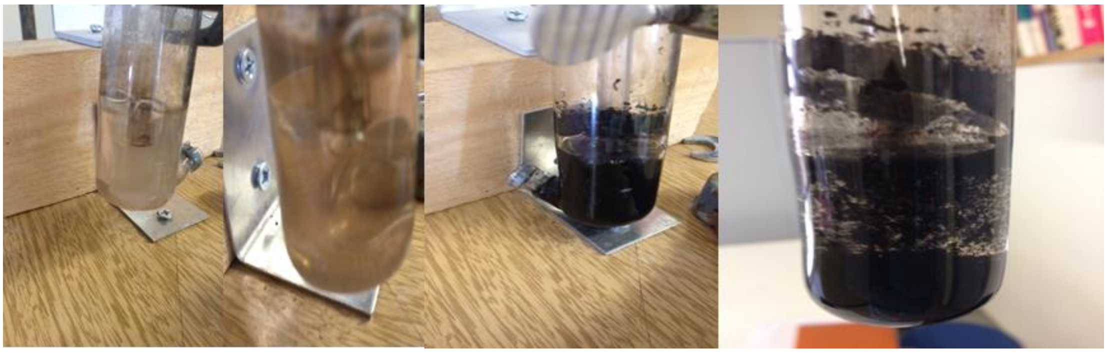

Figure 8: PbAc Solution

3.5. Characterization of Şırnak Asphaltite

For characterization of Şırnak asphaltite residue and gaseous products, Proximate analysis, Elemental analysis, thermogravimetric analysis, Nuclear Magnetic Resonance methods and mass spectrometry.

3.5.1. Proximate Analysis

Proximate analysis of Şırnak asphaltite is used to determine ash, volatile matter, humidity and fixed carbon percentages of material. Proximate analysis is performed using Perkin Elmer Pyris 1 TGA device.

3.5.2. Elemental Analysis

Elemental analysis of Şırnak asphaltite is used to determine initial and final elemental composition of the asphaltite processed. Elemental analysis is performed using LECO, CHNS-932 device.

3.5.3. Thermogravimetric Analysis

Thermogravimetric analysis (Shimadzu DTG 60H) is used to determine volatile behavior of the asphaltite at different temperatures. TGA is performed between 25 °C to 900 °C with 10°C/min ramp under N_2 atmosphere. To obtain oxidation behavior of the asphaltite, TGA experiment is also carried out under O_2 atmosphere. Total gas flow of TGA system is 60 sccm.

Samples processed for TGA are unprocessed, pyrolyzed and hydrogenated Şırnak asphaltite samples.

3.5.4. Nuclear Magnetic Resonance Spectra

To evaluate which structural groups in the coal structure is affected by the process, Nuclear Magnetic Resonance Spectroscopy method is applied. Carbon and Hydrogen NMR methods are used for that purpose. Liquid NMR experiments are carried out using Bruker Liquid NMR, Bruker Avance 300 MHz, Magritek Spinsolve 43 MHz Benchtop NMR. For liquid NMR experiments, DMSO is used as solvent when necessary.

Room temperature ^{13}C direct polarization Magic Angle Spinning (MAS) NMR experiments of selected samples were performed at 11.7 T. The Larmor frequency for ^{13}C is 125.8 MHz. A Bruker 4 mm HBB MAS probe and a Bruker Avance spectrometer were used. A ^{13}C 90-degree pulse width of 4.7 us was measured on solid adamantane, which is also a secondary reference of ^{13}C (the methylene signal was set to 34.48 ppm relative to TMS). The spinning rate was 12.5 kHz. The ^{13}C spectra were acquired with continuous-wave ^{1}H decoupling. The ^{1}H decoupling strength was 50 kHz. A short recycle delay of 5 s was used. 3200 scans were accumulated.[2] (Kanca, Dodd, Reimer, & Uner, 2016)

Glass wools used to plug the asphaltite samples in microreactor setup is divided according to their significant color change. Each divided sample is analyzed using Proton NMR.

When shielding effect is observed, graphic reference method is used for better analysis of similar peaks in stacked NMR graphs. Graphs that belong to raw NMR spectra can be found in Appendix C and Appendix D.

3.5.5. Detailed Hydrocarbon Analysis

Liquid products obtained from pyrolysis and hydrogenation of Şırnak asphaltite is analyzed using Detailed Hydrocarbon Analysis[3]. Sulfur in liquid products are analyzed using ASTM D 5504, where sulfur range for that analysis is 1-1000 ppm. Liquid product analysis is performed according to ASTM D 5431.

3.6. Dry Reforming Experimental Setup

For dry reforming experiments, a home-built experimental setup is used. Quartz tubular reactors with ID: 4 mm and L: 350 mm are use placed inside a home-built temperature-controlled oven. 1 gram of catalyst to be tested is placed in the middle of the reactor and fixed using glass wool. Inlet gas streams passes through a calibrated mass flow controller. Outlet stream of the reactor passes through 2 cold traps to capture unreacted benzene. Gaseous products are analyzed using HP 5890 Series II gas chromotograph equipped with Carboxen 1010 plot column. Outlet stream flow

---

[2] Solid State NMR experiments are performed by Dr. Jun Xu from Berkeley University.
[3] Detailed Hydrocarbon Analysis is performed by METU PAL (ODTÜ Petrol Araştırma Merkezi)

rate is checked using a bubble flow meter. Schematic drawing of xperimental setup can be found in Figure 9.

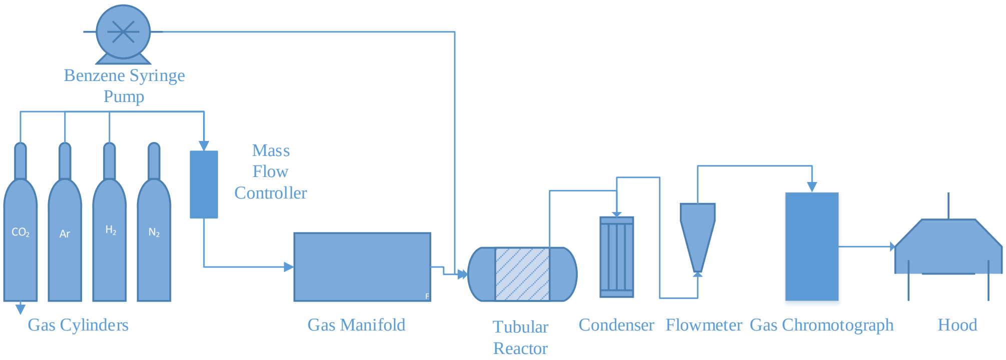

Figure 9: Schematic Drawing of Dry Reforming Experimental Setup

Reduction of the catalyst is performed at 600°C under continuous 40 sccm of argon (70%) and hydrogen (30%) mixture flow for 2 hours. Activity tests are performed using argon, CO_2 and benzene, with total gas flow of 60 sccm. Benzene is supplied using a syringe pump and heated, then swept by carrier gasses. Activity test are run up to 5 hours.

CHAPTER 4

RESULTS AND DISCUSSION

4.1. Thermal Characterization of Şırnak Asphaltite and Biomass

For thermal characterization of Şırnak asphaltite and biomass, synergetic effect was analyzed using thermogravimetric analysis. Pure and mixed samples were then subjected to steam distillation up to 450°C and resulting products were collected in different temperature ranges. In steam distillation experiments, 40 grams of samples were used and 30 ml of water is added to reactor. Collected samples were analyzed using ^{1}H and ^{13}C NMR.

4.1.1. Thermogravimetric Analysis

Şırnak asphaltite was subjected to TGA with biomass (pepper plant waste) for synergetic effect investigation and product characterization. To investigate the synergetic effect of co-processing Şırnak asphaltite and pepper plant waste, dried, <150 mesh samples were used. TGA of asphaltite, biomass and their 25:75, 50:50 and 75:25 ratio mixtures were performed up to 500°C under nitrogen atmosphere. Local maxima points of derivative TGA data is used to find out effect of synergy between asphaltite and biomass.

Sample information of materials analyzed can be found in Table 7.

Table 7: Synergetic Effect Investigation TGA Sample Information

Sample No	**Sample Content**
1	Pure Şırnak Asphaltite
2.1	75% Ş.A. and 25% Biomass
2.2	
2.3	
3.1	50% Ş.A. and 50% Biomass
3.2	
3.3	
4.1	25% Ş.A. and 75% Biomass
4.2	
4.3	
5	Pure Biomass

To avoid any problems of bad mixing, 3 samples of each mixed material was prepared for TGA. Derivative TGA (DrTGA) results were normalized. Normalization was performed according to following formula:

$$Normalized\ DrTGA\ (\frac{1}{sec}) = \frac{Derivative\ TGA\ (\frac{mg}{sec})}{Initial\ sample\ weight\ (mg)}$$

TGA graphs of samples can be found in Figure 10 to Figure 14.

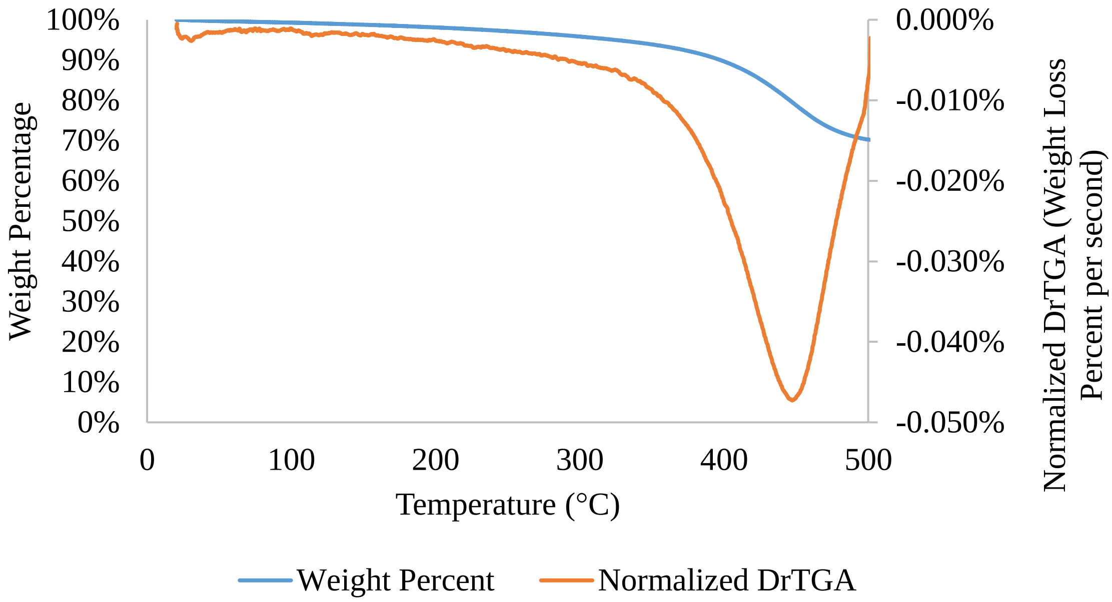

Figure 10: TGA of Pure Şırnak asphaltite under Nitrogen Atmosphere

Using Figure 10, analyzed Şırnak asphaltite has lost almost all light volatiles including water, since only 2% weight loss is observed below 150°C. Hence, used Şırnak asphaltite is “dead” asphalite.

Only one major peak is observed in Derivative TGA of Şırnak asphaltite, which started around 200°C and peaked 450°C.

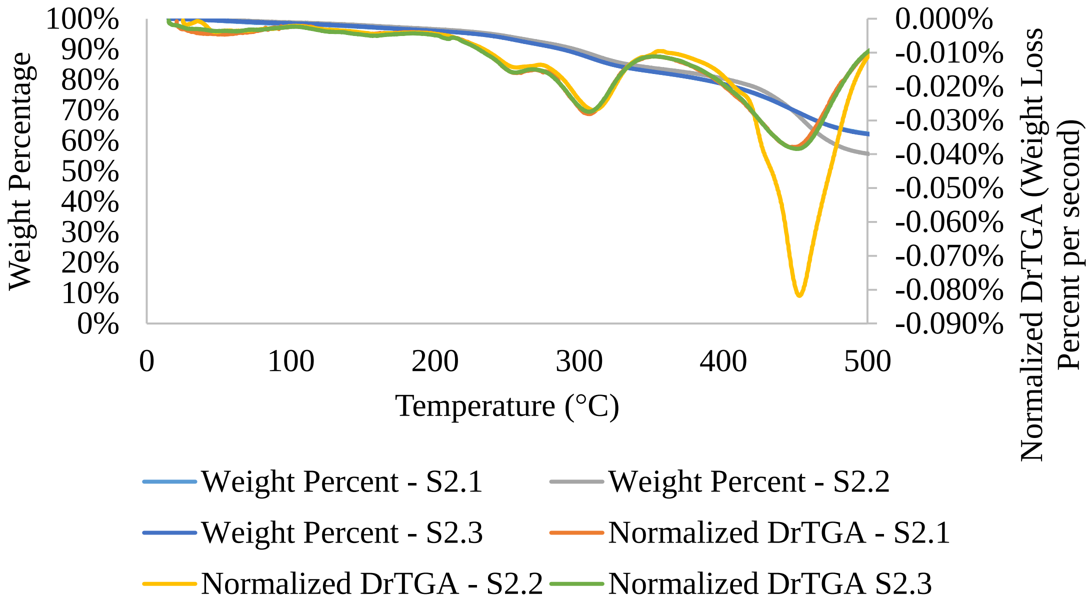

Figure 11: TGA of 75% Şırnak asphaltite and 25% Biomass Mixture under Nitrogen Atmosphere

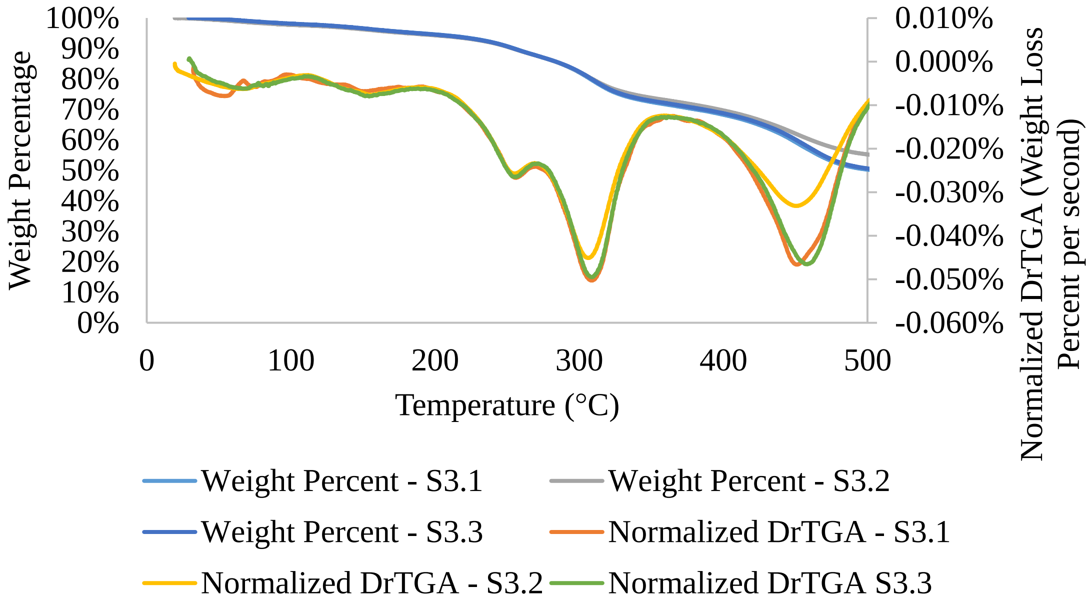

Figure 12: TGA of 50% Şırnak asphaltite and 50% Biomass Mixture under Nitrogen Atmosphere

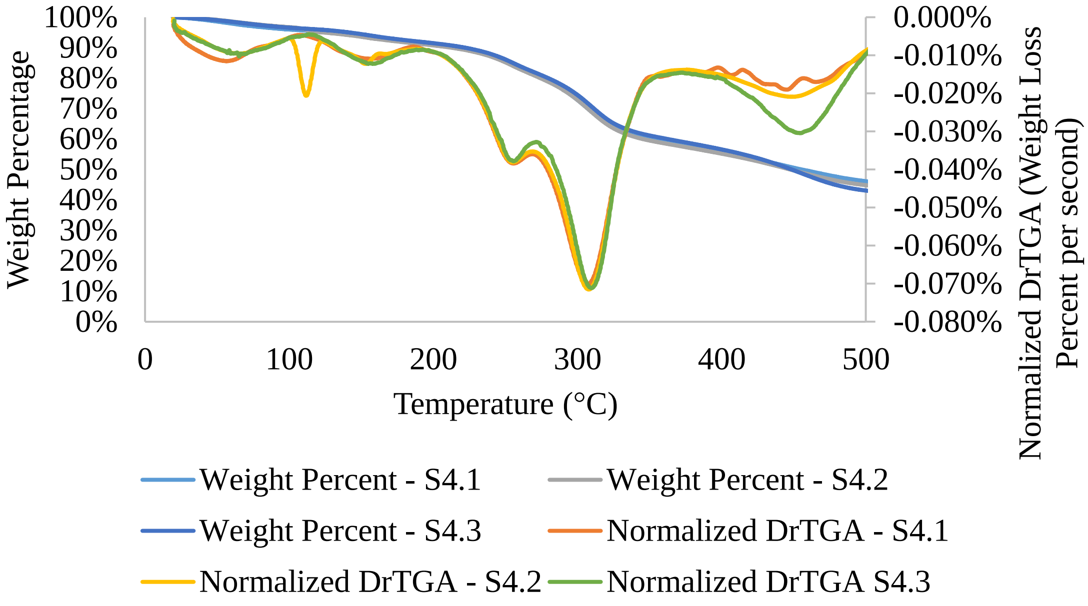

Figure 13: TGA of 25% Şırnak asphaltite and 75% Biomass Mixture under Nitrogen Atmosphere

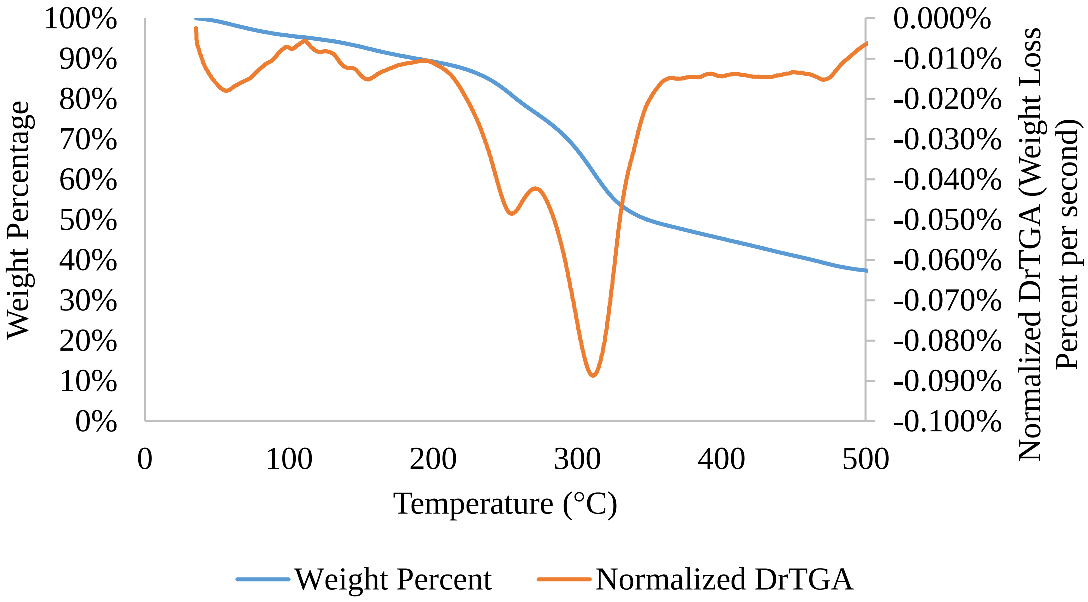

Figure 14: TGA of Pure Biomass under Nitrogen Atmosphere

TGA of mixed samples, Samples 2, 3 and 4, shows that 2nd samples of each mixtures, 2.2, 3.2 and 4.2, shows different behaviors than 1st and 3rd samples. For the analysis part, 1st samples of mixtures are used.

For the analysis of TGA data, total weight loss at 500 °C and all major peaks are investigated. Sample calculation for analysis can be found in Appendix B. Sample information, initial weight and weight at 500°C can be found in Table 8.

Table 8: Sample Information of TGA Data

Sample No	**Material**	**Sample Weight (mg)**	**Weight at 500°C (mg)**
1	Pure Ş.A.	8.84	6.21
2	75% Ş.A. + 25% Biomass	10.97	6.84
3	50% Ş.A. + 50% Biomass	6.75	3.39
4	25% Ş.A. + 75% Biomass	8.27	3.81
5	Pure Biomass	6.42	2.40

Total weight loss percent at 500°C, expected theoretical weight loss and weight loss improvement can be found in Table 9. Expected theoretical weight loss is calculated according to following formula.

$$\begin{aligned} Expected\ Loss\ \left(\frac{mg}{sec}\right) &= \left(\frac{DrTGA\ of\ Ş.A. * Initial\ Weight\ of\ Sample * Weight\%\ of\ Ş.A.}{Initial\ Weight\ of\ Ş.A.}\right) \\ &+ \left(\frac{DrTGA\ of\ B.M. * Initial\ Weight\ of\ Sample * Weight\%\ of\ B.M.}{Initial\ Weight\ of\ B.M.}\right) \end{aligned}$$

Table 9: Actual Weight Loss and Expected Theoretical Weight Loss of Pure and Mixed Materials

Sample	Total Weight Loss	Expected Theoretical Weight Loss	Weight Loss Improvement
Pure Ş.A.	29.78%	N/A	N/A
75% Ş.A. + 25% Biomass	37.66%	38.00%	-0.90%
50% Ş.A. + 50% Biomass	49.81%	46.22%	7.76%
25% Ş.A. + 75% Biomass	53.91%	54.45%	-0.99%
Pure Biomass	62.67%	N/A	N/A

Major peaks in pure samples are identified and to see synergetic effect at different temperatures, weight loss of mixtures in determined temperatures are analyzed.

1st major weight loss is observed for biomass around 55°C. Analysis can be found in Table 10.

Table 10: Weight loss of Samples around 55°C

Sample	Temperature (°C)	DrTGA (mg/sec)	Expected Loss (mg/sec)	Deviation
Pure Ş.A.	53.8	-0.00013	N/A	N/A
75% Ş.A. + 25% Biomass	54.1	-0.00051	-0.00061	-17%
50% Ş.A. + 50% Biomass	54.1	-0.00053	-0.00066	-19%
25% Ş.A. + 75% Biomass	56.4	-0.00095	-0.00114	-17%
Pure Biomass	56.7	-0.00115	N/A	N/A

For all mixtures, theoretical expected weight loss is decreased for peak around 55°C.

2nd major weight loss is observed for biomass around 155°C. Analysis can be found in Table 11.

Table 11: Weight loss of Samples around 155°C

Sample	**Temperature (°C)**	**DrTGA (mg/sec)**	**Expected Loss (mg/sec)**	**Deviation**
Pure Ş.A.	155.17	-0.000160	N/A	N/A
75% Ş.A. + 25% Biomass	154.88	-0.000496	-0.00057	-12%
50% Ş.A. + 50% Biomass	151.00	-0.000462	-0.00057	-19%
25% Ş.A. + 75% Biomass	155.9	-0.000900	-0.00098	-8%
Pure Biomass	155.05	-0.000970	N/A	N/A

For all mixtures, theoretical expected weight loss is decreased for peak around 155°C.

3rd major weight loss is observed for biomass around 255°C. Analysis can be found in Table 12.

Table 12: Weight loss of Samples around 255°C

Sample	**Temperature (°C)**	**DrTGA (mg/sec)**	**Expected Loss (mg/sec)**	**Deviation**
Pure Ş.A.	254.5	-0.00034	N/A	N/A
75% Ş.A. + 25% Biomass	256.7	-0.00176	-0.00165	7%
50% Ş.A. + 50% Biomass	254.5	-0.0018	-0.00176	2%
25% Ş.A. + 75% Biomass	255.6	-0.00318	-0.00308	3%
Pure Biomass	254.5	-0.00311	N/A	N/A

A synergetic effect is observed for the peak around 255°C. Observed weight loss for each mixture are higher than theoretical calculated loss.

4th major weight loss is observed for biomass around 310°C. Analysis can be found in Table 13.

Table 13: Weight Loss of Samples around 310°C

Sample	**Temperature (°C)**	**DrTGA (mg/sec)**	**Expected Loss (mg/sec)**	**Deviation**
Pure Ş.A.	311.1	-0.0005	N/A	N/A
75% Ş.A. + 25% Biomass	307.3	-0.00309	-0.00290	6%
50% Ş.A. + 50% Biomass	308.8	-0.00339	-0.00318	7%
25% Ş.A. + 75% Biomass	307.0	-0.00579	-0.00561	3%
Pure Biomass	311.0	-0.00568	N/A	N/A

Synergetic effect is also observed for the peak around 310°C for all mixtures. Observed weight loss for each mixture are higher than theoretical calculated loss.

5th major weight loss is observed for Şırnak asphaltite around 450°C. Analysis can be found in Table 14.

Table 14: Weight Loss of Samples around 450°C

Sample	Temperature (°C)	DrTGA (mg/sec)	Expected Loss (mg/sec)	Deviation
Pure Ş.A.	447.2	-0.00418	N/A	N/A
75% Ş.A. + 25% Biomass	446.6	-0.00416	-0.00426	-2%
50% Ş.A. + 50% Biomass	451.1	-0.00315	-0.00206	53%
25% Ş.A. + 75% Biomass	444.9	-0.00157	-0.00322	-51%
Pure Biomass	447.0	-0.00088	N/A	N/A

For the peak around 450°C, there is no significant effect observed for Sample 2, 53% increase in weight loss is observed for Sample 3 and 51% decrease in weight loss is observed for Sample 4.

6th major weight loss is observed for biomass around 470°C. Analysis can be found in Table 15.

Table 15: Weight Loss of Samples around 470°C

Sample	Temperature (°C)	DrTGA (mg/sec)	Expected Loss (mg/sec)	Deviation
Pure Ş.A.	470.1	-0.00287	N/A	N/A
75% Ş.A. + 25% Biomass	470.1	-0.00303	-0.00308	-2%
50% Ş.A. + 50% Biomass	470.1	-0.00252	-0.00161	57%
25% Ş.A. + 75% Biomass	470.1	-0.00138	-0.00233	-41%
Pure Biomass	470.3	-0.00098	N/A	N/A

For the peak around 470°C, there is no significant effect observed for Sample 2, 57% increase in weight loss is observed for Sample 3 and 41% decrease in weight loss is observed for Sample 4.

TGA results indicate that, in accordance with the theory, there is a synergetic effect in weight loss in co-processing of the reactants. Synergetic effect found to be highest when the mixing ratio is 50:50. For all mixing rates, weight loss of mixture is lower than theoretical expected value when the major loss is originated from biomass. However, when the asphaltite is the major source of the weight loss, around 50% increase in weight loss is obtained for mixture with mixing ratio of 50:50.

4.1.2. Chemical Characterization by Steam Distillation Fractionation

To investigate the synergetic effect of biomass and Şırnak asphaltite with steam distillation, biomass, Şırnak asphaltite and biomass 50:50 mixture and Şırnak asphaltite experiments are carried out. Samples that could be obtained after each experiment can be found in Table 16.

Table 16: Steam Distillation Experiment Sample Information

	Delivery Tube	100°C	100°C - 150°C	150°C - 250°C	250°C - 350°C	350°C – 450°C
Biomass	X	X	X	X	X	X
50:50 Mixture of Biomass and Şırnak asphaltite	-	X	X	X	X	X
Şırnak asphaltite	-	-	X	X	X	X

4.1.2.1. NMR Spectra of Obtained Samples

^{1}H-NMR and ^{13}C-NMR Spectra of obtained liquid samples in condenser are taken. Nothing but noise is obtained in ^{13}C-NMR Spectra. ^{1}H-NMR stacked graphs can be found in Figure 16, Figure 17 and Figure 18. For characterization, Figure 15 is used.

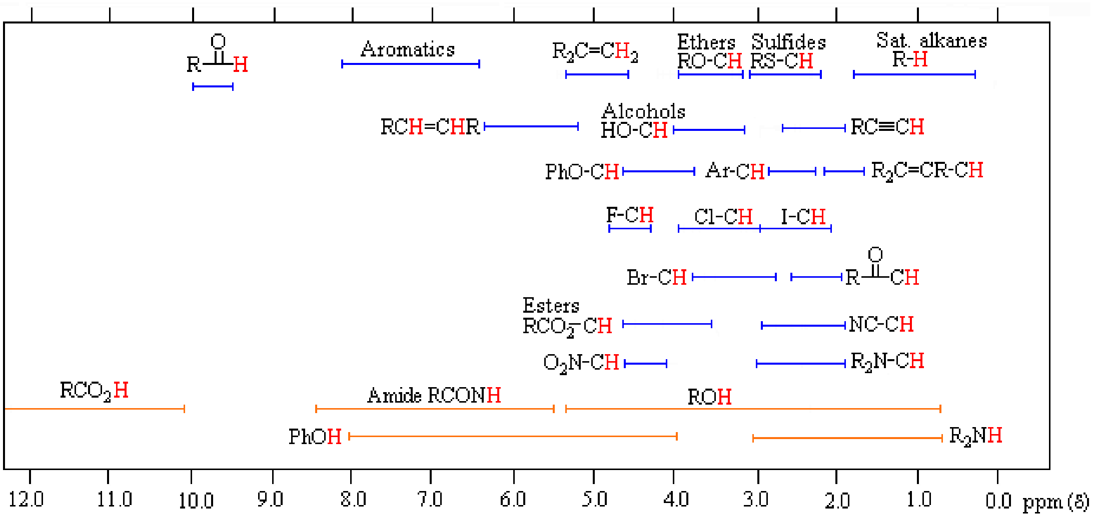

Figure 15: Chemical Shift Reference Table (University of Potsdam(n.d.))

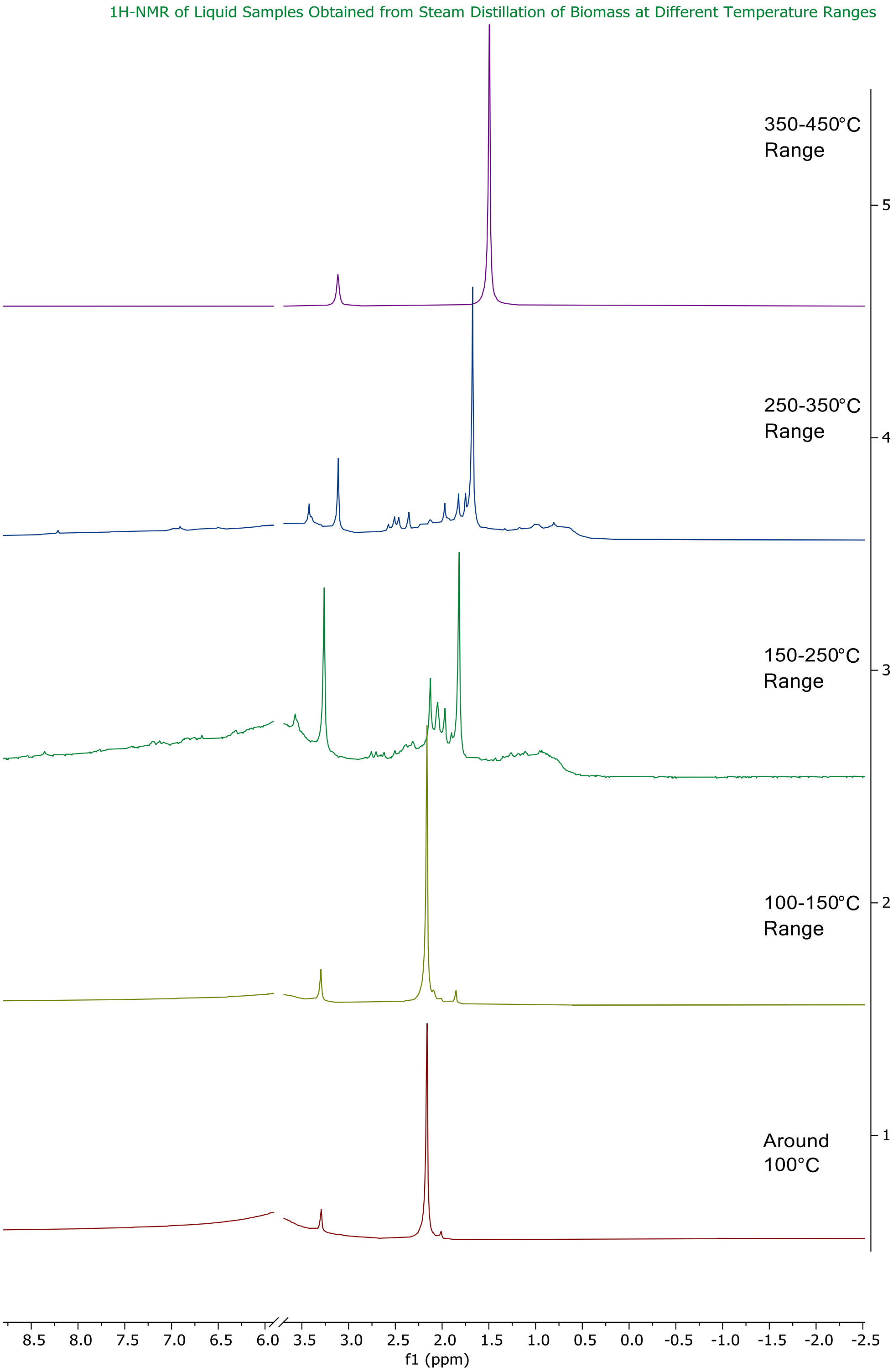

Figure 16: Stacked ^{1}H-NMR of Liquid Sample Obtained from Steam Distillation of Biomass at Different Temperature Ranges

In Figure 16, major shift is observed around 4.8 ppm, which corresponds to water. For 100°C and 100°C-150°C range, second major peak is observed around 2.2 ppm. As temperature increases, this peak is observed to move upfield. This shielding effect is occurring because of the presence of a more electronegative atom. Considering this NMR belongs to biomass, shielding effect probably occurs due to presence of nitrogen. Samples of 150°C - 250°C range and 250°C - 350°C range shows significant and broad peaks around 1 ppm and 2-3.5 ppm range. Broad peaks around 1 ppm belongs to $-CH_3$ groups and broad peaks around 2-3.5 ppm range belongs to $-CH_2$ group. Those peaks are not observed for 350°C - 450°C range, which is a probable result of obtaining volatiles between 150°C - 350°C range.

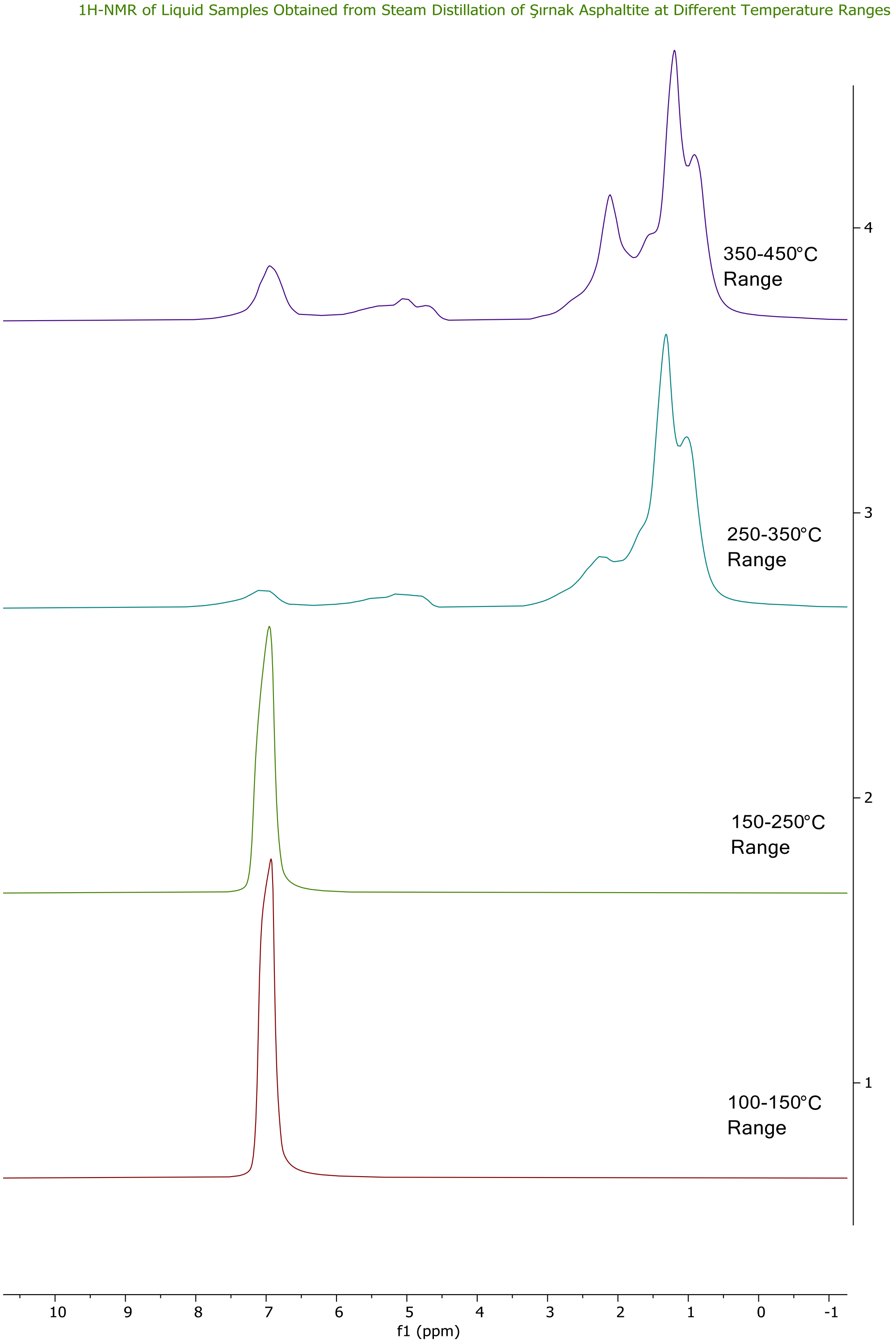

Figure 17: Stacked ^{1}H-NMR of Liquid Sample Obtained from Steam Distillation of Şırnak asphaltite at Different Temperature Ranges

In Figure 17, major shift is observed around 0.5 ppm, which corresponds to water. For 100°C - 150°C and 150°C-250°C range, no other major peak is observed. As temperature increases, this peak is observed to move upfield. This shielding effect is occurring because of the presence of a more electronegative atom. Considering this NMR belongs to asphaltite, shielding effect probably occurs due to presence of sulfur atoms. Samples of 250°C - 350°C range and 350°C - 450°C range shows significant and broad peaks below and above major (water) peak. Broad peaks around below water peak belongs to $-CH_3$ groups and broad peaks just above water range belongs to $-CH_2$ group. -2 ppm peak in both 250°C - 350°C range and 350°C - 450°C, shows -CH group and peak around 0.7 ppm shows aromatics.

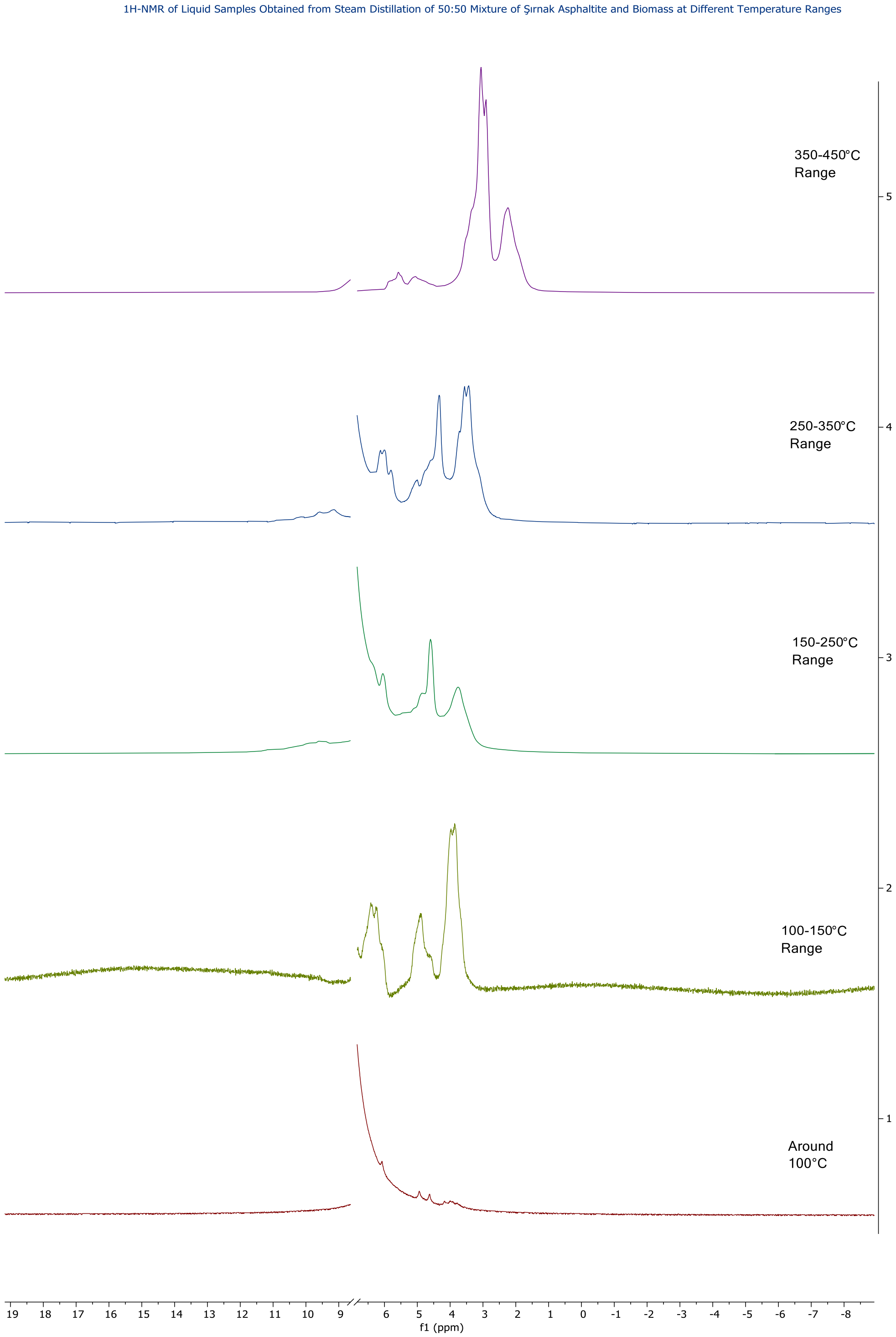

Figure 18: Stacked ^{1}H-NMR of Liquid Samples Obtained from Steam Distillation of 50:50 Mixture of Şırnak asphaltite and Biomass at Different Temperature Ranges

Although, ^{1}H-NMR spectra of samples have shown chemical shifts, neither peaks nor peak intensities follow a pattern. Probable reasons are heterogeneous nature of products and heavy product's inability to escape reactor system. However, in line with the TGA peak analysis results, different shifts in mixed sample's NMR after 250°C are observed, which can be attributed to synergetic effect.

4.2. Pyrolysis, Hydrogenation and Oxidation of Şırnak Asphaltite

4.2.1. Elemental Analysis

With 5 grams of Şırnak asphaltite sample, oxidesulfurization, hydrodesulfurization and pyrolysis experiments are carried out. Using elemental analysis, raw asphaltite residue C, H, N and S mass percent is obtained and can be found in Table 17.

Table 17: Raw Asphaltite and Process Residue Elemental Analysis

	Asphaltite (Raw Material Sample)		Reactor Residue after Oxi-desulfurization		Reactor Residue after Hydrogenation		Reactor Residue after Pyrolysis	
	Mass (gr)	Mass percent (%)	Mass (gr)	Mass percent (%)	Mass (gr)	Mass percent (%)	Mass (gr)	Mass percent (%)
C	2.679	53.6	1.222	42.2	1.249	40.4	1.064	38.7
H	0.259	5.2	0.035	1.20	0.024	0.80	0.037	1.30
N	0.040	0.8	0.028	1.00	0.023	0.70	0.027	1.00
S	0.391	7.8	0.233	8.00	0.248	8.00	0.199	7.20

4.2.2. NMR Analysis

NMR analysis was conducted on the samples collected on the glass wools placed at the end of the 5 mm Pyrex tubular reactor where pyrolysis and hydrogenation reactions were carried out. The liquid products were impregnated on the glass wool in the cold zone after the furnace. The glass wool was carefully removed and the organic molecules were extracted by dissolving them in deuterated DMSO solvent for subsequent NMR analysis.

In hydrogenation experiments, glass wool distances are determined starting from exit of the pyrex reactor. 14.5 cm of glass wool is obtained from hydrogenation experiments where glass wool at the coal interface is classified as glass wool 14.5 cm. However, in pyrolysis experiments, glass wool distances are determined starting from the coal/glass wool interface.

Glass wool classification and sample information can be found in Table 18.

Table 18: Glass Wool NMR Analysis Sample Information

Lab Sample #	NMR Sample #	Explanation	NMR Type
-	1	TCE+DMSO	Proton
-	2	TCE	Proton
I-1	3	Pyrolysis 10-11 cm	Proton
I-2	4	Pyrolysis 8-10 cm	Proton
I-3	5	Pyrolysis 7-8 cm	Proton
I-4	6	Pyrolysis 6.5-7 cm	Proton
I-5	7	Pyrolysis 4.5-6.5 cm	Proton
I-6	8	Pyrolysis Coal Char	Proton
II-1	21	Hydrogenation 0-5 cm	Proton
II-2	22	Hydrogenation 5-6.5 cm	Proton
II-3	23	Hydrogenation 6.5-9.5 cm	Proton
II-4	24	Hydrogenation 9.5-12 cm	Proton
II-5	25	Hydrogenation 12-14.5 cm	Proton
II-6	26	Hydrogenation Coal Char	Proton
-	-	Şırnak asphaltite	Carbon/Proton
-	-	Şırnak asphaltite tar	Carbon/Proton

^{1}H-NMR spectra of pyrolysis samples given in Table 18 can be found in Figure 19 and hydrogenation samples can be found in Figure 20.

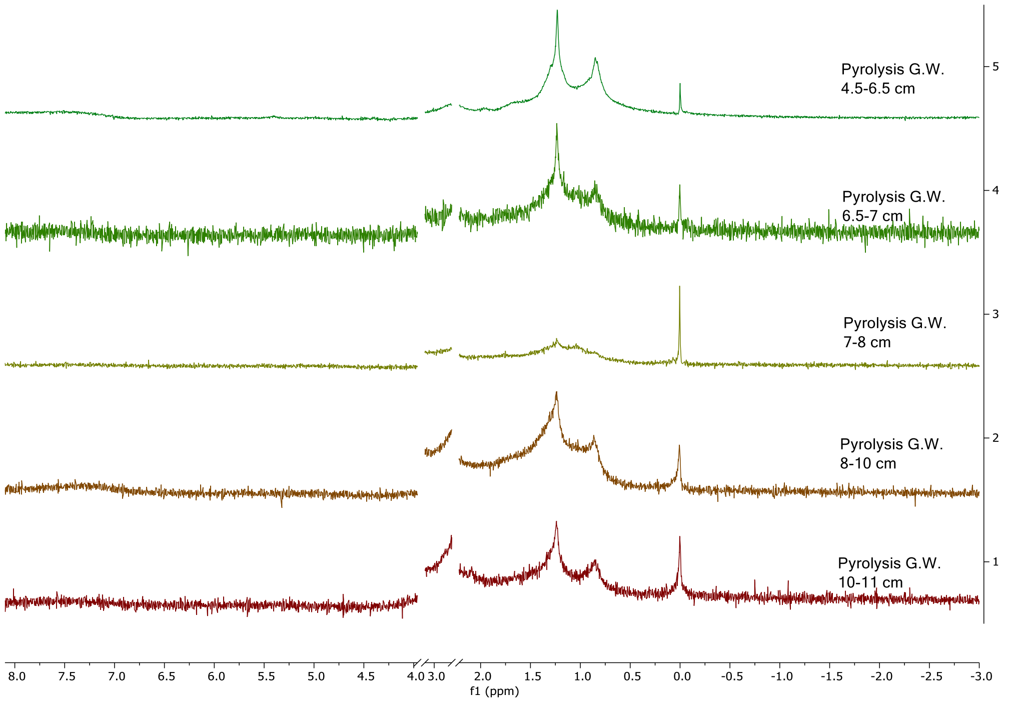

Figure 19: ^{1}H-NMR of Glass Wools Obtained from Şırnak Asphaltite Pyrolysis

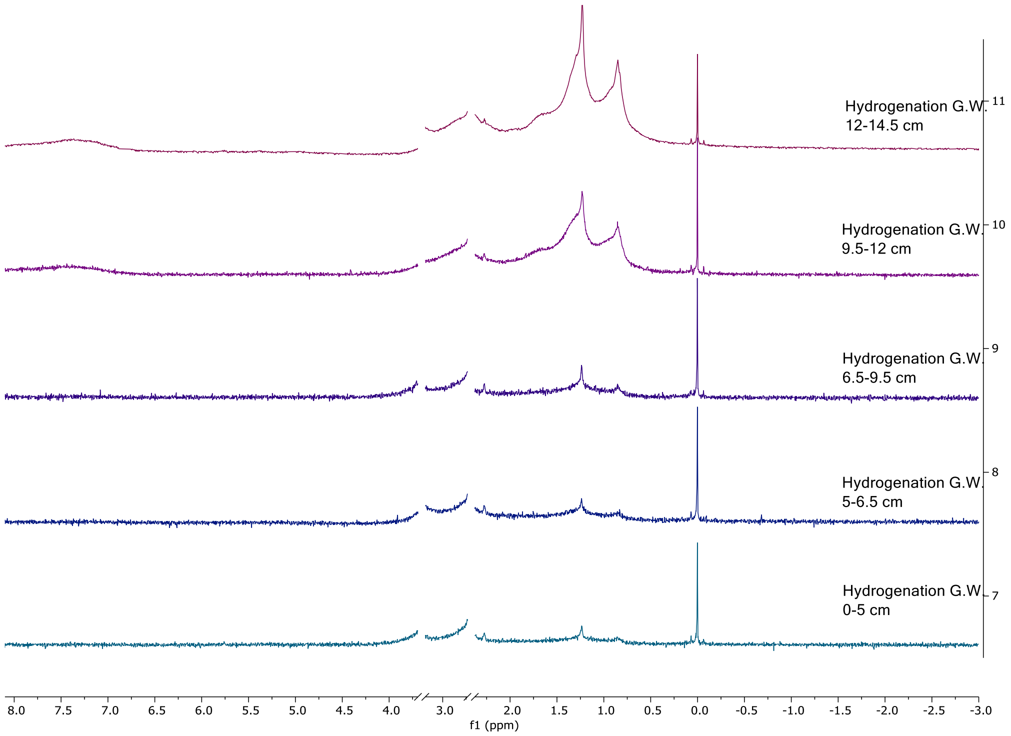

Figure 20: ^{1}H-NMR of Glass Wools Obtained from Şırnak Asphaltite Hydrogenation

4.2.3. Eschka Analysis

Eschka analysis of Şırnak asphaltite can be found in Table 19.

Table 19: Şırnak Asphaltite Eschka Analysis

Type of Sulfur Compound	Mass Percent (%)
Total Sulfur Compounds	8.05
Sulfatic Compounds	0.15
Pyrite	1.59
Organic Sulfur Compounds	6.31

Eschka analysis shows the necessity of chemical processing of Şırnak asphaltite, since physical methods cannot remove organic forms of sulfur compounds, which corresponds to 78% of the total sulfur compounds.

4.2.4. Proximate Analysis

Proximate analysis of Şırnak asphaltite results are presented in Figure 21.

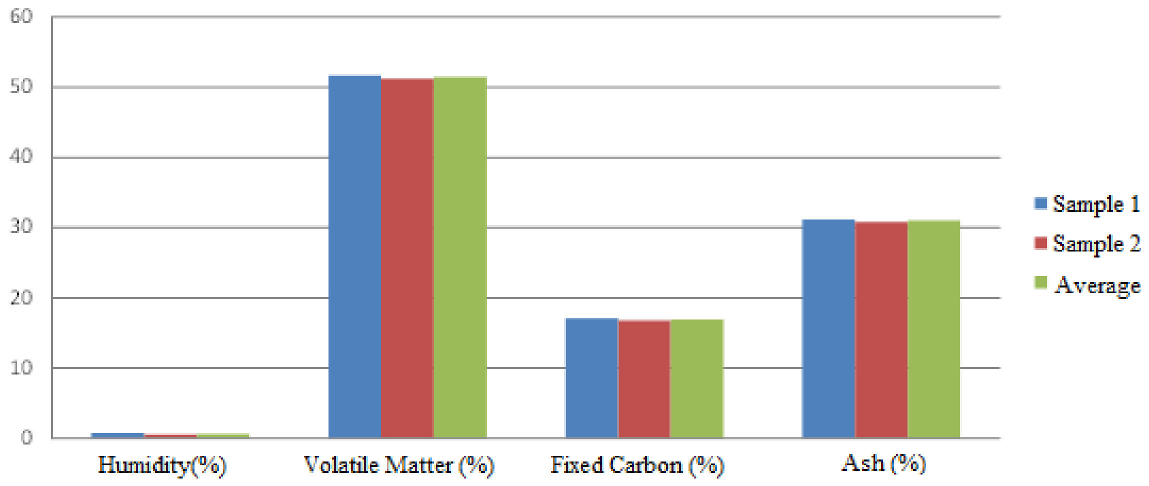

Figure 21: Şırnak Asphaltite Proximate Analysis

Average of analyzed samples shows that humidity is 0.6%, volatile matter is 51.5%, fixed carbon is 16.9% and ash is 31% of the Şırnak asphaltite.

4.2.5. Mass Spectroscopy Data

In pyrolysis of Şırnak asphaltite experiments, amu-2 is followed for H_2 evolution with respect to time. H_2 evolution graph of asphaltite pyrolysis experiment can be seen in Figure 22.

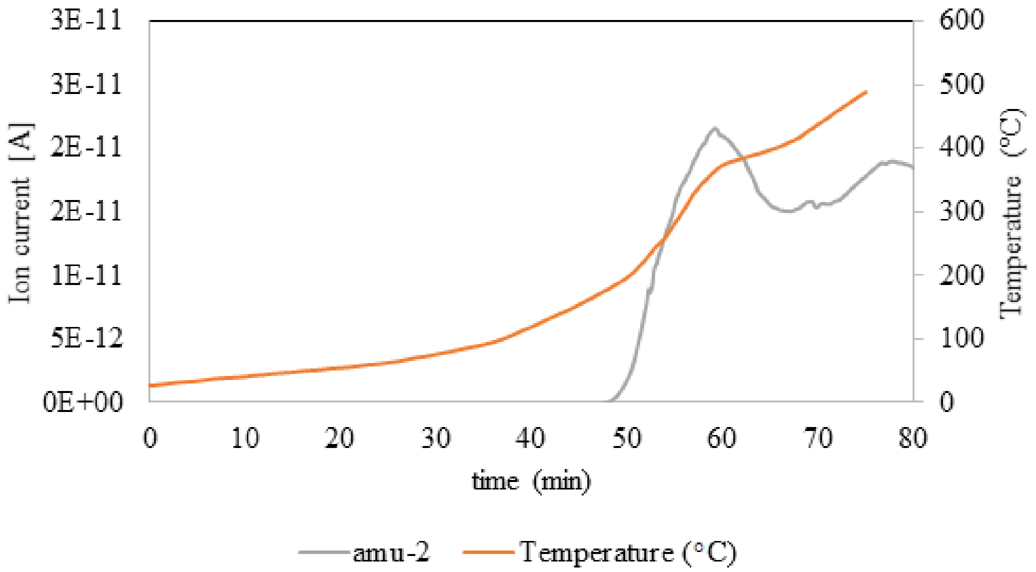

Figure 22: Hydrogen Evolution during Pyrolysis of Şırnak Asphaltite with respect to Time

It is observed that hydrogen evolution in pyrolysis experiment starts at 180°C and peak is reached at 340°C.

Methane formation during pyrolysis is followed from amu-15 and amu-16 signals. Methane formation can be seen in Figure 23.

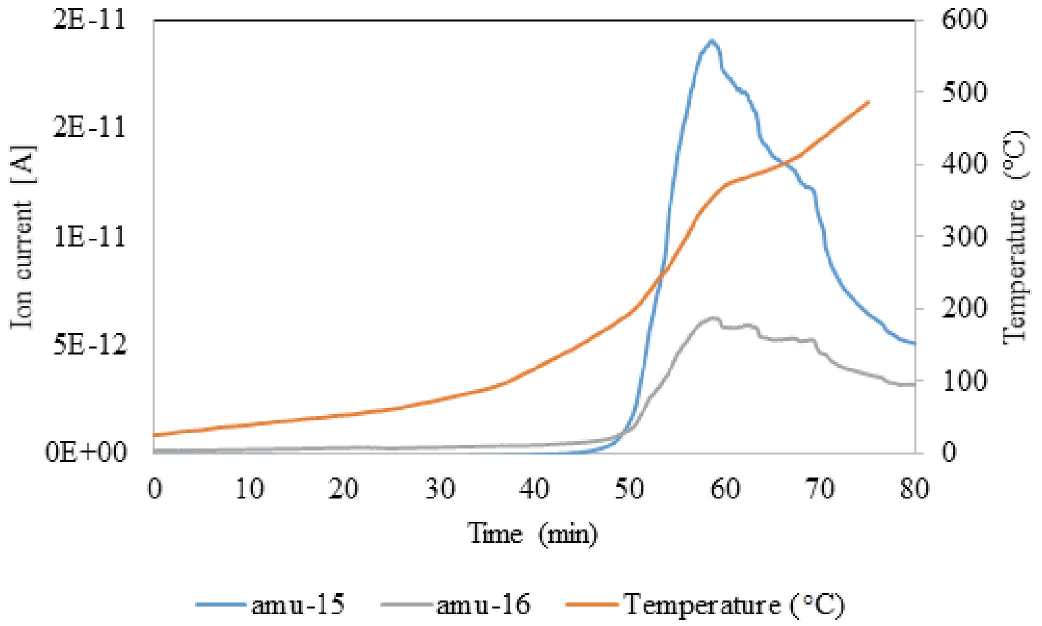

Figure 23: Methane Evolution Graph during Pyrolysis of Şırnak Asphaltite with respect to Time

Methane formation started around 180°C and reached its peak around 370°C.

Carbon monoxide formation during pyrolysis is followed from amu-27 and amu-28 signals. CO formation graph can be seen in Figure 24.

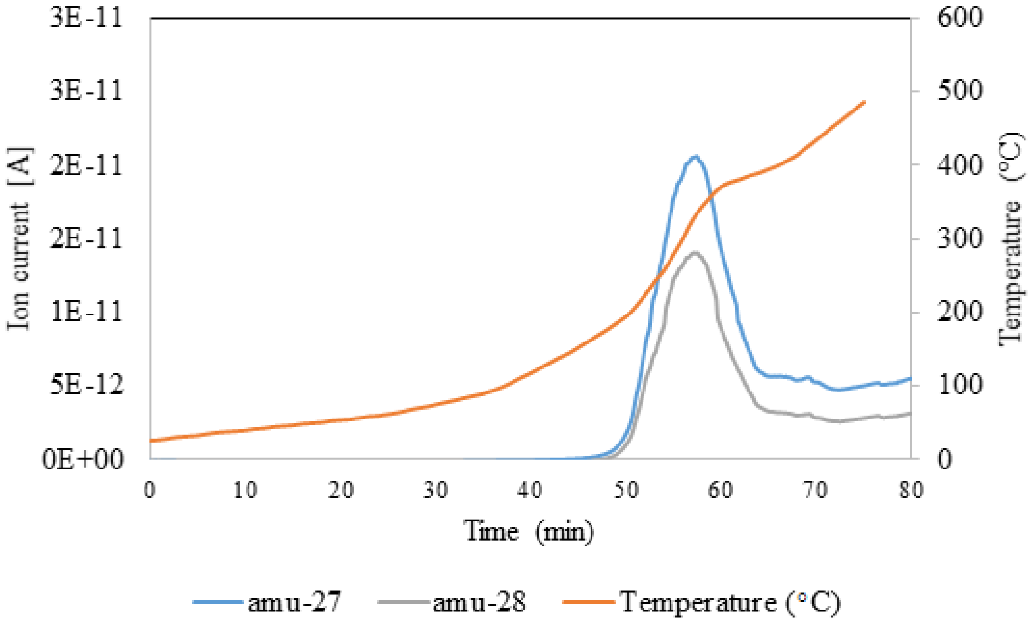

Figure 24: CO Formation Graph during Pyrolysis of Şırnak Asphaltite with respect to Time

It is observed that CO formation has reached its peak around 340°C and an almost steady signal is obtained after 400°C. CO formation shows formation of oxygen compounds which further reacts to form CO (partial combustion). Considering the hydrogen evolution shows similar trend to CO formation, water decomposition after 250°C is the source of the oxygen.

4.2.6. Asphaltite Samples NMR Analysis

^{13}C superimposed NMR spectra of raw asphaltite, hydrogenated asphaltite liquid product and hydrogenated asphaltite residue can be found in Figure 25.

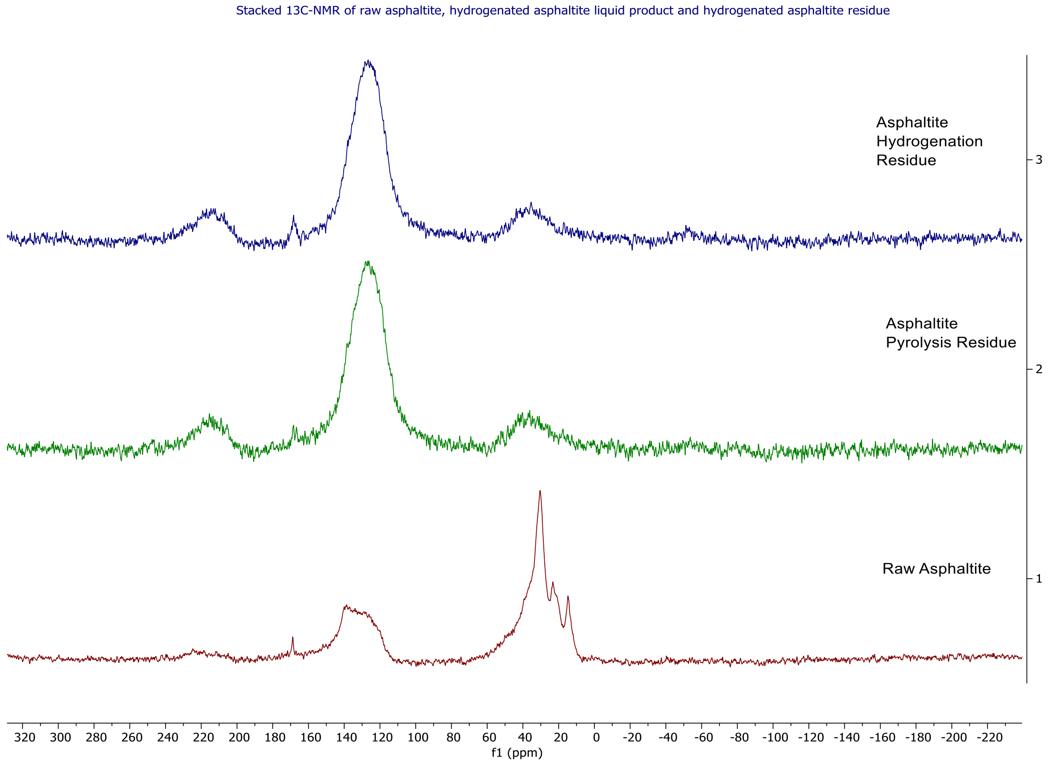

Figure 25: Stacked ^{13}C-NMR of Raw Asphaltite, Hydrogenated Asphaltite Liquid Product and Hydrogenated Asphaltite Residue

Figure 25 indicates that, major carbon compounds obtained as liquid product are alkanes (peak around 35 ppm) and aromatics (peak around 130 ppm).

4.2.7. Detailed Hydrocarbon Analysis

Detailed hydrocarbon analysis for different particle size of liquid product of pyrolysis and hydrogenation of Şırnak asphaltite samples is performed. Detailed hydrocarbon analysis is performed to obtain percent distribution of n-paraffins, i-paraffins, olefins, naphtenes and aromatics of C_6 to C_{26}.

n-Paraffin distribution can be found in Figure 26.

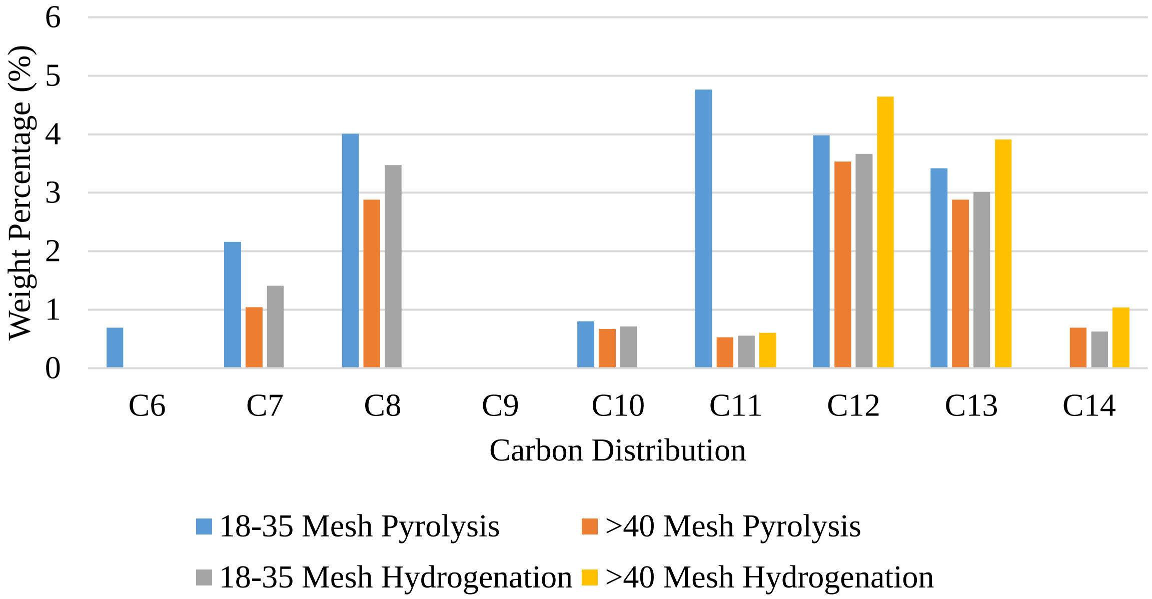

Figure 26: n-Paraffin Distribution of Liquid Obtained from 18-35 Mesh and >40 Mesh Şırnak asphaltite Particles' Pyrolysis and Hydrogenation

i-Paraffin distribution can be found in Figure 27.

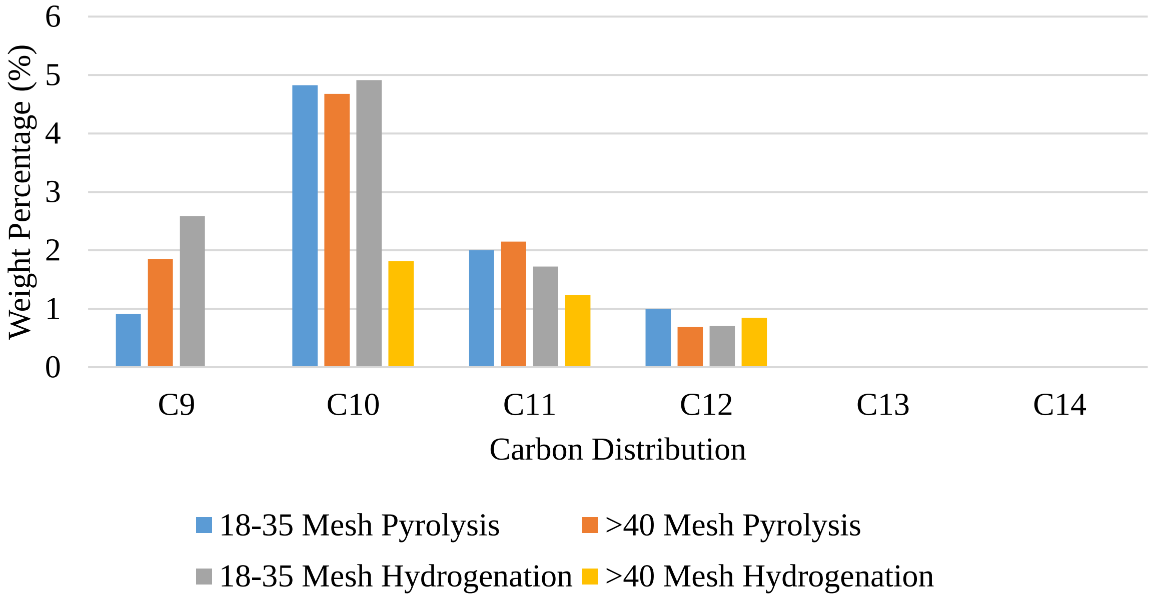

Figure 27: i-Paraffin Distribution of Liquid Obtained from 18-35 Mesh and >40 Mesh Şırnak Asphaltite Particles' Pyrolysis and Hydrogenation

Olefin distribution can be found in Figure 28.

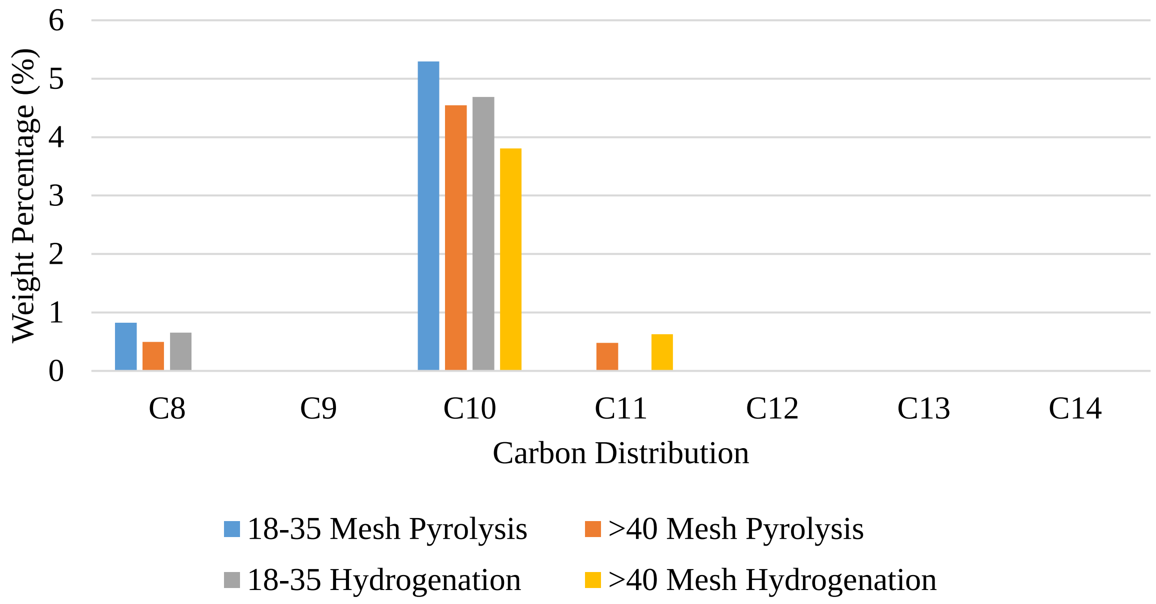

Figure 28: Olefin Distribution of Liquid Obtained from 18-35 Mesh and >40 Mesh Şırnak Asphaltite Particles’ Pyrolysis and Hydrogenation

Naphthene distribution can be found in Figure 29.

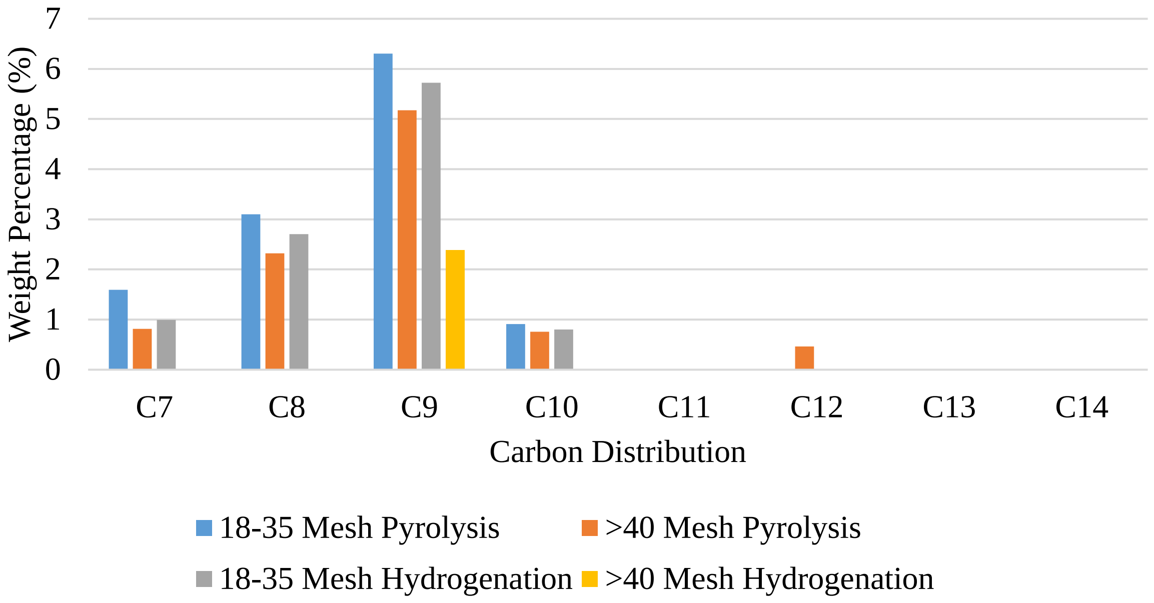

Figure 29: Naphtene Distribution of Liquid Obtained from 18-35 Mesh and >40 Mesh Şırnak Asphaltite Particles' Pyrolysis and Hydrogenation

Aromatic distribution can be found in Figure 30.

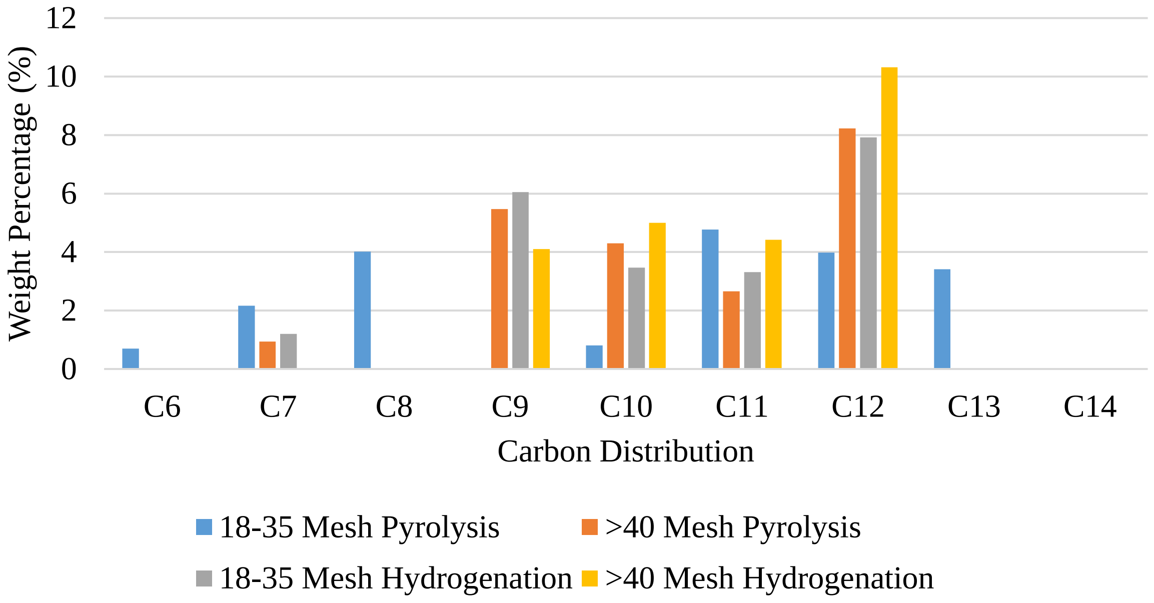

Figure 30: Aromatics Distribution of Liquid Obtained from 18-35 Mesh and >40 Mesh Şırnak Asphaltite Particles' Pyrolysis and Hydrogenation

Due to experimental limitations, varying amounts of hydrocarbons could not be identified. Unknown percentages can be found in Figure 31.

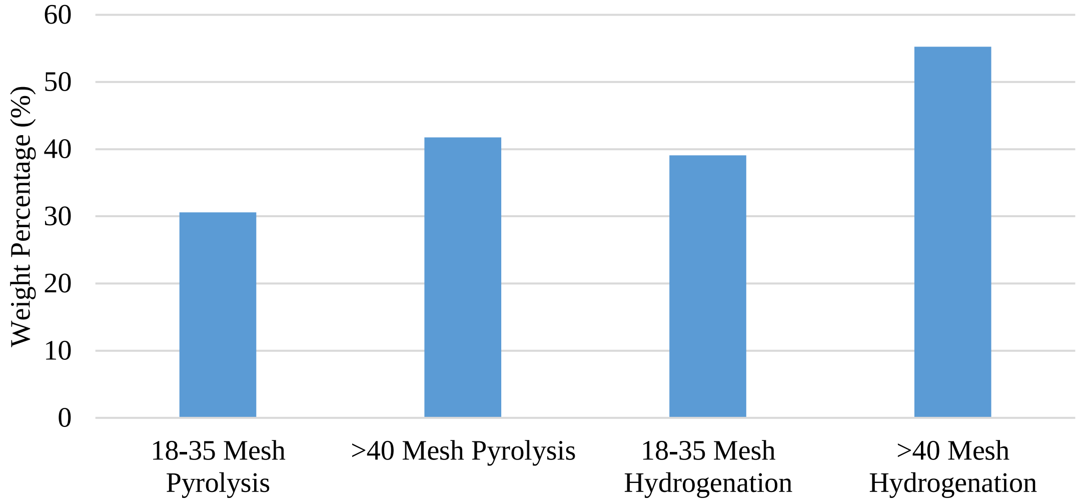

Figure 31: Unknown Percentages of Liquid Obtained from 18-35 Mesh and >40 Mesh Şırnak Asphaltite Particles' Pyrolysis and Hydrogenation

Finally, liquid products' Octane Number is also calculated. Results can be found in Figure 32.

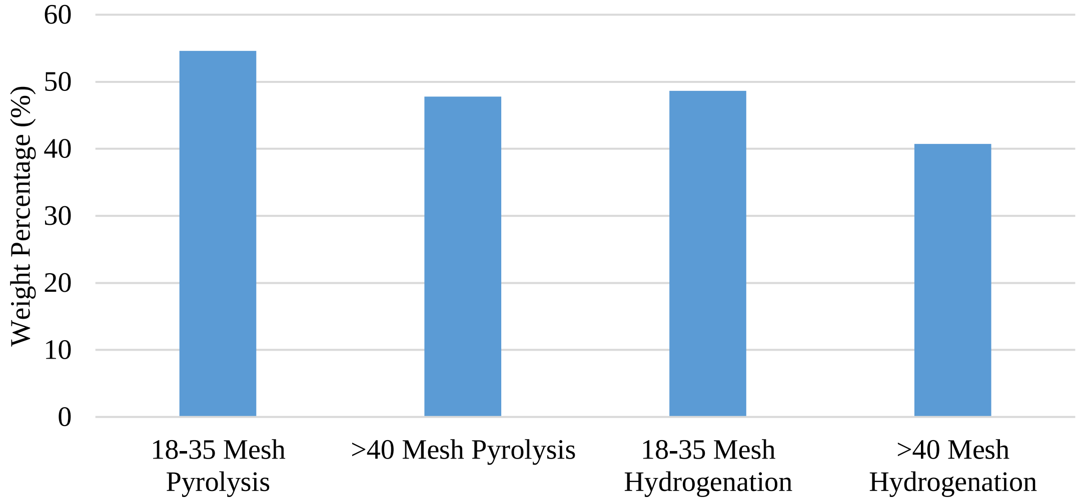

Figure 32: Calculated Octane Numbers of Liquid Obtained from 18-35 Mesh and >40 Mesh Şırnak Asphaltite Particles' Pyrolysis and Hydrogenation

It is observed that Octane numbers of liquid products are almost proportional with known percentage of the liquid sample analyzed. This has occurred since octane number is calculated from the individual component contributions. Sulfur content is analyzed to be greater than 1000 ppm for all samples, where 1000 ppm is the maximum concentration that can be analyzed in DHA.

Judging by detailed hydrocarbon analysis, it is possible to obtain valuable liquid products from Şırnak asphaltite by hydrogenation in atmospheric conditions and mild temperatures. Detailed hydrocarbon analysis has also shown that there is around 20% by weight aromatics in the products.

4.2.8. Thermogravimetric Analysis

To investigate the effects of pyrolysis and hydrogenation on the Şırnak asphaltite residue, TGA of unprocessed, pyrolyzed and hydrogenated samples under nitrogen and air atmosphere is performed.

Comparative TGA results of unprocessed, pyrolyzed and hydrogenated asphaltite samples under air atmosphere can be found in Figure 33 and comparative DrTGA results of unprocessed, pyrolyzed and hydrogenated asphaltite samples under air atmosphere can be found in Figure 35.

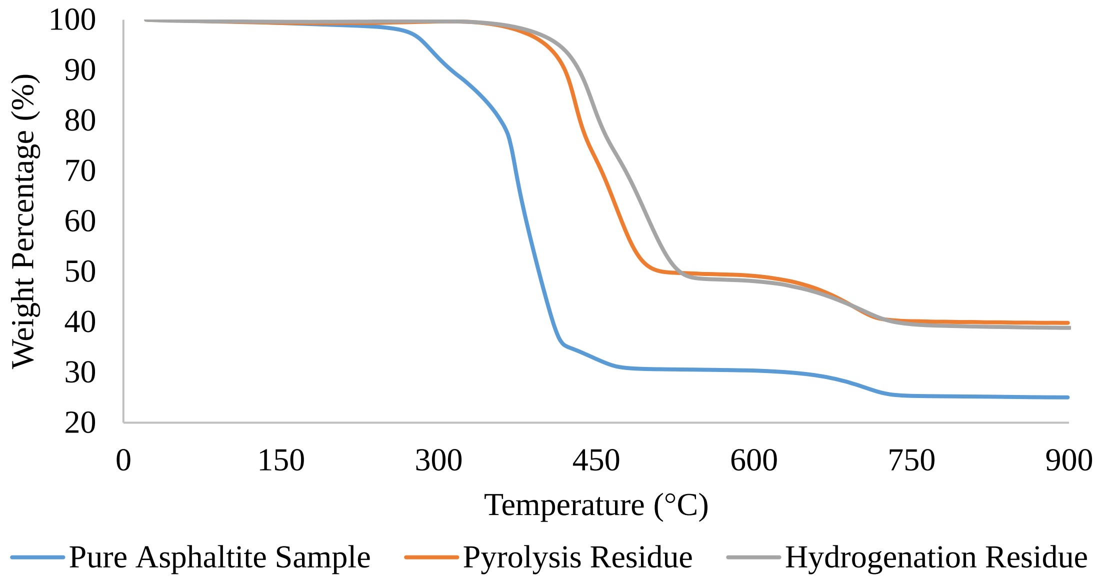

Figure 33: Comparative TGA Results of Unprocessed, Pyrolyzed and Hydrogenated Asphaltite Samples Under Air Atmosphere up to 900°C

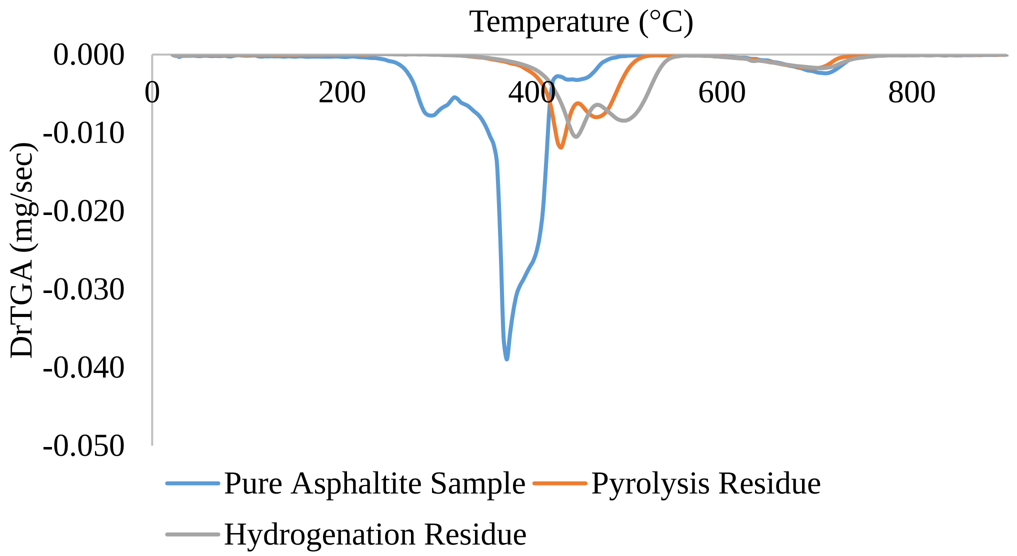

Figure 34: Comparative Derivative TGA Results of Unprocessed, Pyrolyzed and Hydrogenated Asphaltite Samples Under Air Atmosphere up to 900°C

Comparative TGA results of unprocessed, pyrolyzed and hydrogenated asphaltite samples under nitrogen atmosphere can be found in Figure 35 and comparative

DrTGA results of unprocessed, pyrolyzed and hydrogenated asphaltite samples under nitrogen atmosphere can be found in Figure 36.

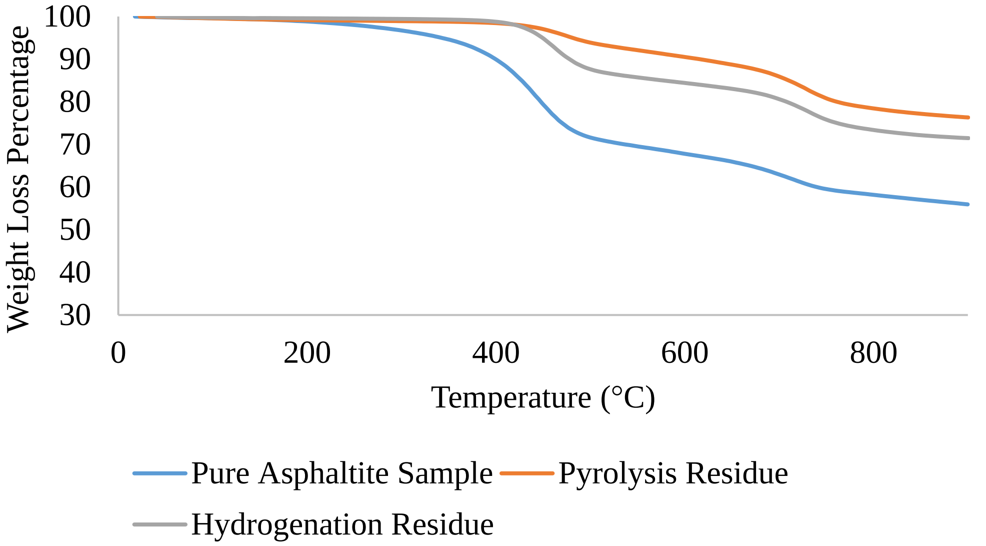

Figure 35: Comparative TGA Results of Unprocessed, Pyrolyzed and Hydrogenated Asphaltite Samples Under Nitrogen Atmosphere up to 900°C

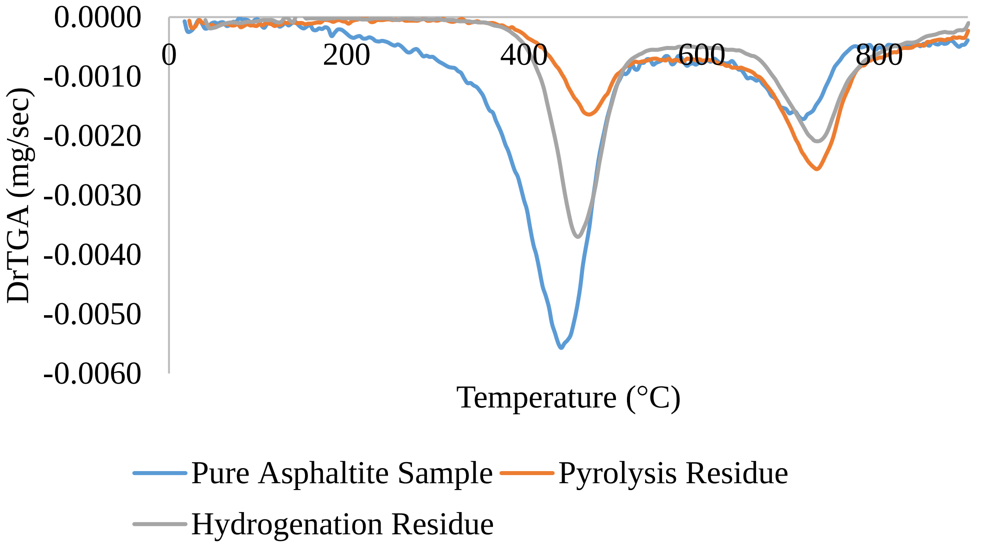

Figure 36: Comparative Derivative TGA Results of Unprocessed, Pyrolyzed and Hydrogenated Asphaltite Samples Under Nitrogen Atmosphere up to 900°C

TGA results demonstrate that, around 50°C temperature difference has occurred inside the reactor during the pyrolysis and hydrogenation experiments. It can also be seen that, up to processing temperature, hydrogenation does not provide any significant effect on total weight loss of the asphaltite.

4.3. Analysis of Asphaltite and Biomass Experiments

All data of Thermal Characterization of Şırnak asphaltite and biomass and Pyrolysis, Hydrogenation and Oxidation of Şırnak asphaltite experiments are analyzed.

Chemical shielding effect is observed for biomass and asphaltite after 150°C. Nitrogen is the main component of shielding for biomass and sulfur is the main component of shielding for asphaltite. Although nitrogen is more electronegative than sulfur, shielding is stronger for asphaltite samples than biomass samples which shows that asphaltite pyrolysis liquid products have more sulfur compounds than nitrogen in biomass pyrolysis liquid products.

Coupling TGA data (Figure 14) and ^{1}H-NMR of Liquid Sample Obtained from Steam Distillation of biomass (Figure 16), weight loss of biomass below 150°C belongs mainly to water. Hemicellulose is expected to maximize decomposition around 310°C and cellulose decomposition is expected to be maximum around 365°C. Considering temperature gradients inside the reactor, hemicellulose and cellulose decompositions are happening mostly together. However, differences in relative peak intensities are observed between samples of 150°C - 250°C range and 250°C - 350°C range which shows difference in decomposition rate of hemicellulose and cellulose. It is also expected using TGA data.

Coupling TGA data (Figure 10) and ^{1}H-NMR of Liquid Sample Obtained from Steam Distillation of Şırnak asphaltite (Figure 17), no major peaks besides water below 250°C is observed in NMR analysis, as expected using TGA data. TGA shows increase in decomposition rate after 250°C. $-CH_3$, $-CH_2$, -CH and aromatics are forming after 250°C. While intensities of all peaks increase by increasing temperature relative intensities of peaks do not change significantly, as it also is observed in glass wool experiments (Figure 19). As TGA data also suggests, only rate of decomposition changes after 250°C, not the type of compound. Mass spectroscopy shows hydrogen, methane and CO formation in gaseous form. These formations also show their peak after 350°C.

Coupling TGA data analysis with ^{1}H-NMR spectra, behavioral change of mixed sample, addition to TGA data (Figure 14) and ^{1}H-NMR of Liquid Sample combination also shows change of decomposition rates. This change indicates synergetic effect in increasing the value of products by co-processing biomass and asphaltite.

Stacked ^{1}H-NMR spectra Şırnak asphaltite pyrolysis glass wool and steam distillation of Şırnak asphaltite at 350-450°C temperature range can be found in Figure 37.

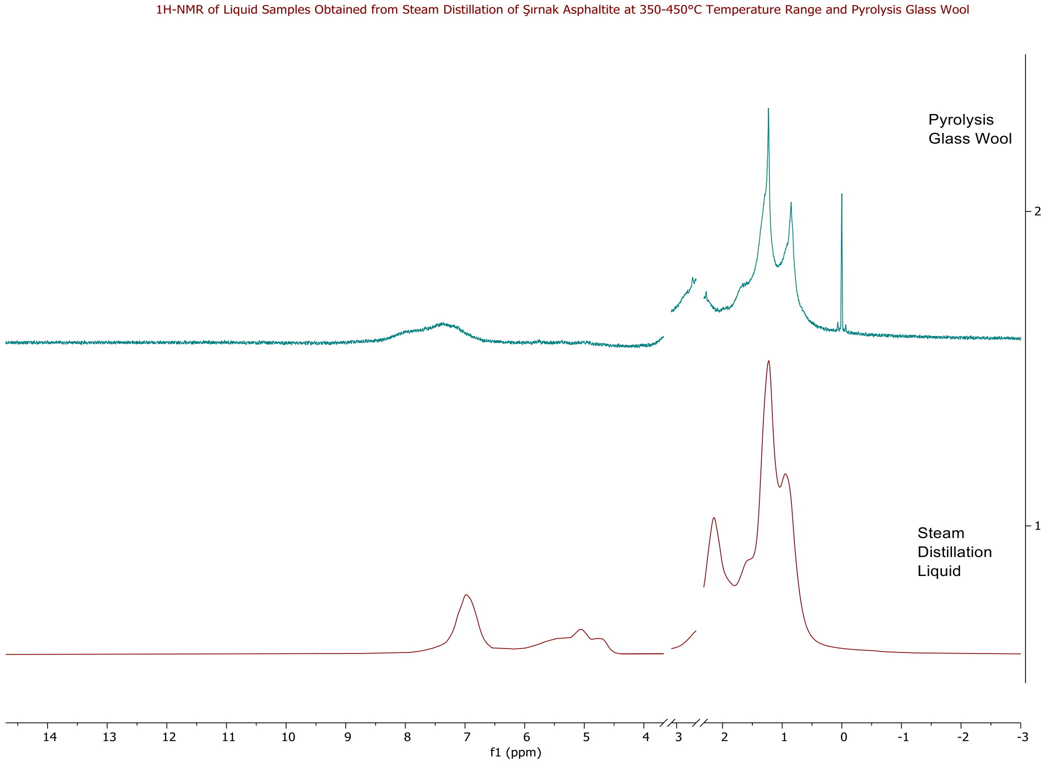

Figure 37: Stacked ^{1}H-NMR spectra Pyrolysis Glass Wool and Steam Distillation of Şırnak Asphaltite at 350-450°C Temperature Range

In Figure 37, it can be seen that pyrolysis glass wool NMR spectra has resulted in wider range of peak shifts. Pyrolysis glass wool has higher aromatics peaks between 2-4 ppm. This is a result of experimental setups, since no loss in delivery tubes or in reactor.

Emphasis is put on aromatics, since they are the major component of tar compounds. Detailed hydrocarbon analysis has shown that 20% of the products are aromatics and NMR data show that those aromatics form after 250°C. After that temperature, tar reforming reaction is needed.

4.4. Characterization of Dry Reforming Catalysts

Characterization of dry reforming catalysts are performed by XRD and TPR experiments.

4.4.1. Ni/$LaCoO_3$

Ni/$LaCoO_3$ characterization is performed by Asst. Prof. Dr. Başar Çağlar. XRD patterns of Ni/$LaCoO_3$ can be seen in Figure 38.

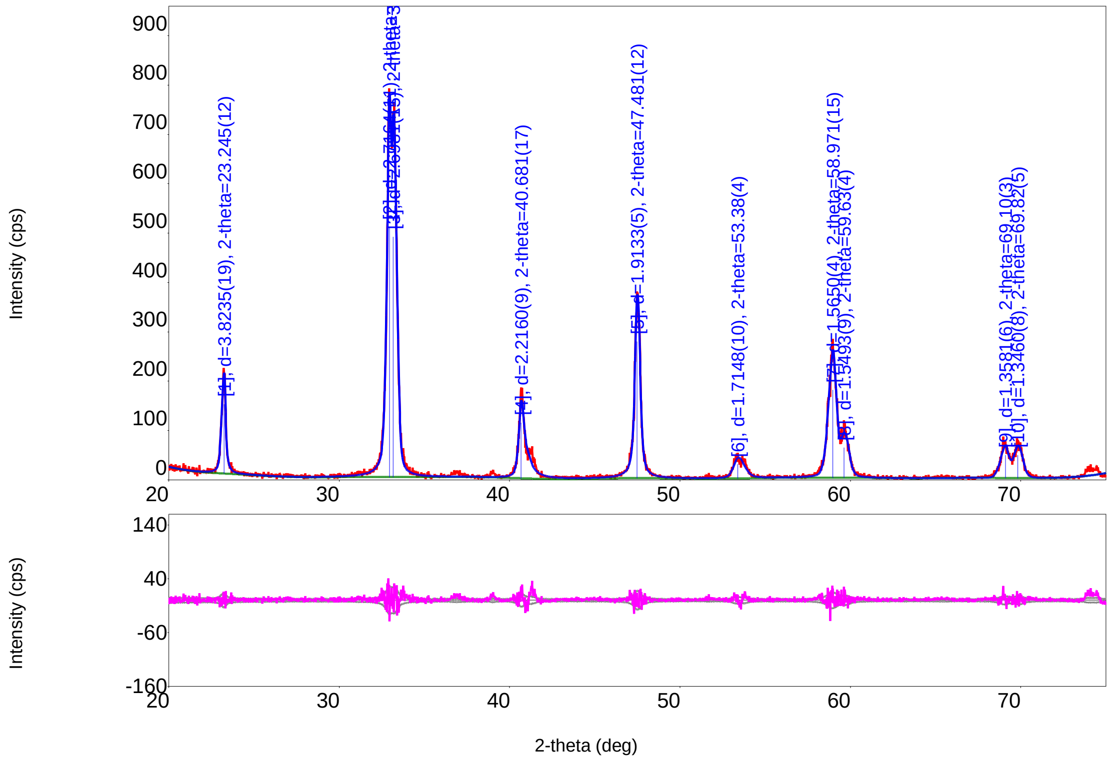

Figure 38: XRD Pattern of Ni/LaCoO3

For characterization comparison of synthesized Ni/$LaCoO_3$, TCD of Ni/$LaCoO_3$ is performed under N_2 atmosphere, TCD results can be seen in Figure 39.

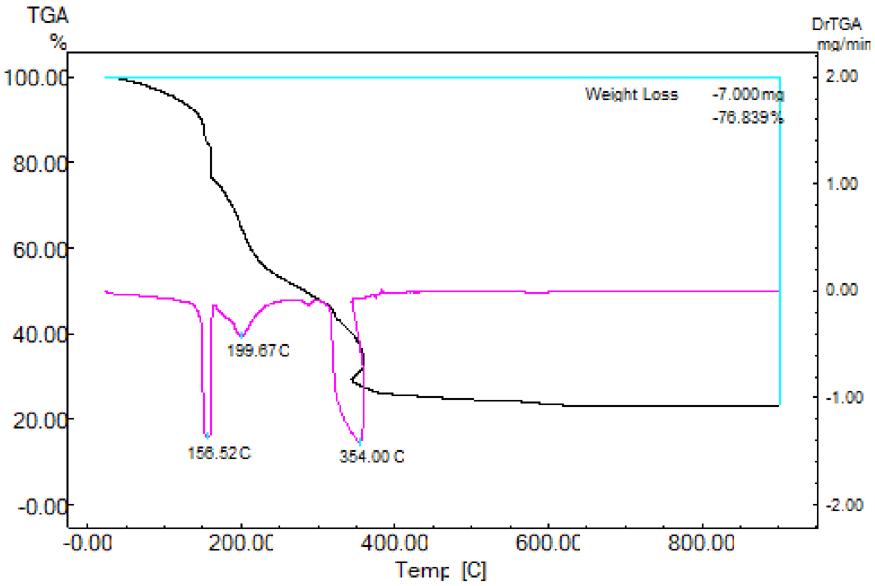

Figure 39: TCD Results of Ni/$LaCoO_3$ Under N_2 Atmosphere

4.4.2. Ni/Al_2O_3

Only TPR is used for characterization of Ni/Al_2O_3. TPR Results can be found in Figure 40.

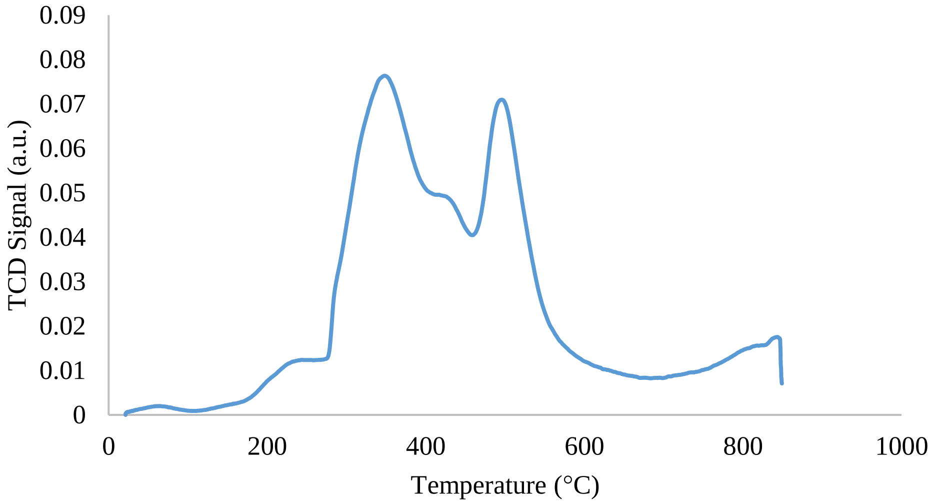

Figure 40: TPR Results of Ni/Al_2O_3

4.5. Dry Reforming Experiments

Using Detailed Hydrocarbon Analysis, it was understood that around 20% of the liquid product is aromatic compounds. Overall process efficiency can be increased using dry reforming experiments by producing hydrogen, methane and carbon monoxide. For that purpose, $Ni/LaCoO_3$ catalyst is selected as novel catalyst and tested against standard Ni/Al_2O_3 on model benzene. Benzene is selected as model aromatic molecule and dry reforming experiments are performed on different temperature ranges and in different benzene to CO_2 ratios. Product gases are analyzed using a gas chromatograph.

Dry reforming of Benzene experiments is planned on 2 different catalysts, $Ni/LaCoO_3$ and Ni/Al_2O_3. Planned experiments can be found in Table 20.

Table 20: Planned Dry Reforming Experiments

Catalyst	Temp. (°C)	CO_2/C_6H_6 ratio	Gas hourly space velocity ($hour^{-1}$)	Weight hourly space velocity of benzene ($hour^{-1}$)	Benzene concentration	Residence time (s)
$Ni/LaCoO_3$	600	6	28000	3.5	100	0.13
$Ni/LaCoO_3$	700	6	28000	3.5	100	0.13
$Ni/LaCoO_3$	800	6	28000	3.5	100	0.13
Ni(15)-Al_2O_3	600	6	28000	3.5	100	0.13
Ni(15)-Al_2O_3	700	6	28000	3.5	100	0.13
Ni(15)-Al_2O_3	800	6	28000	3.5	100	0.13
$Ni/LaCoO_3$	800	12	28000	3.5	100	0.13
$Ni/LaCoO_3$	800	3	28000	3.5	100	0.13
$Ni/LaCoO_3$	800	6	14000	3.5	100	0.26

4.5.1. Conversion Rate

From planned experiments, Ni(15)-Al_2O_3 at 600 °C and 700 °C and Ni/$LaCoO_3$ at 800°C while CO_2/C_6H_6 ratio is 3, gas flow stopped due to increased pressure drop in the reactor. This problem is assumed to be occurring due to carbon deposition on the catalyst. It is understood that Ni/$LaCoO_3$ either has higher resistance than Ni(15)-Al_2O_3 or carbon deposition reactions are slower on Ni/$LaCoO_3$. Hence, those experiments' conversion rate is not reported.

Catalyst performance is evaluated in 3 metric, CO_2 conversion, (Produced Hydrogen (moles))/(Fed Benzene (moles)) and (Produced Carbon Monoxide (moles))/(Fed Carbon Dioxide (moles)).

4.5.1.1. Ni/$LaCoO_3$ Experiments

Ni/$LaCoO_3$ performance is tested at 600 °C with CO_2/C_6H_6=6. Performance graph can be found in Figure 41.

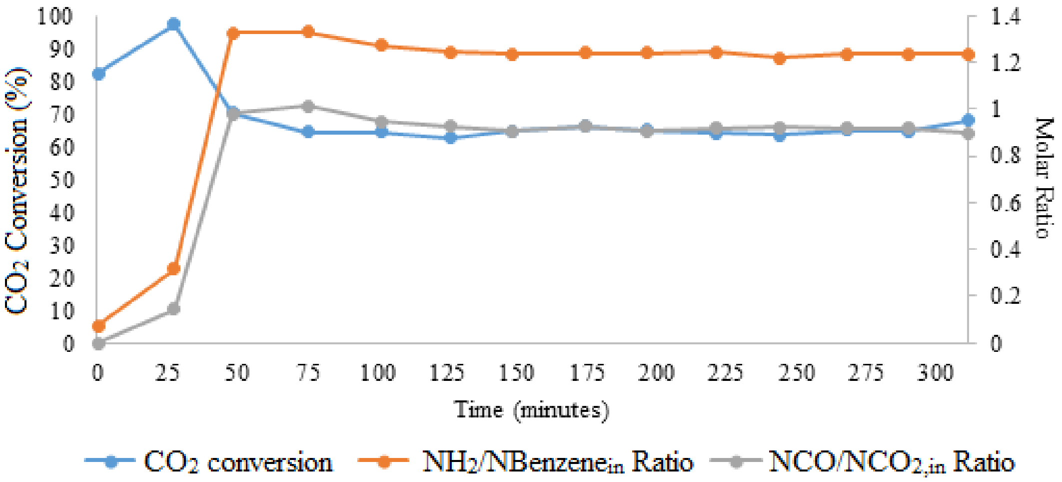

Figure 41: Results of Dry Reforming Experiments using Ni/$LaCoO_3$ as Catalyst at 600°C with CO_2/C_6H_6 ratio of 6

Ni/$LaCoO_3$ performance is tested at 700 °C with CO_2/C_6H_6=6. Performance graph can be found in Figure 42.

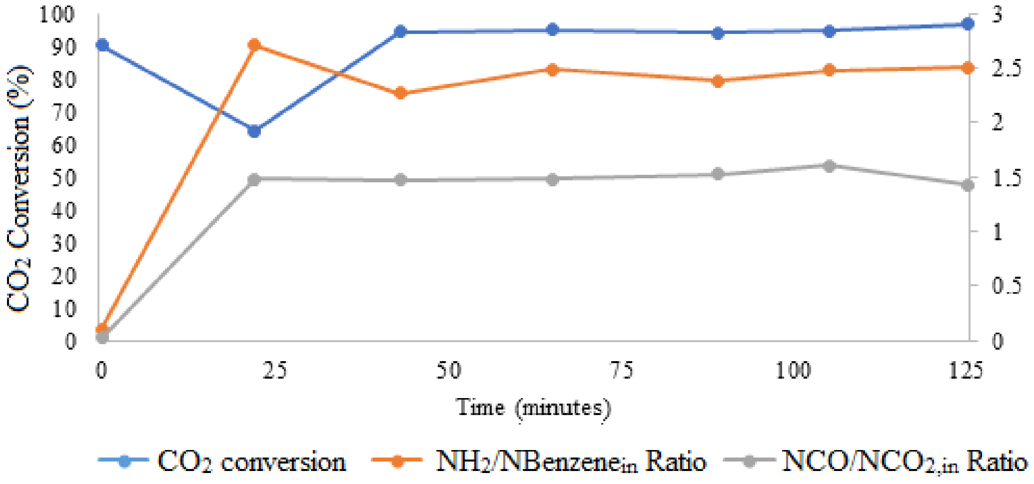

Figure 42: Results of Dry Reforming Experiments using Ni/$LaCoO_3$ as Catalyst at 700 °C CO_2/C_6H_6 ratio of 6

Ni/$LaCoO_3$ performance is tested at 800 °C with CO_2/C_6H_6=6. Performance graph can be found in Figure 43.

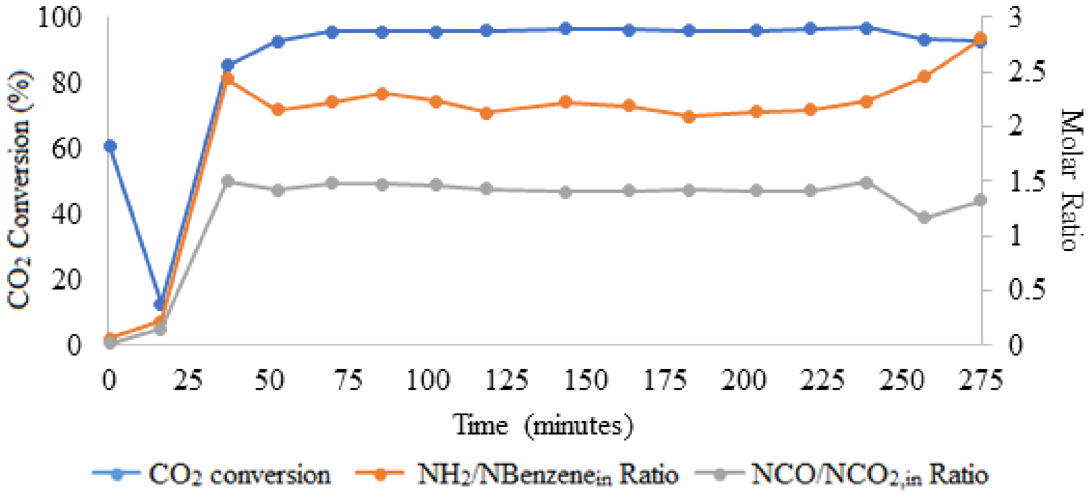

Figure 43: Results of Dry Reforming Experiments using Ni/$LaCoO_3$ as Catalyst at 800 °C CO_2/C_6H_6 ratio of 6

Ni/$LaCoO_3$ performance is tested at 800 °C with CO_2/C_6H_6=12. Performance graph can be found in Figure 44.

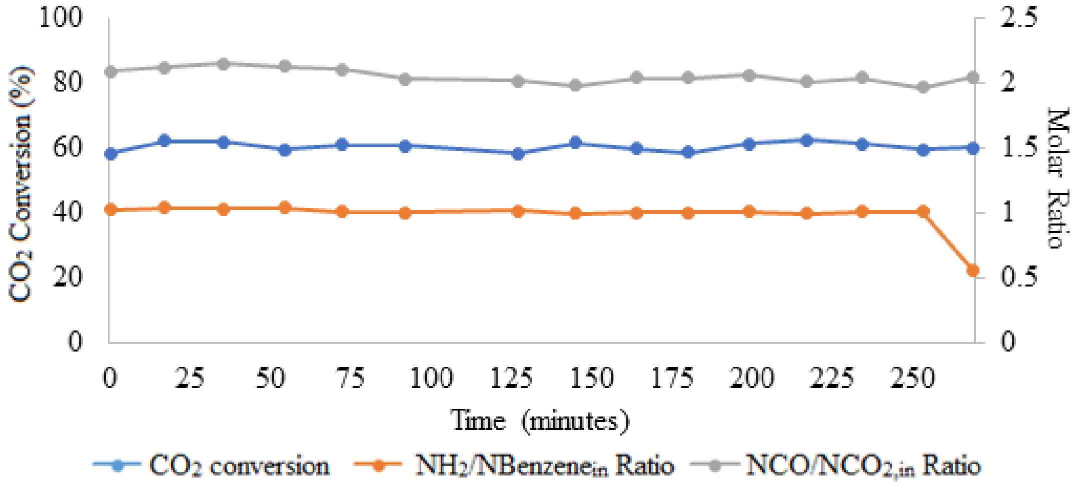

Figure 44: Results of Dry Reforming Experiments using Ni/$LaCoO_3$ as Catalyst at 800 °C with CO_2/C_6H_6 ratio of 12

As expected, increase in reaction temperature increases almost every performance metric. For $CO_2/C_6H_6=6$, at every temperature, the first data seems to be outlier. This can be a result of adsorption reactions. After the surface saturates, reaction seems to follow steady state.

4.5.1.2. Ni/Al_2O_3 Experiments

Ni/Al_2O_3 catalyst is tested at 600 °C, 700 °C and 800 °C. $NiAl_2O_3$ catalyst only performed at 800 °C. Results can be seen in Figure 45.

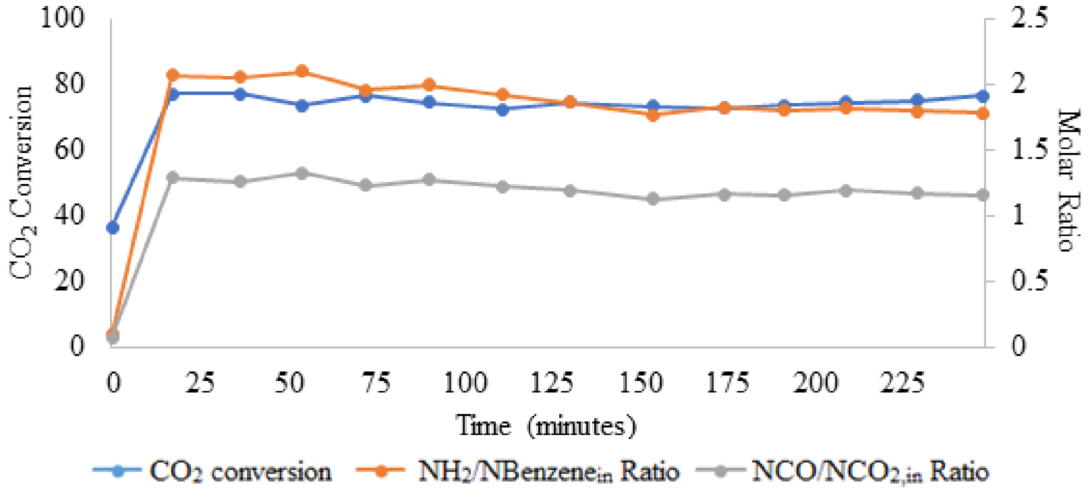

Figure 45: Results of Dry Reforming Experiments using Ni/Al_2O_3 as Catalyst at 800 °C with CO_2/C_6H_6 ratio of 6

Dry reforming experiments have shown that, Ni/$LaCoO_3$ can effectively convert 96% of CO_2 around 800°C. In lower temperatures, 600°C and 700°C coke deposition is decreasing catalyst efficiency.

CHAPTER 5

CONCLUSION

The purpose of this study is increasing the value of Şırnak asphaltite in environmentally friendly way, synergetic effect investigation of co-processing of biomass and Şırnak asphaltite while characterization of products obtained and improving process efficiency by dry reforming on perovskite oxide, which can also encapsulate CO_2. For this purpose, <150 mesh Şırnak asphaltite and waste pepper plant samples are prepared by using size reduction methods and a grinding calibration curve is obtained for asphaltite. Synergetic effect in co-processing of Şırnak asphaltite and biomass is obtained at the mixing ratio of 50:50. For processing of the mixture, considering both asphaltite and biomass has moisture unless dried, steam distillation is selected as processing technique and resulting liquids are collected and analyzed using ^1H and ^{13}C NMR. Şırnak asphaltite is also subjected to pyrolysis and hydrogenation, where produced liquids are captured on glass wools and analyzed using ^1H and ^{13}C NMR, gaseous products are analyzed using mass spectroscopy and residue is analyzed using TGA and elemental analysis. Dry reforming on $Ni/LaCoO_3$ is performed using benzene as model compound.

To conclude, although high sulfur content of Şırnak asphaltite makes it hard to utilize this important energy source in direct combustion, experiments have shown that it is possible to increase its value by co-processing it with biomass. Using biomass increases the overall weight loss of asphaltite processing, which demonstrates the presence of synergetic effect between asphaltite and biomass. Co-processing efficiency can be further improved by dry reforming on $Ni/LaCoO_3$ efficiency by removal of tar compounds with 97%.

REFERENCES

1. Adegoroye, A. (2004). The characterisation of tars produced during the gasification of sewage sludge in a spouted bed reactor. Fuel. doi:10.1016/s0016-2361(04)00128-0

2. Agarwal, G., & Lattimer, B. (2014). Physicochemical, kinetic and energetic investigation of coal–biomass mixture pyrolysis. Fuel Processing Technology, 124, 174-187. doi:10.1016/j.fuproc.2014.03.005

3. Alam, H., Moghaddam, A., & Omidkhah, M. (2009). The influence of process parameters on desulfurization of Mezino coal by HNO3/HCl leaching. Fuel Processing Technology, 90(1), 1-7. doi:10.1016/j.fuproc.2008.06.009

4. Attia, Y. A., Weiwen, L. 1987. In Processing and Utilization of High Sulfur Coals, vol. II. New York: Elsevier.

5. Ballice, L., & Sağlam, M. (2003). Co-pyrolysis of Göynük-oil shale and Şırnak-asphaltite from Turkey and analysis of co-pyrolysis products by capillary GC total stream sampling technique☆. *Fuel*, *82*(5), 511–522. doi: 10.1016/s0016-2361(02)00326-5

6. Boncukcuoğlu, R., Kocakerim, M., & Erşahan, H. (1994). Kinetics of desulphurization of Nevşehir - Dadaği coal with ferric chloride solutions. Fuel Processing Technology, 38(1), 31-44. doi:10.1016/0378-3820(94)90041-8

7. Borah, D., & Baruah, M. K. (2001). Kinetic and thermodynamic studies on oxidative desulphurisation of organic sulphur from Indian coal at 50–150°C. Fuel Processing Technology, 72(2), 83-101. doi:10.1016/s0378-3820(00)00132-6

8. Borah, D., Baruah, M. K., & Gogoi, P. C. (2005). Model study of pyrite demineralization by hydrogen peroxide oxidation at 30 °C in the presence of metal ions (Ni2 , Co2 and Sn2). Fuel Processing Technology, 86(7), 769-779. doi:10.1016/j.fuproc.2004.08.003

9. Borah, D., Baruah, M., & Haque, I. (2002). Oxidation of high sulphur coal. Part 2. Desulphurisation of organic sulphur by hydrogen peroxide in presence of metal ions. Fuel and Energy, 43(3), 170. doi:10.1016/s0140-6701(02)85577-1

10. Brage, C., Yu, Q., Chen, G., & Sjöström, K. (2000). Tar evolution profiles obtained from gasification of biomass and coal. Biomass and Bioenergy, 18(1), 87-91. doi:10.1016/s0961-9534(99)00069-0

11. Clean coal technologies in Japan: Technological innovation in the coal industry. (2006). Kawasaki: New Energy and Industrial Technology Development Organization.

12. Collot, A.G., Zhuo, Y., Dugwell, D.R., Kandiyoti R. (2000). Co-pyrolysis and co-gasification of coal and biomass in bench-scale fixed-bed and fluidised bed reactors. Fuel and Energy Abstracts, 41(4), 232. doi:10.1016/0140-6701(00)92755-3

13. Demir, E. (2009). CLEANING OF ŞIRNAK KARATEPE ASPHALTITES (Unpublished master's thesis). Middle East Technical University.

14. Demirbaş, A. (2002). Demineralization and desulfurization of coals via column froth flotation and different methods. Energy Conversion and Management, 43(7), 885-895. doi:10.1016/s0196-8904(01)00088-7

15. Demirbas, A. (2006). Desulfurization of Organic Sulfur from Lignite by an Electron Transfer Process. Energy Sources, Part A: Recovery, Utilization, and Environmental Effects, 28(14), 1295-1301. doi:10.1080/00908310500451931

16. Demirbas, A., & Balat, M. (2004). Coal Desulfurization via Different Methods. Energy Sources, 26(6), 541-550. doi:10.1080/00908310490429669

17. El-Rub, Z. A., Bramer, E. A., & Brem, G. (2004). Review of Catalysts for Tar Elimination in Biomass Gasification Processes. Industrial & Engineering Chemistry Research, 43(22), 6911-6919. doi:10.1021/ie0498403

18. Evans, R. J., & Milne, T. A. (1987). Molecular characterization of the pyrolysis of biomass. Energy & Fuels, 1(2), 123-137. doi:10.1021/ef00002a001

19. Evans, R. J., & Milne, T. A. (1987). Molecular characterization of the pyrolysis of biomass. 2. Applications. Energy & Fuels, 1(4), 311-319. doi:10.1021/ef00004a001

20. Fan, C.W., Dong, G.W., Markuszewski, R., Wheelock, T.D. 1987, Sayfa 172-182. Processing and Utilization of High Sulfur Coals vol. II. New York: Elsevier.

21. Friedman, S., LaCount, R.B., Warzinski, R.P. 1977. Coal Desulfurization, Chemical and Physical Methods. Am. Chem. Soc. Symp. Ser., 164-172

22. Garcia, R., Moinelo, S. R., Lafferty, C. J., & Snape, C. E. (1991). Pyrolytic desulfurization of some high-sulfur coals. Energy & Fuels, 5(4), 582-586. doi:10.1021/ef00028a009

23. Gerber, M. A. (2007). Review of Novel Catalysts for Biomass Tar Cracking and Methane Reforming.

24. Gürü, M. 2004. "Desulphurization of coal by selective oxidative agent permanganate solution", Eighth International Combustion Symposium, Gazi University, Ankara, Turkey, 606–615.

25. Gürü, M. and Alıcılar, A. 2001b. Removal of sulfur in fuel oil by holding in ash with organic based metallic compounds. J. Inst. Sci. Technol. Gazi Univ., 14: 435–444.

26. Holmes, J., Cochran, H., Edwards, M., Joy, D., & Lantz, P. (1977). Evaluation of Coal Carbonization Processes. Coal Processing Technology, 3.

27. ICCT. (2016, June). A technical summary of Euro 6/VI vehicle emission standards. Retrieved September 20, 2018, from http://www.theicct.org/sites/default/files/publications/ICCT_Euro6-VI_briefing_jun2016.pdf

28. Jukic, A. (2016, February 10). Petroleum Refining. Retrieved October 21, 2018, from https://www.scribd.com/document/298860357/Petroleum-Refining

29. Jung, W. Y., Song, Y. I., Lim, K. T., Lee, G. D., Lee, M. S., & Hong, S. (2015). Catalytic Oxidation of Benzene Over LaCoO3 Perovskite-Type Oxides Prepared Using Microwave Process. Journal of Nanoscience and Nanotechnology, 15(1), 652-655. doi:10.1166/jnn.2015.8330

30. Kanca, A., Dodd, M., Reimer, J. A., & Uner, D. (2016). Following the structure and reactivity of Tuncbilek lignite during pyrolysis and hydrogenation. Fuel Processing Technology, 152, 266–273. doi: 10.1016/j.fuproc.2016.06.014

31. Kara, H., & Ceylan, R. (1988). Removal of sulphur from four Central Anatolian lignites by NaOH. Fuel, 67(2), 170-172. doi:10.1016/0016-2361(88)90258-x

32. Kawatra, S. K., & Eisele, T. C. (2001). Coal desulfurization: High-efficiency preparation methods. New York: Taylor & Francis.

33. Krerkkaiwan, S., Fushimi, C., Tsutsumi, A., & Kuchonthara, P. (2013). Synergetic effect during co-pyrolysis/gasification of biomass and sub-bituminous coal. Fuel Processing Technology, 115, 11-18. doi:10.1016/j.fuproc.2013.03.044

34. Lalvani, S., Pata, M., & Coughlin, R. W. (1983). Sulphur removal from coal by electrolysis. Fuel, 62(4), 427-437. doi:10.1016/0016-2361(83)90006-6

35. Liu, Q., Hu, H., Zhu, S., Zhou, Q., Li, W., Wei, X., & Xie, K. (2005). Desulfurization of Coal by Pyrolysis and Hydropyrolysis with Addition of KOH/NaOH. Energy & Fuels, 19(4), 1673-1678. doi:10.1021/ef0497053

36. Lompa-Krzymien, L. (1982). Complete removal of sulphur from coal using solutions containing cupric ions. Fuel, 61(9), 871-873. doi:10.1016/0016-2361(82)90319-2

37. Longwell, J., Rubin, E., & Wilson, J. (1995). Coal: Energy for the future. Progress in Energy and Combustion Science, 21(4), 269-360. doi:10.17226/4918

38. Luo, G., Kang, L., Zhu, M., & Dai, B. (2014). Highly active phosphotungstic acid immobilized on amino functionalized MCM-41 for the oxidesulfurization of dibenzothiophene. Fuel Processing Technology, 118, 20-27. doi:10.1016/j.fuproc.2013.08.001

39. Mei, H., Mei, B., & Yen, T. F. (2003). A new method for obtaining ultra-low sulfur diesel fuel via ultrasound assisted oxidative desulfurization☆. Fuel, 82(4), 405-414. doi:10.1016/s0016-2361(02)00318-6

40. Mesroghli, S., Yperman, J., Jorjani, E., Carleer, R., & Noaparast, M. (2015). Evaluation of microwave treatment on coal structure and sulfur species by reductive pyrolysis-mass spectrometry method. Fuel Processing Technology, 131, 193-202. doi:10.1016/j.fuproc.2014.11.005

41. Palmer, S., & Hippo, E. (1991). Chemical coal cleaning using selective oxidation. doi:10.2172/6148319

42. S, Kasper (1981). Coal Conversion Chemistry.

43. Silopi Electric. (2019). Retrieved from http://www.cinergroup.com.tr/en/energy-and-mining/silopi-electric

44. Simell, P. A., Hakala, N. A., Haario, H. E., & Krause, A. O. (1997). 97/01498 Catalytic decomposition of gasification gas tar with benzene as the model compound. Fuel and Energy Abstracts, 38(2), 118. doi:10.1016/s0140-6701(97)84319-6

45. Singh, K., & Zondlo, J. (2017). Co-processing coal and torrefied biomass during direct liquefaction. Journal of the Energy Institute, 90(4), 497-504. doi:10.1016/j.joei.2016.06.001

46. Srivastava, V. C. (2012). ChemInform Abstract: An Evaluation of Desulfurization Technologies for Sulfur Removal from Liquid Fuels. ChemInform, 43(18). doi:10.1002/chin.201218271

47. Statistical Review of World Energy: Energy economics: Home. (2019). Retrieved from https://www.bp.com/en/global/corporate/energy-economics/statistical-review-of-world-energy.html

48. Torres, W., Pansare, S. S., & Goodwin, J. G. (2007). Hot Gas Removal of Tars, Ammonia, and Hydrogen Sulfide from Biomass Gasification Gas. Catalysis Reviews, 49(4), 407-456. doi:10.1080/01614940701375134

49. University of Potsdam. (n.d.). Proton Chemical Shift Ranges. Retrieved August 2, 2019, from https://www2.chemistry.msu.edu/faculty/reusch/OrgPage/nmr.htm.

50. Üner, D. (2017). Advances in refining catalysis. Boca Raton: CRC Press/Taylor & Francis Group.

51. Verkade, J. G., Mohan, T., & Angelici, R. J. (1995). U.S. Patent No. US5437696A. Washington, DC: U.S. Patent and Trademark Office.

52. Wang, C. (2017). Co-pyrolysis Characteristic and Parameters Optimization of Low Rank Coal and Eichhornia Crassipes. Proceedings of the 2017 6th International Conference on Energy and Environmental Protection (ICEEP 2017). doi:10.2991/iceep-17.2017.130

53. World Coal Association. (n.d.). What is Coal. Retrieved May 1, 2015, from http://www.worldcoal.org/coal/what-is-coal/

54. World Enegy Council. (2013). World Enegy Resources: Coal.

55. Yaman, S., & Küçükbayrak, S. (1996). Oxydesulfurization of a Turkish Lignite Using Trona Solutions. Energy Sources, 18(4), 461-471. doi:10.1080/00908319608908782

56. Zhang, G., Du, Y., Zhang, Y., & Xu, Y. (2014). Desulfurization reaction model and experimental analysis of high sulfur coal under hydrogen atmosphere. Journal of Industrial and Engineering Chemistry, 20(2), 487-493. doi:10.1016/j.jiec.2013.05.006

57. Zhang, L., Xu, S., Zhao, W., & Liu, S. (2007). Co-pyrolysis of biomass and coal in a free fall reactor. Fuel, 86(3), 353-359. doi:10.1016/j.fuel.2006.07.004

APPENDICES

A. Sample Calculation for Asphaltite Size Reduction

Tablo 1: Size Reduction Experimental Data

t=15 min	**Empty (gr)**	**Full**
Undersize Vessel	254,1	295,41
Sieve and Undersize Vessel	515,55	615,6
t=45 min	**Empty (gr)**	**Full**
Undersize Vessel	254	326,77
Sieve and Undersize Vessel	515,39	615,46
t=60 min	**Empty (gr)**	**Full**
Undersize Vessel	254,06	332,32
Sieve and Undersize Vessel	515,16	615,56

$$\begin{aligned} &< 150 \text{ Mesh Particle Size Percentage} \\ &\qquad = (Full\ Weight\ of\ Undersize\ Vessel \\ &\qquad - Empty\ Weight\ of\ Undersize\ Vessel) \\ &\qquad /(Full\ Weight\ of\ Sieve\ and\ Undersize\ Vessel \\ &\qquad - Empty\ Weight\ of\ Sieve\ Undersize\ Vessel) \end{aligned}$$

At t=15 minutes,

$$< 150 \text{ Mesh Particle Size Percentage} = \frac{295{,}41\ gr - 254{,}1\ gr}{615{,}6\ gr - 515{,}55\ gr} = \frac{41{,}31\ gr}{100{,}05\ gr}$$

$$= 41{,}29\%$$

B. Sample Calculation for Steam Distillation TGA Analysis

Expected theoretical weight loss is calculated according to following formula:

$$\begin{aligned} ExpectedWL\% = {} & (Total\ Weight\ Loss\ of\ \text{Ş}.A.* Weight\%\ of\ \text{Ş}.A.) \\ & + (Total\ Weight\ Loss\ of\ Biomass * Weight\%\ of\ Biomass) \end{aligned}$$

C. NMR Spectra of Steam Distillation Experiments

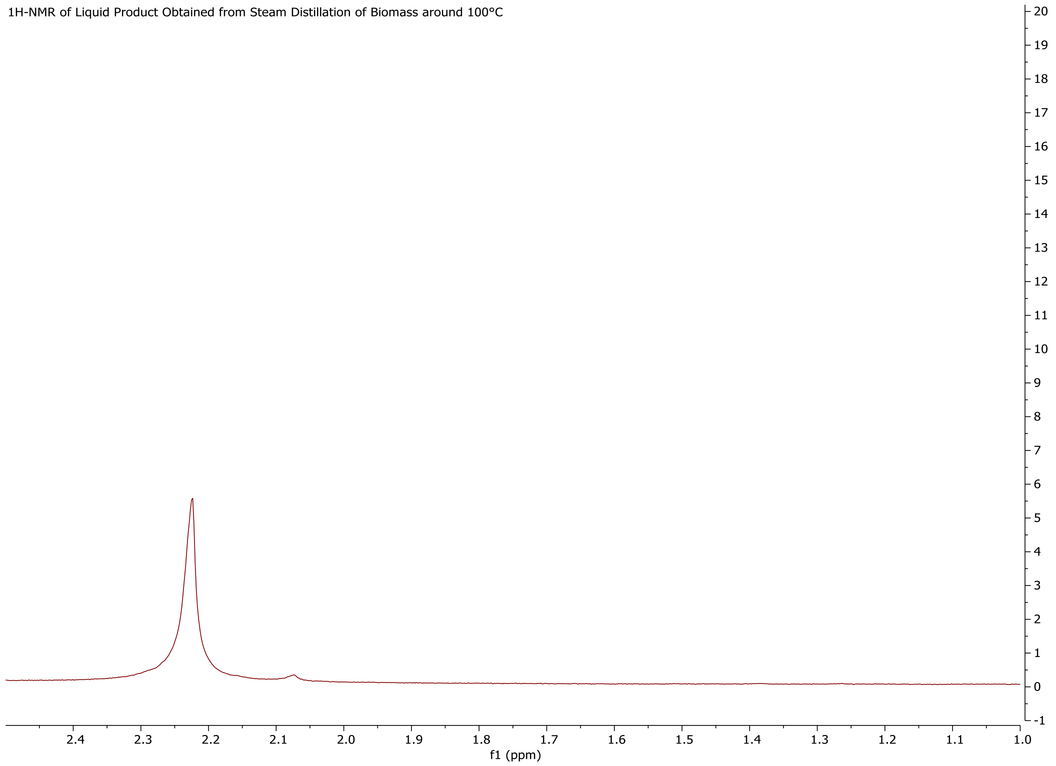

Figure 46: ^{1}H-NMR of Liquid Product Obtained from Steam Distillation of Biomass around 100°C

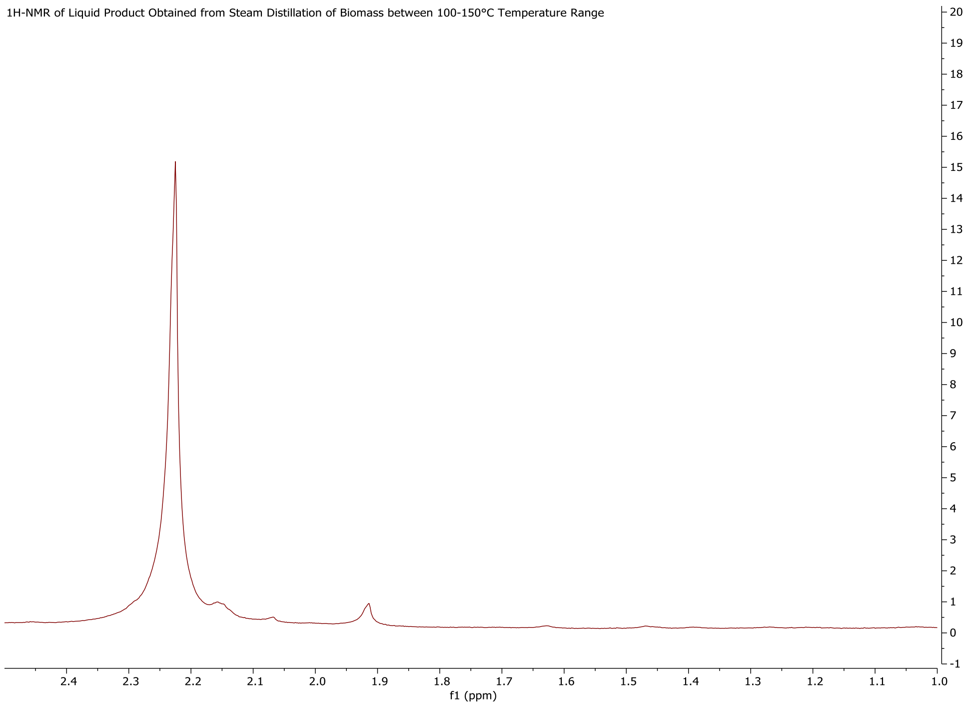

Figure 47: ^{1}H-NMR of Liquid Product Obtained from Steam Distillation of Biomass between 100-150°C Temperature Range

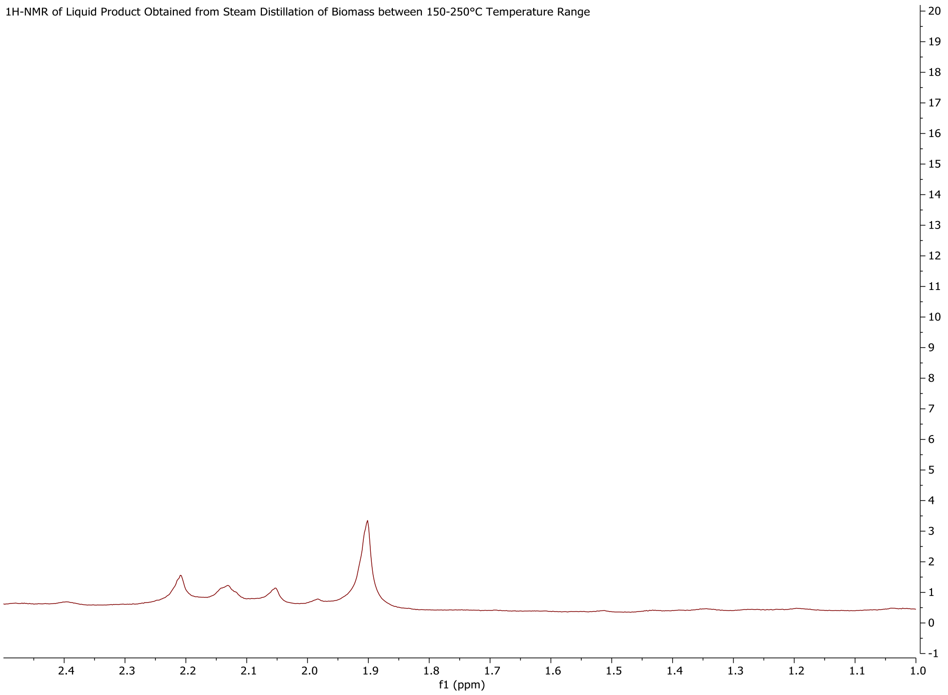

Figure 48: ^{1}H-NMR of Liquid Product Obtained from Steam Distillation of Biomass between 150-250°C Temperature Range

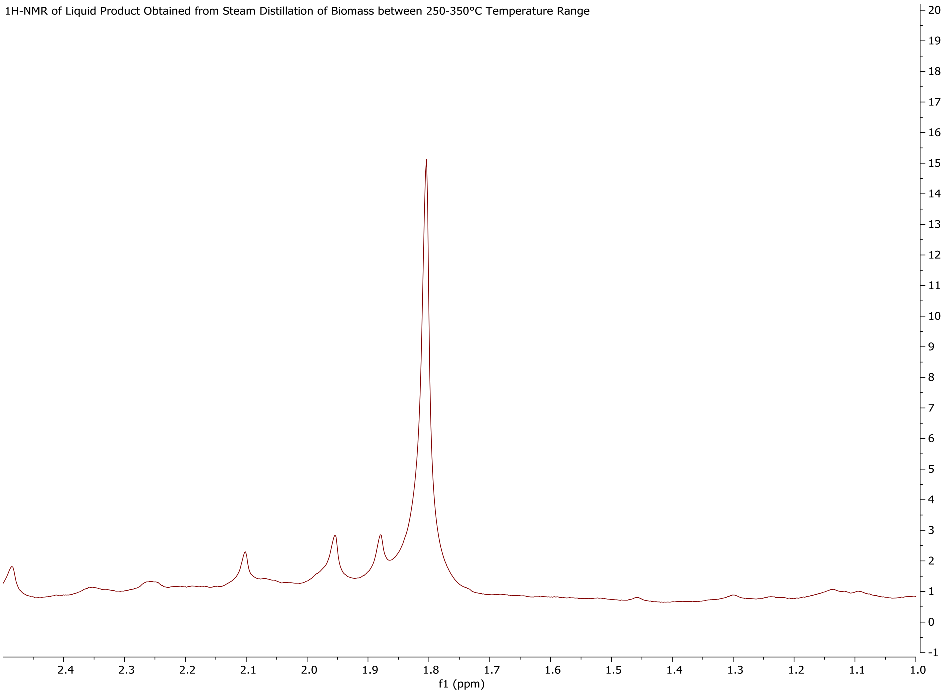

Figure 49: ^{1}H-NMR of Liquid Product Obtained from Steam Distillation of Biomass between 250-350°C Temperature Range

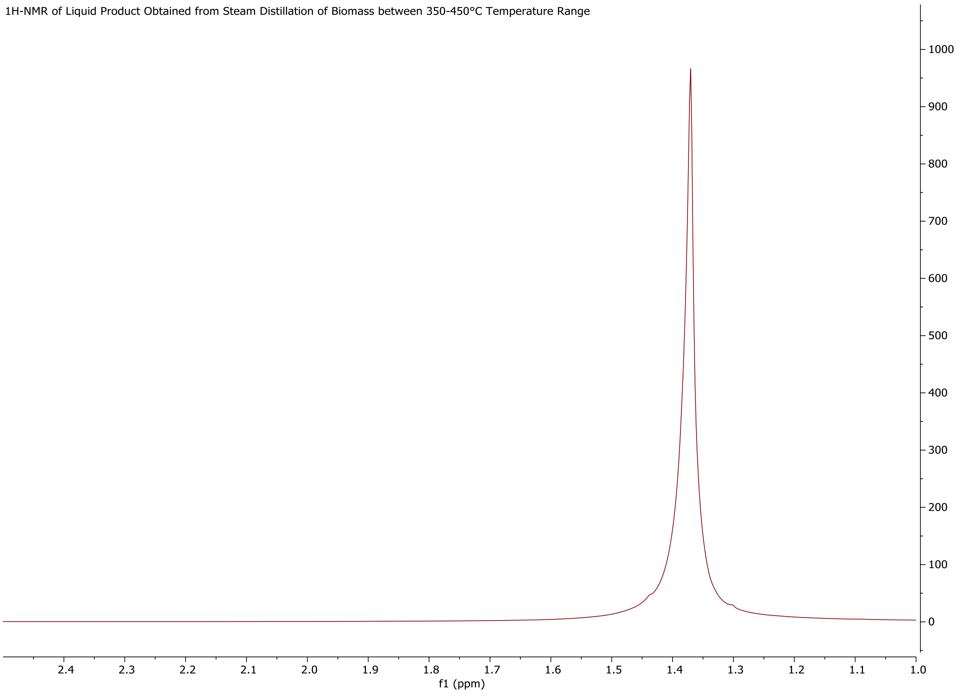

Figure 50: ^{1}H-NMR of Liquid Product Obtained from Steam Distillation of Biomass between 350-450°C Temperature Range

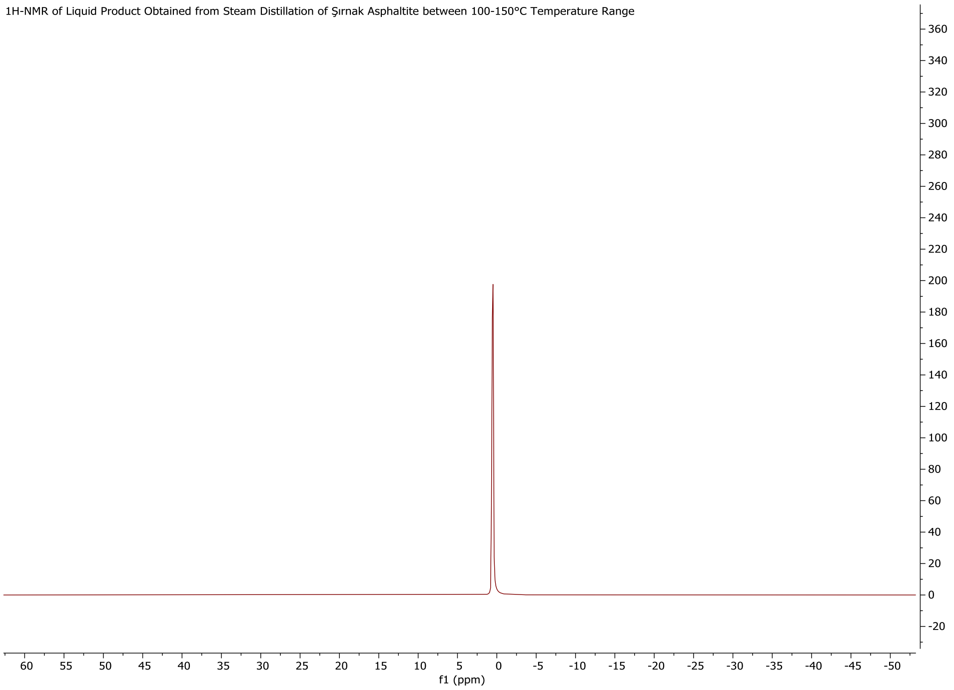

Figure 51: ^{1}H-NMR of Liquid Product Obtained from Steam Distillation of Şırnak Asphaltite between 100-150°C Temperature Range

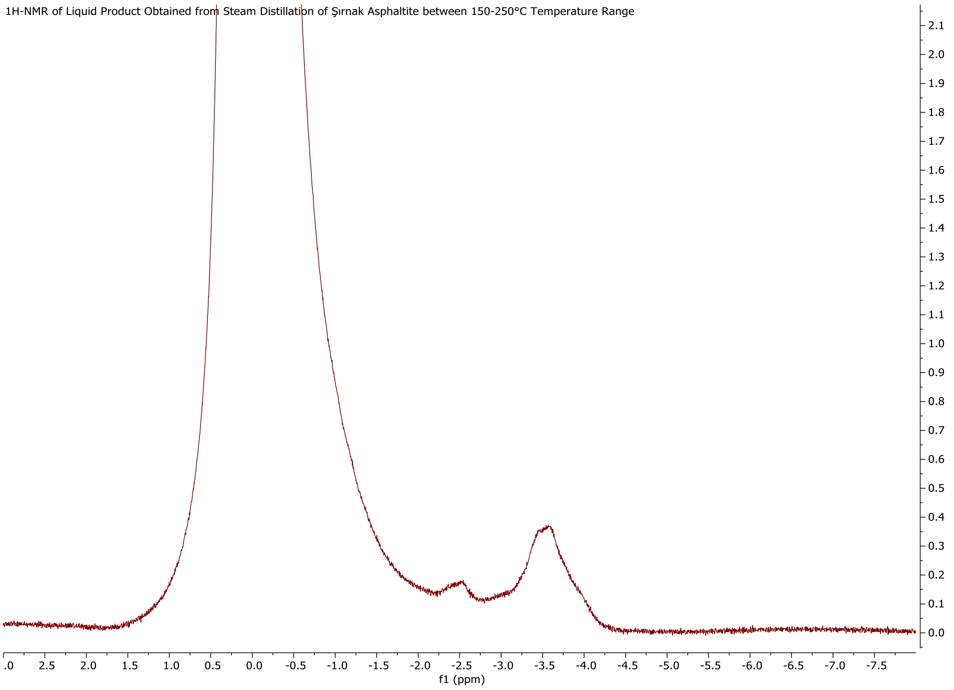

Figure 52: ^{1}H-NMR of Liquid Product Obtained from Steam Distillation of Şırnak Asphaltite between 150-250°C Temperature Range

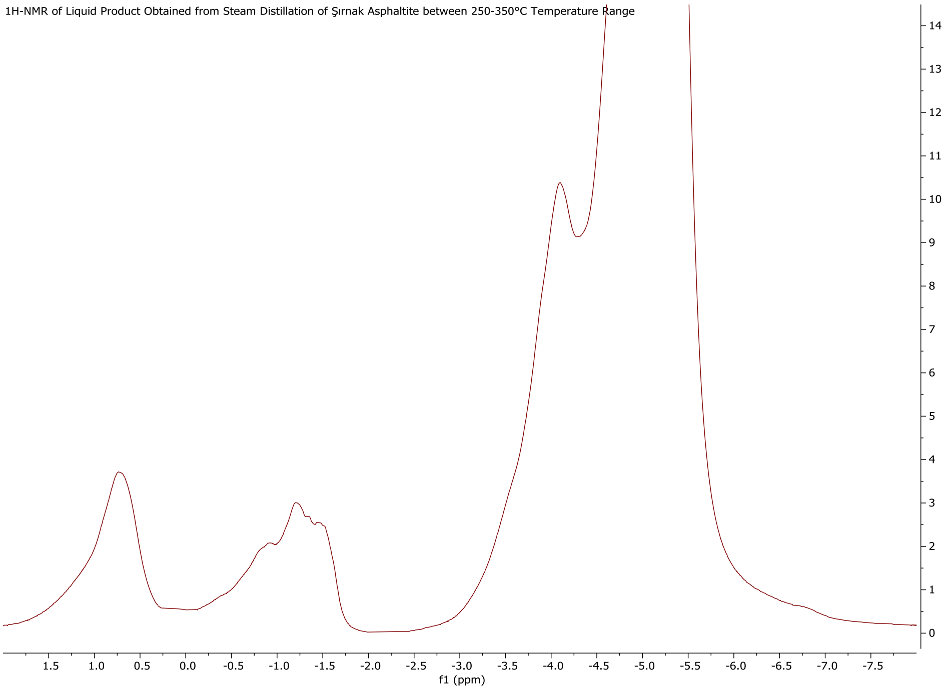

Figure 53: ^{1}H-NMR of Liquid Product Obtained from Steam Distillation of Şırnak Asphaltite between 250-350°C Temperature Range

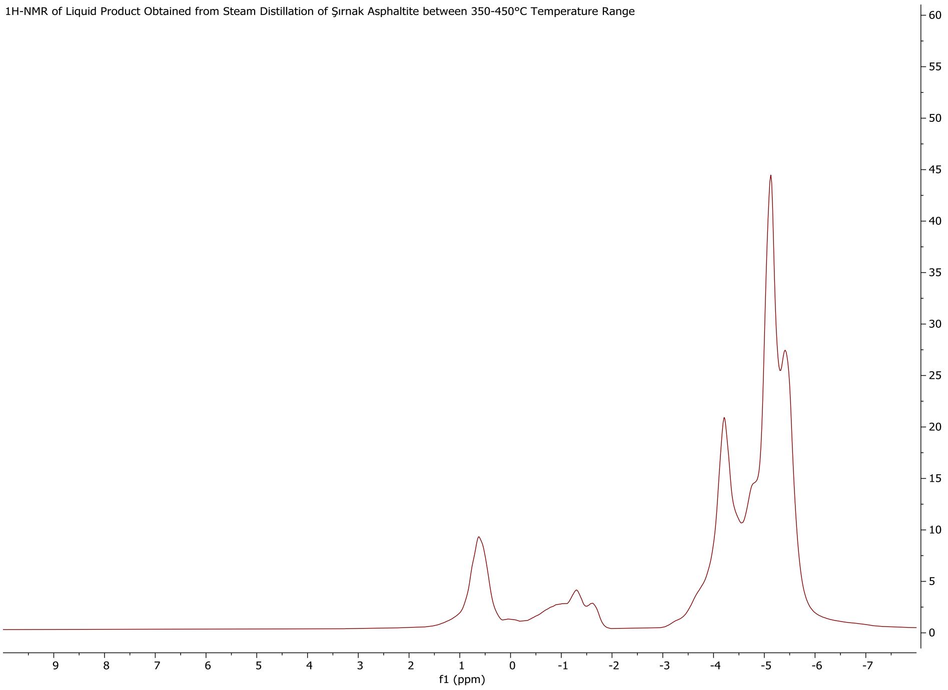

Figure 54: ^{1}H-NMR of Liquid Product Obtained from Steam Distillation of Şırnak Asphaltite between 350-450°C Temperature Range

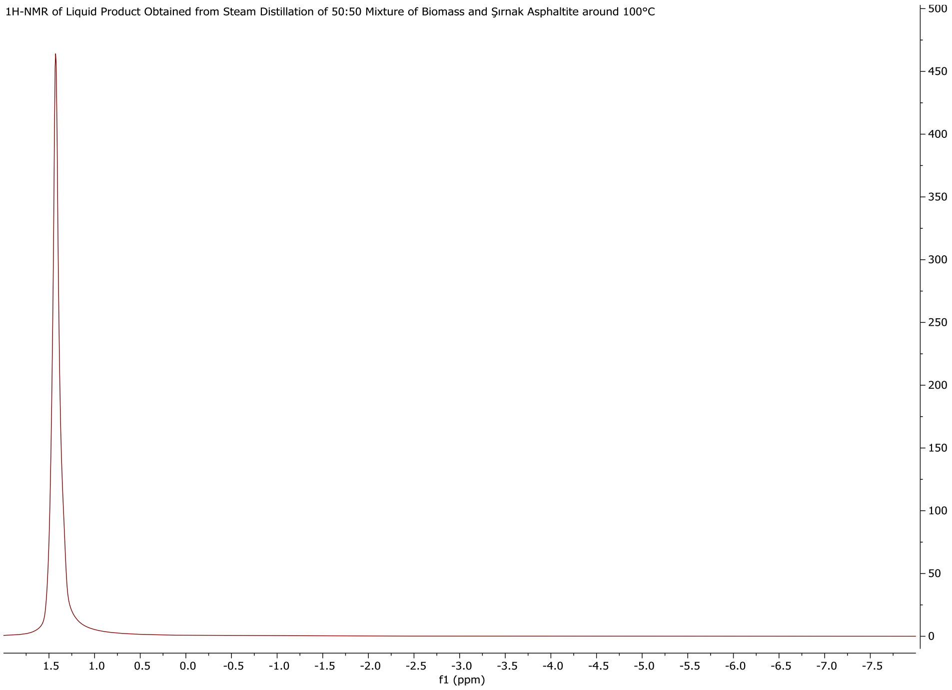

Figure 55: ^{1}H-NMR of Liquid Product Obtained from Steam Distillation of 50:50 Mixture of Biomass and Şırnak Asphaltite around 100°C

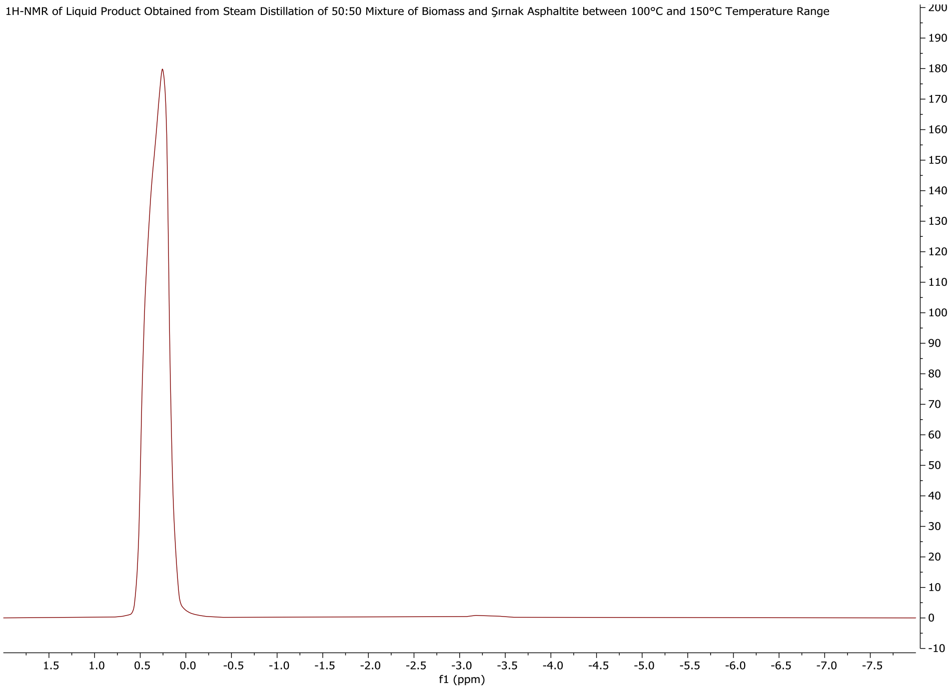

Figure 56: 1H-NMR of Liquid Product Obtained from Steam Distillation of 50:50 Mixture of Biomass and Şırnak Asphaltite between 100°C and 150°C Temperature Range

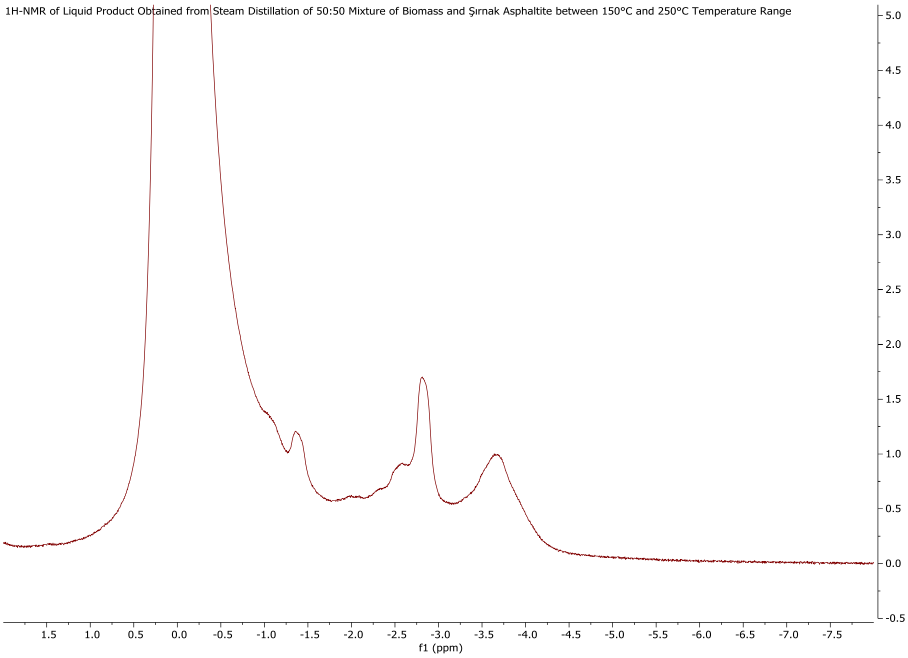

Figure 57: ^{1}H-NMR of Liquid Product Obtained from Steam Distillation of 50:50 Mixture of Biomass and Şırnak Asphaltite between 150°C and 250°C Temperature Range

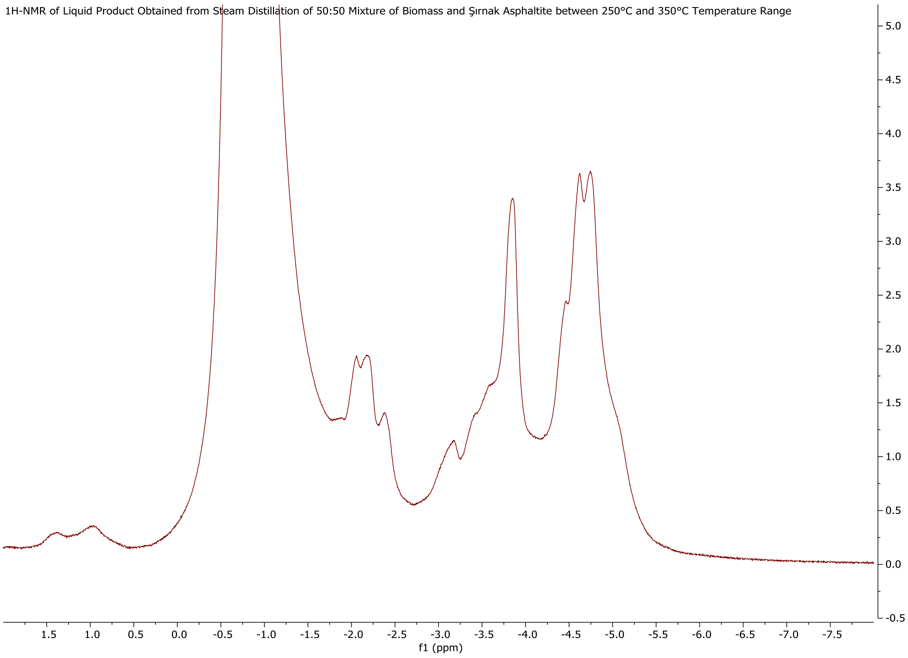

Figure 58: ^{1}H-NMR of Liquid Product Obtained from Steam Distillation of 50:50 Mixture of Biomass and Şırnak Asphaltite between 250°C and 350°C Temperature Range

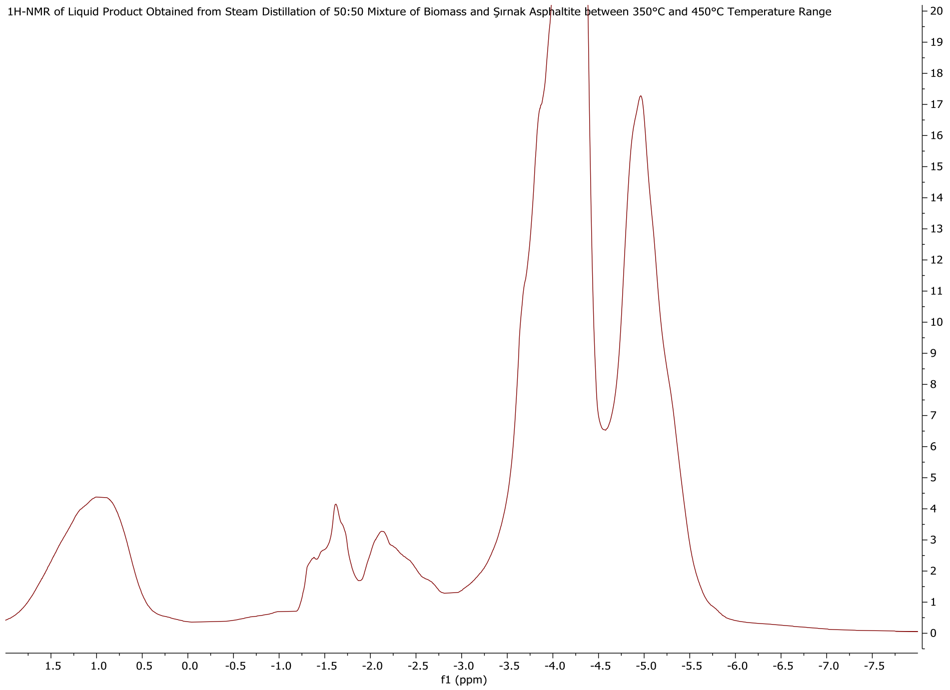

Figure 59: : ^{1}H-NMR of Liquid Product Obtained from Steam Distillation of 50:50 Mixture of Biomass and Şırnak Asphaltite between 350°C and 450°C Temperature Range

D. Glass Wool NMR Spectra

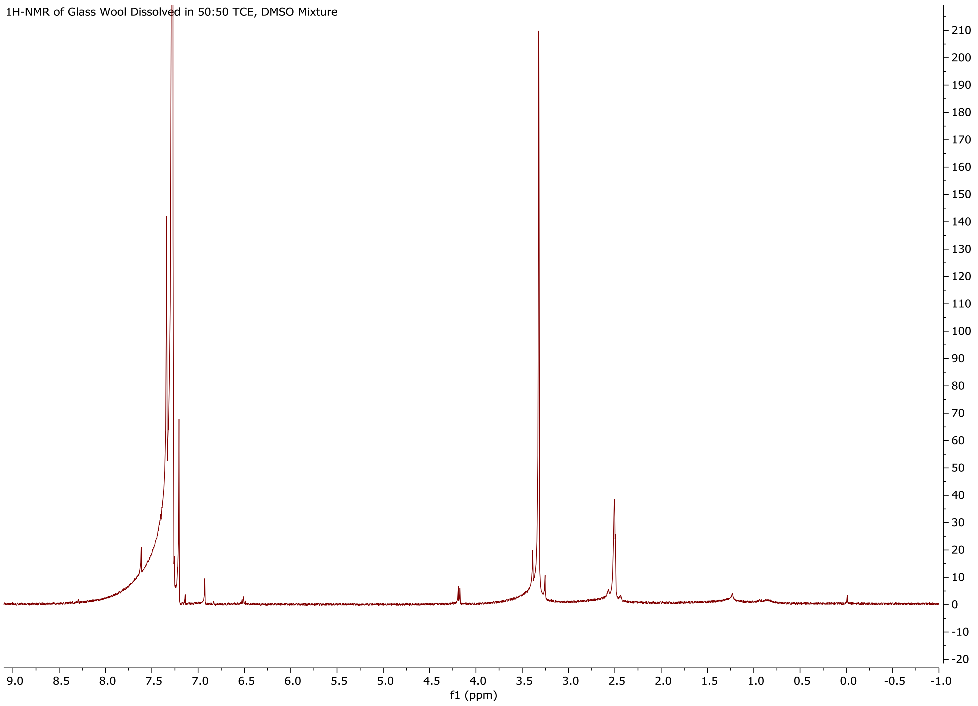

Figure 60: ^{1}H-NMR of Glass Wool Dissolved in 50:50 TCE, DMSO Mixture

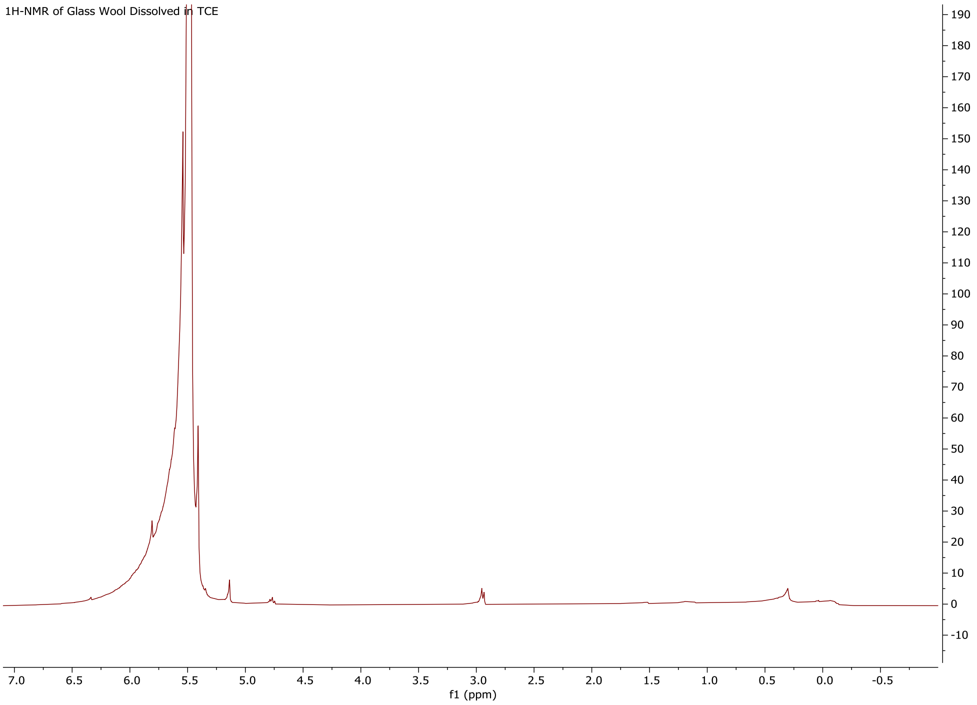

Figure 61: ^{1}H-NMR of Glass Wool Dissolved in TCE

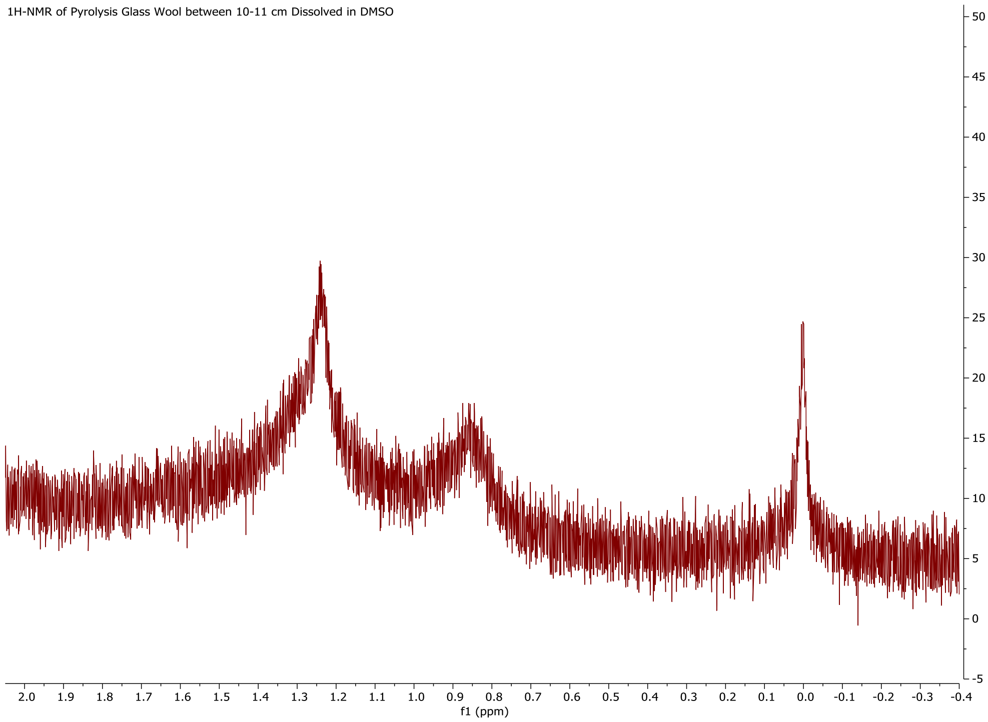

Figure 62: ^{1}H-NMR of Pyrolysis Glass Wool between 10-11 cm Dissolved in DMSO

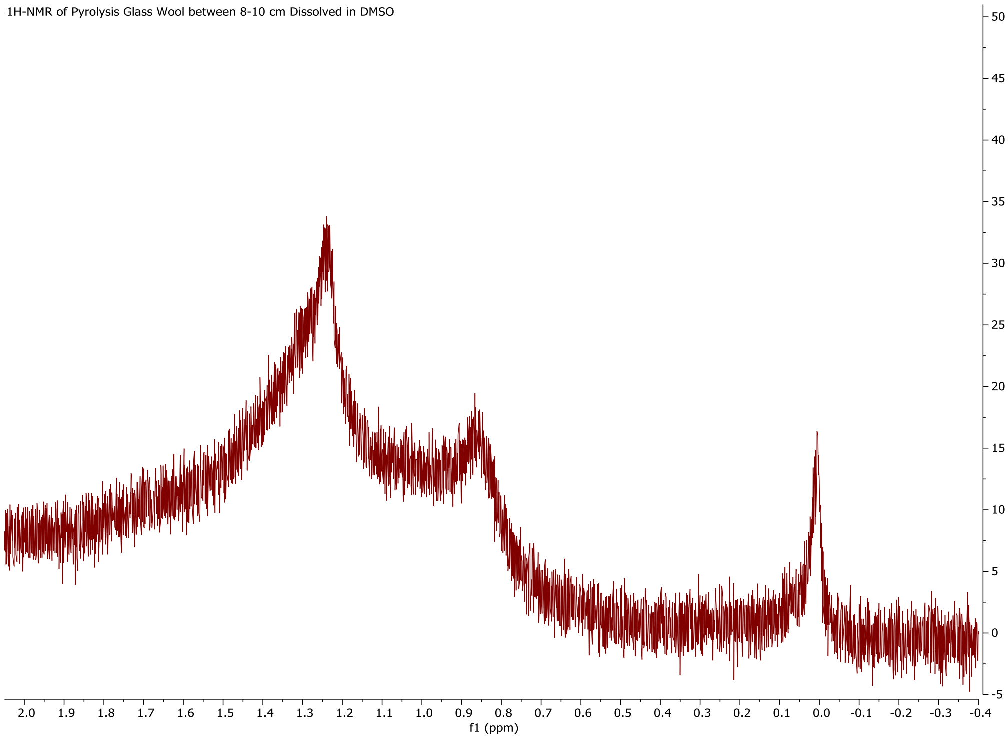

Figure 63: ^{1}H-NMR of Pyrolysis Glass Wool between 8-10 cm Dissolved in DMSO

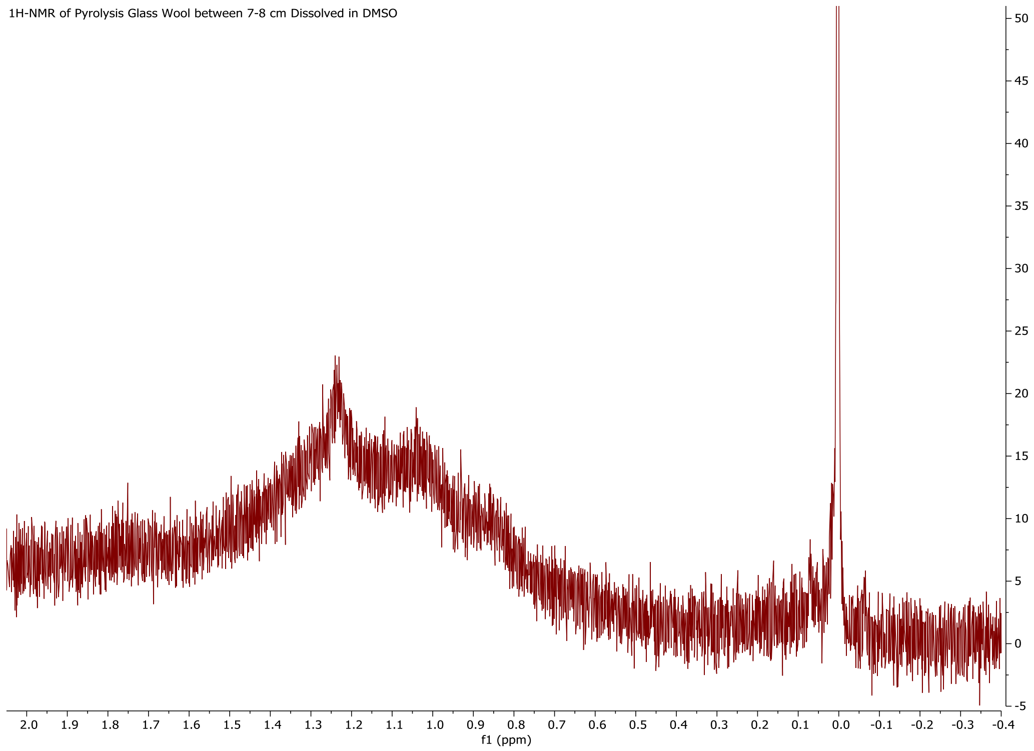

Figure 64: ^{1}H-NMR of Pyrolysis Glass Wool between 7-8 cm Dissolved in DMSO

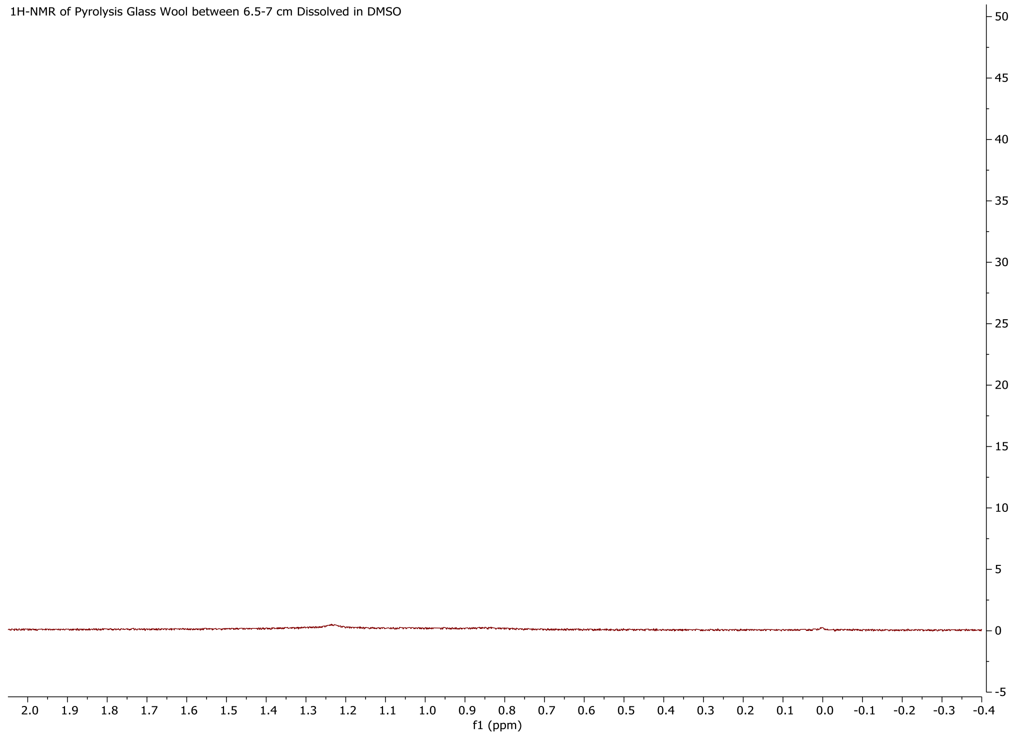

Figure 65: ^{1}H-NMR of Pyrolysis Glass Wool between 6.5-7 cm Dissolved in DMSO

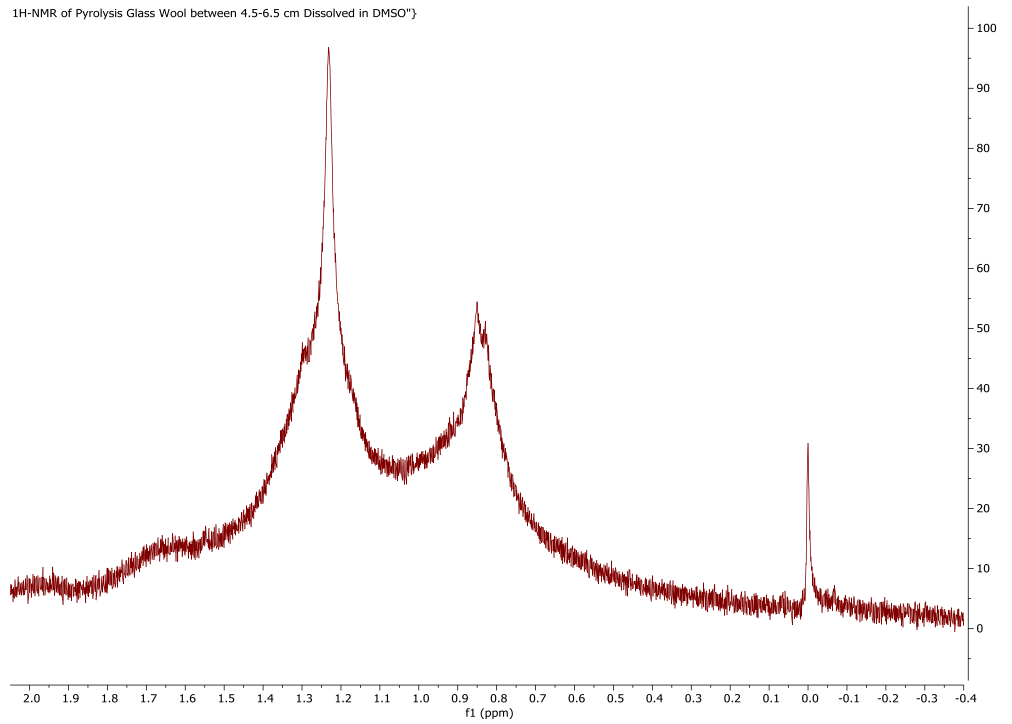

Figure 66: ^{1}H-NMR of Pyrolysis Glass Wool between 4.5-6.5 cm Dissolved in DMSO

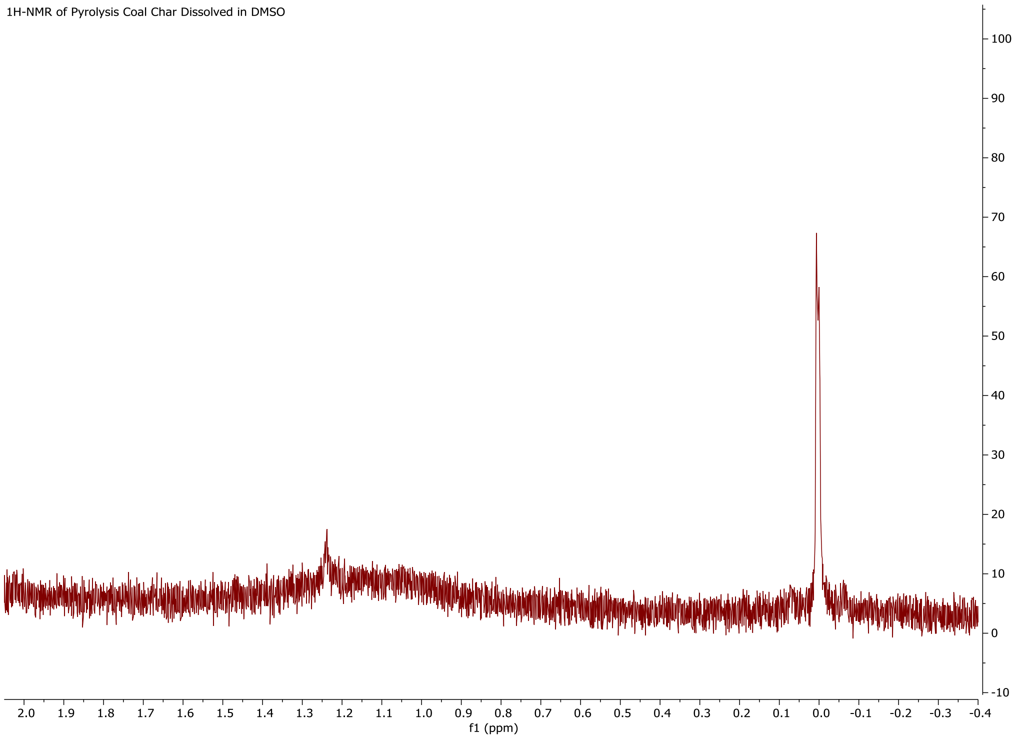

Figure 67: ^{1}H-NMR of Pyrolysis Coal Char Dissolved in DMSO

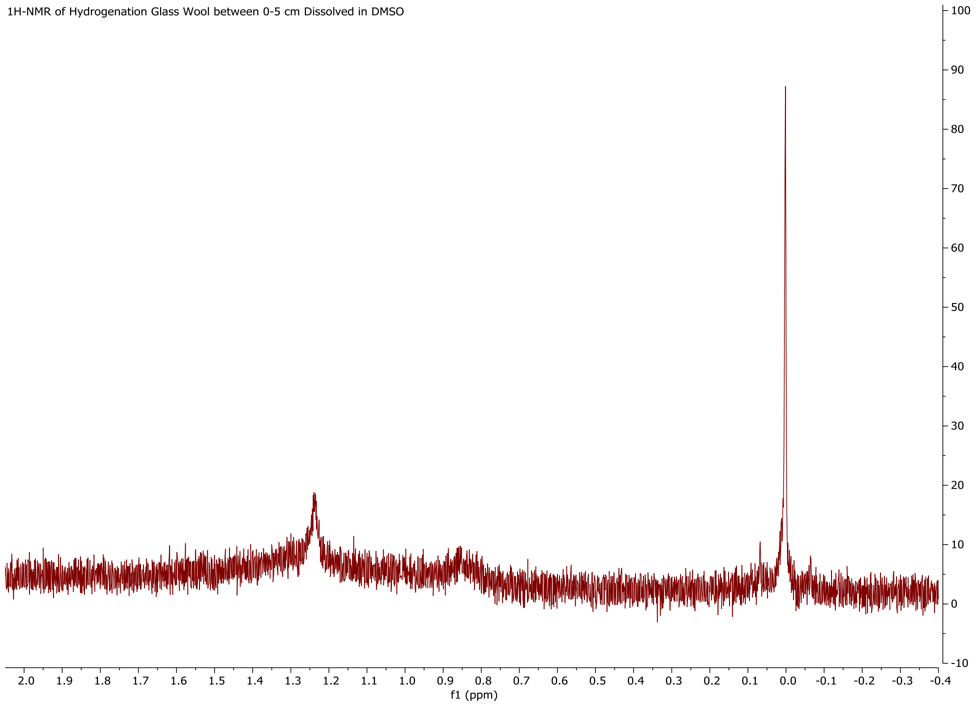

Figure 68: ^{1}H-NMR of Hydrogenation Glass Wool between 0-5 cm Dissolved in DMSO

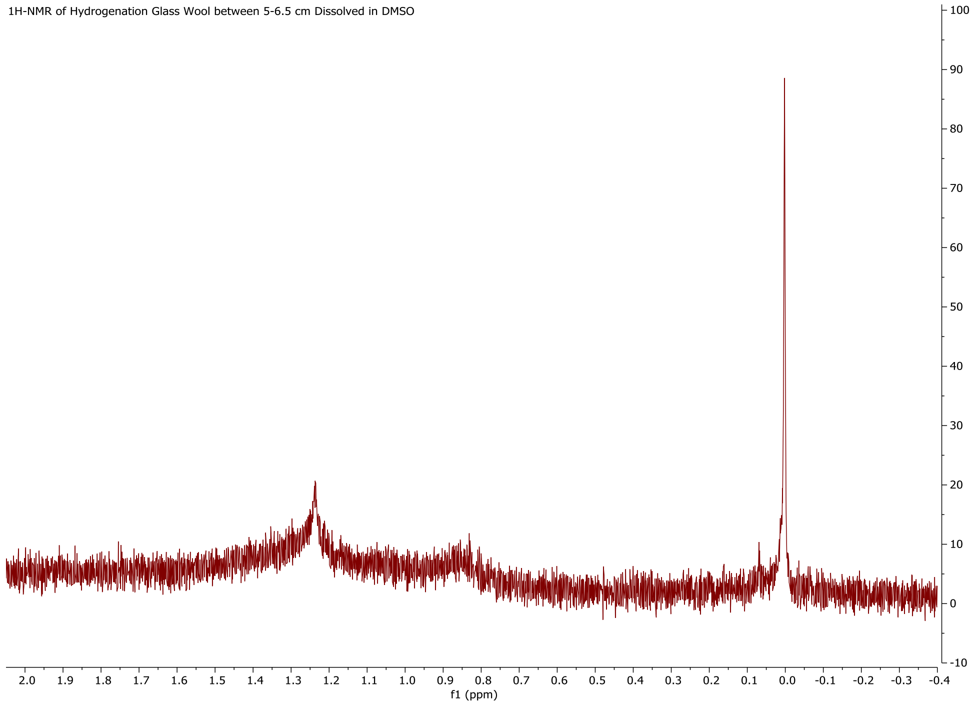

Figure 69: ^{1}H-NMR of Hydrogenation Glass Wool between 5-6.5 cm Dissolved in DMSO

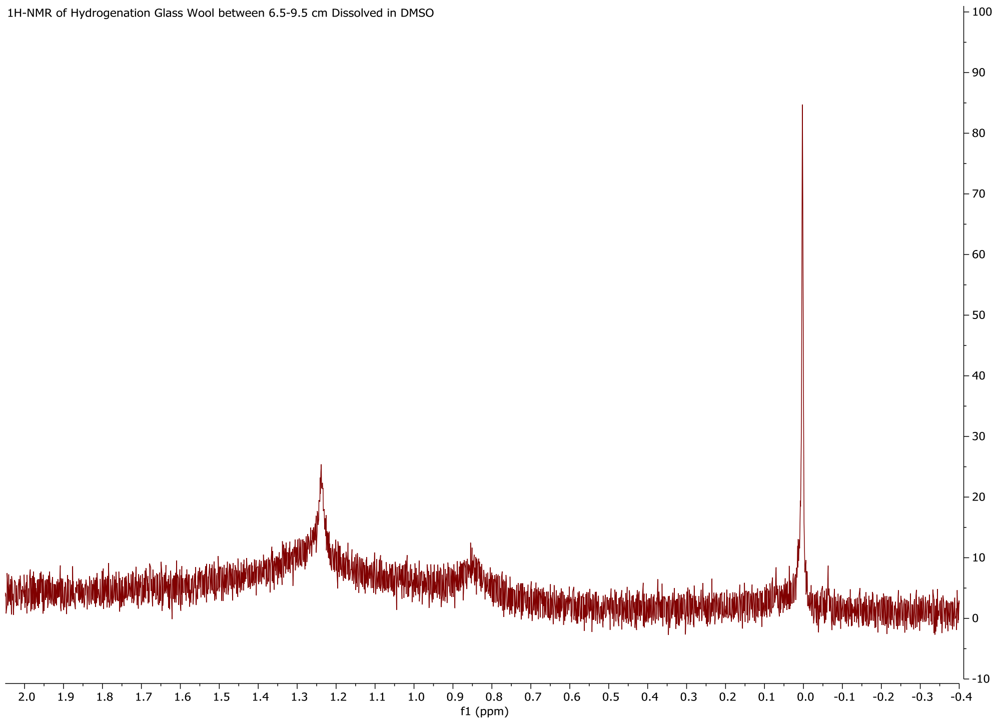

Figure 70: 1H-NMR of Hydrogenation Glass Wool between 6.5-9.5 cm Dissolved in DMSO

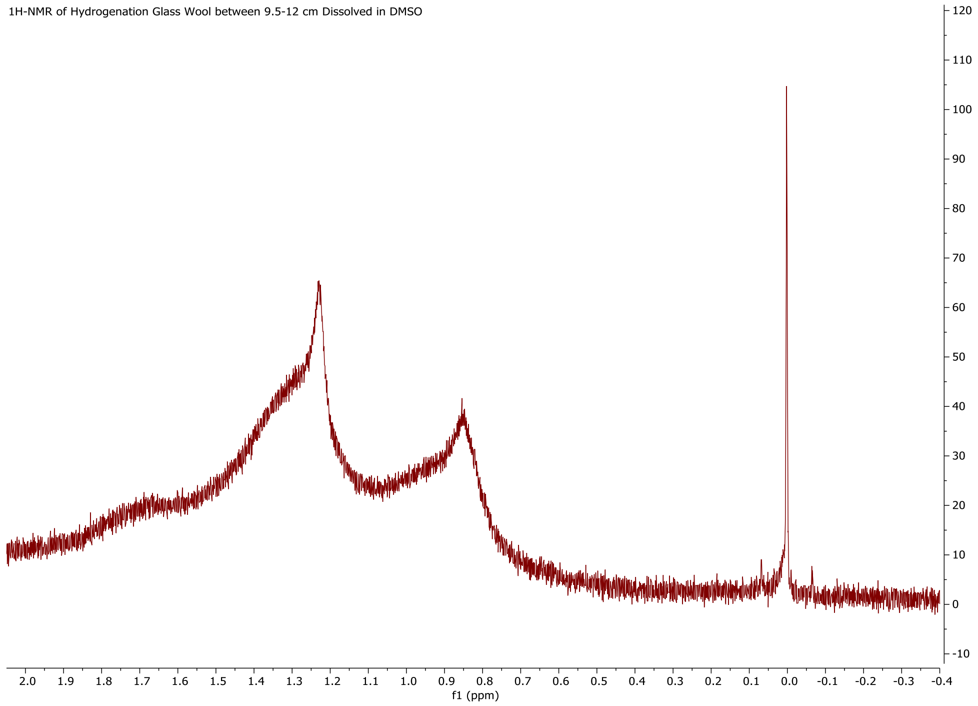

Figure 71: ^{1}H-NMR of Hydrogenation Glass Wool between 9.5-12 cm Dissolved in DMSO

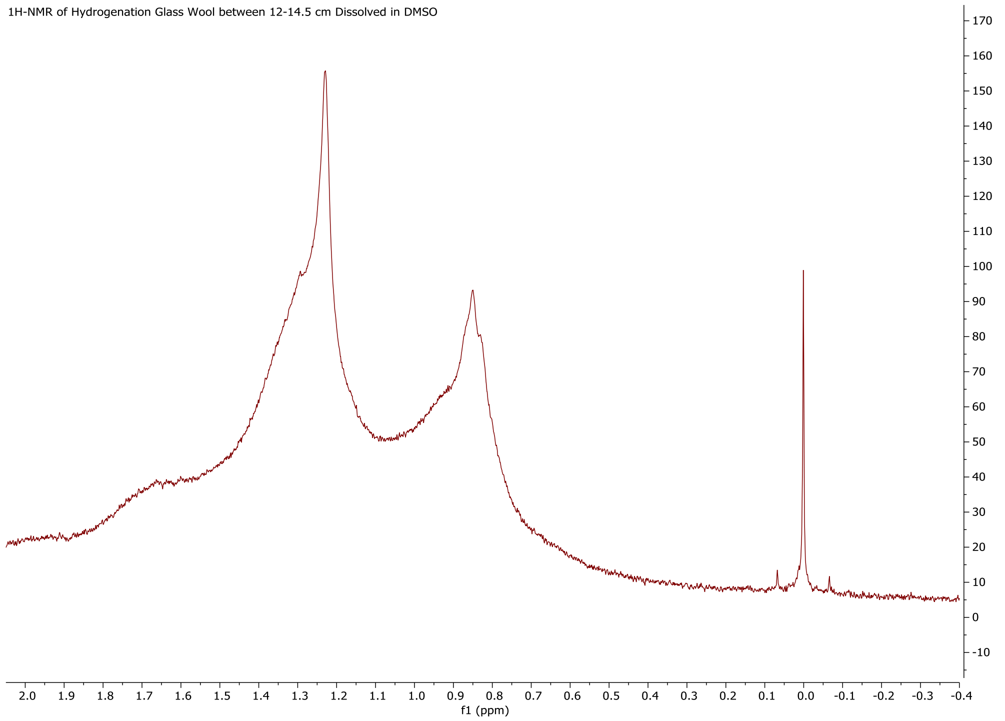

Figure 72: ^{1}H-NMR of Hydrogenation Glass Wool between 12-14.5 cm Dissolved in DMSO

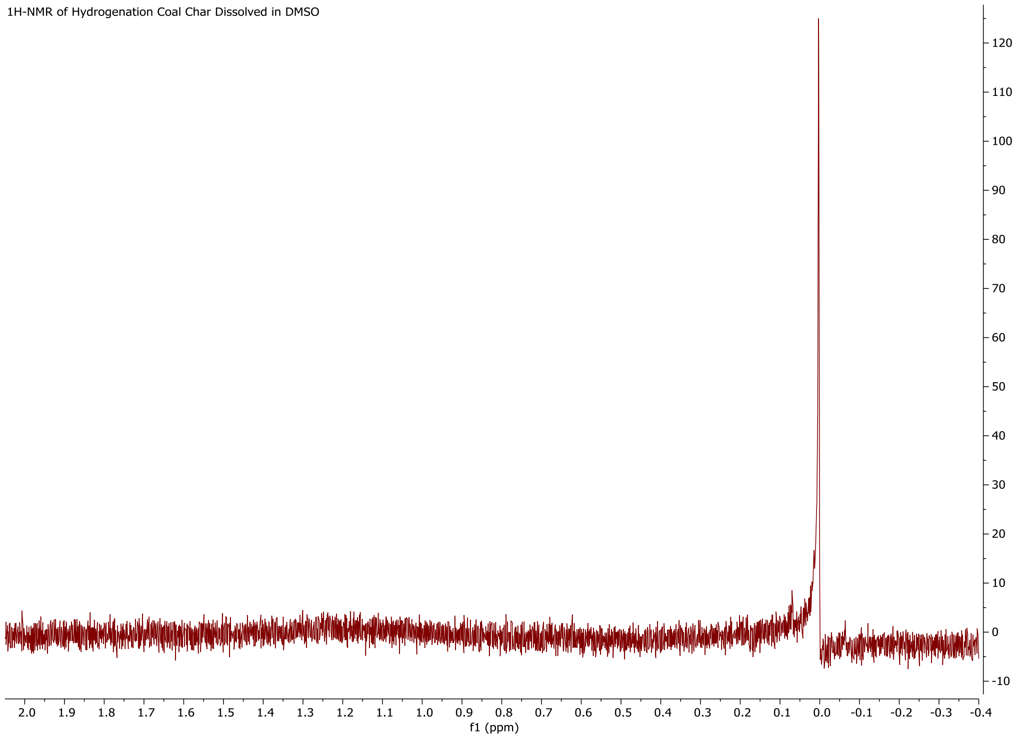

Figure 73: ^{1}H-NMR of Hydrogenation Asphaltite Char Dissolved in DMSO

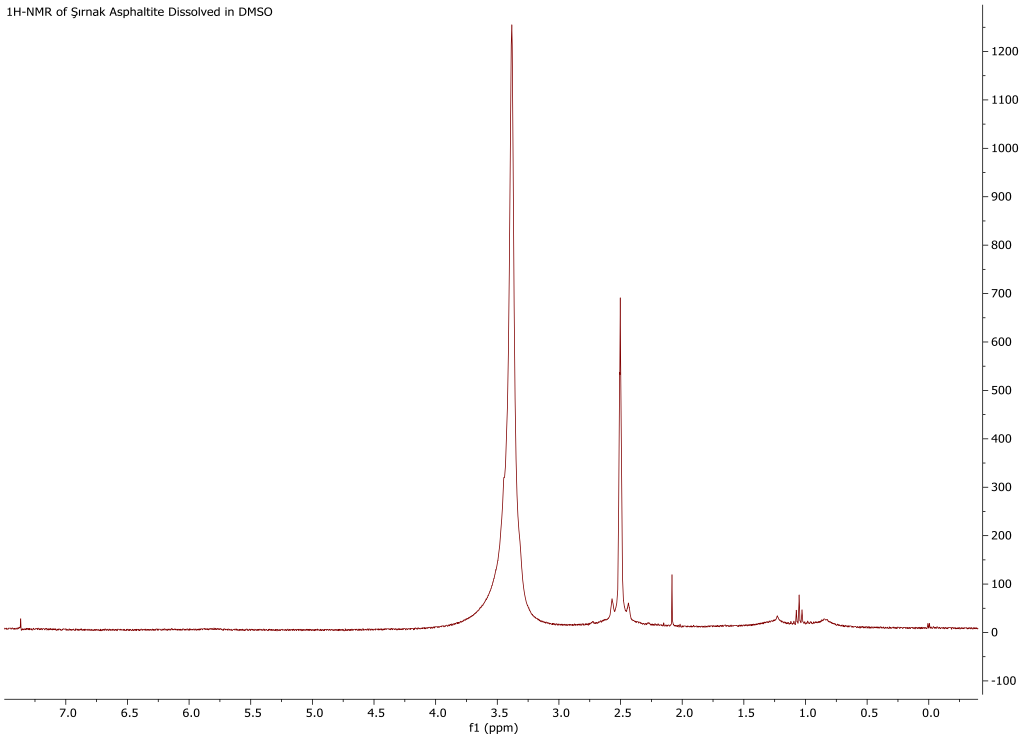

Figure 74: ^{1}H-NMR of Şırnak Asphaltite Dissolved in DMSO

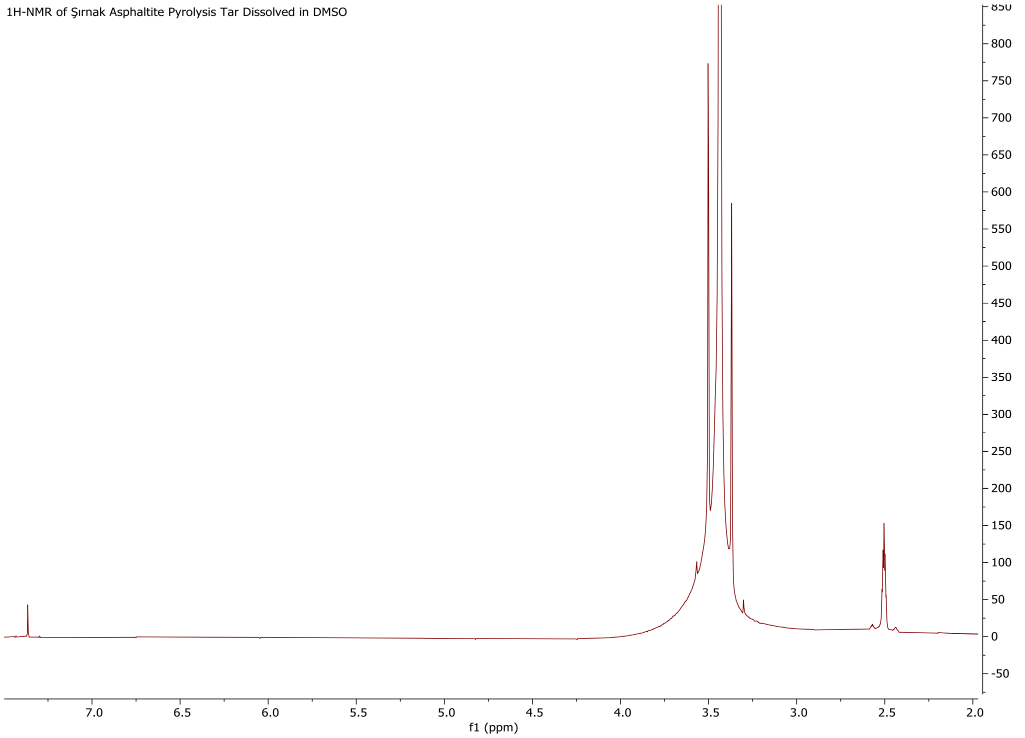

Figure 75: ^{1}H-NMR of Şırnak Asphaltite Pyrolysis Tar

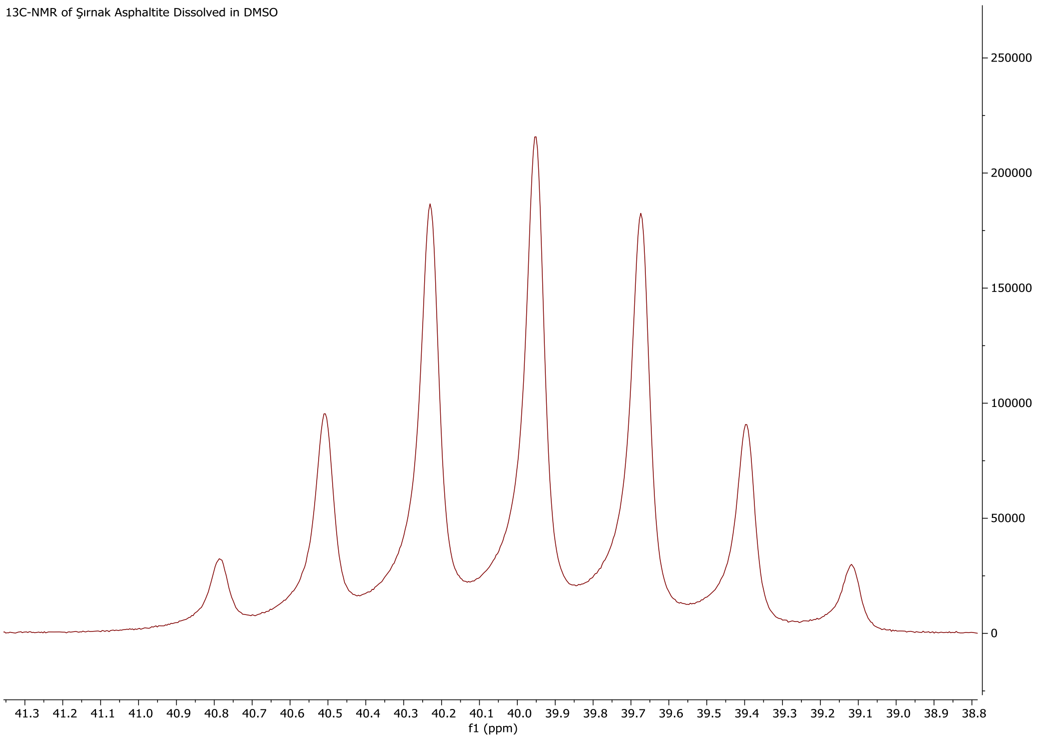

Figure 76: ^{13}C NMR of Şırnak Asphaltite

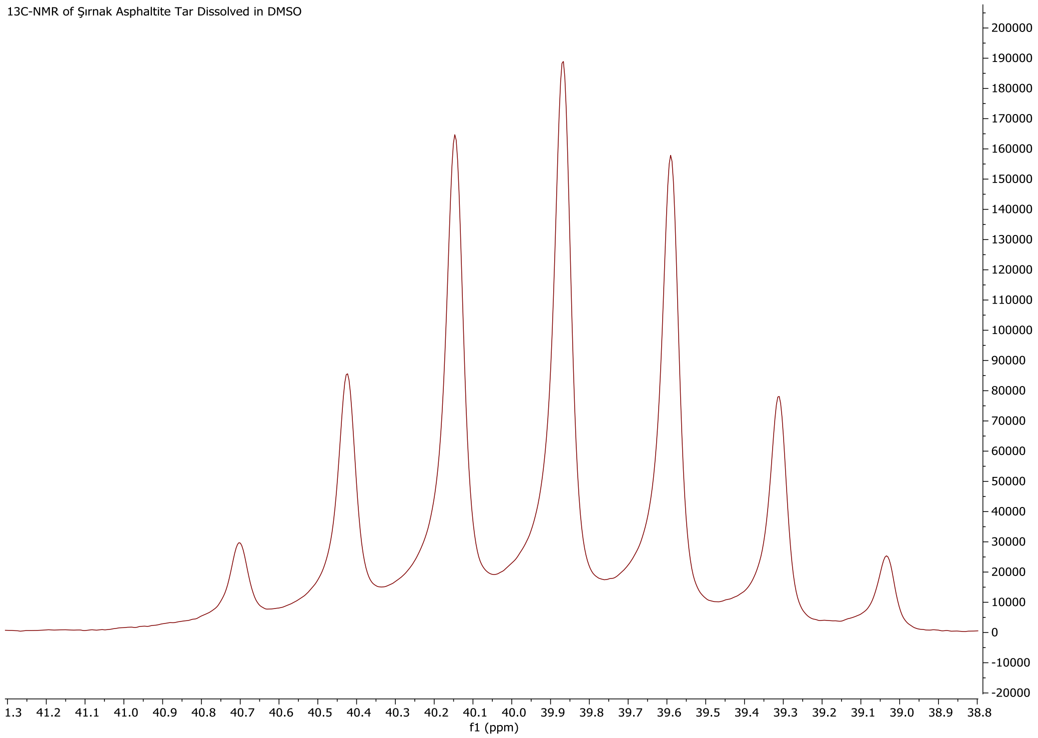

Figure 77: ^{13}C NMR of Şırnak Asphaltite Tar Dissolved in DMSO

E. SEM Images of Steam Distillation Residue

SEM Images of Şırnak asphaltite TGA Residue, pepper plant waste TGA residue and Sample 3 TGA Residue. 3kx Images can be found in Figure 78, Figure 85 and Figure 86.

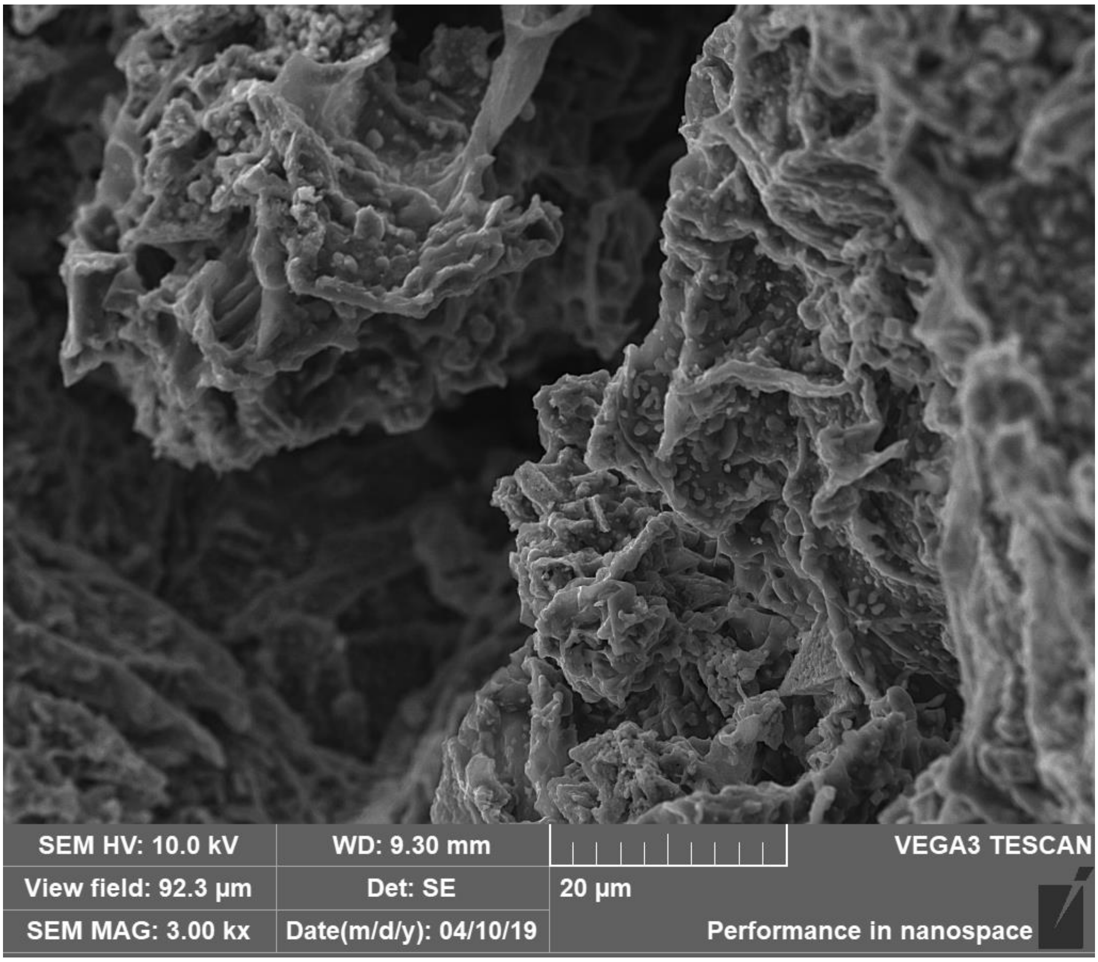

Figure 78: 3.00 kx SEM Image of Şırnak Asphaltite Steam Distillation Residue

F. Detailed Hydrocarbon Analysis Results

Table 21: 18-35 mesh Şırnak Asphaltite Pyrolysis Liquid Product Sample Detailed Hydrocarbon Analysis

	n-Paraffins	i-Paraffins	Olefins	Naphtenes	Aromatics	Oxygenates	Total
C1							0
C2							0
C3							0
C4							0
C5							0
C6	0.693						0.693
C7	2.161			1.595	1.166		4.922
C8	4.009		0.825	3.099			7.933
C9		0.915		6.306	6.856		14.077
C10	0.802	4.827	5.296	0.909	3.853		15.687
C11	4.764	2			4.724		11.488
C12	3.981	0.995			6.219		11.195
C13	3.416						3.416
C14							0
Total	19.826	8.737	6.121	11.909	22.818	0	69.411
						Total unknowns	30.589
						Grand total	100

Table 22: >40 mesh Şırnak Asphaltite Pyrolysis Liquid Product Sample Detailed Hydrocarbon Analysis

	n-Paraffins	**i-Paraffins**	**Olefins**	**Naphtenes**	**Aromatics**	**Oxygenates**	**Total**
C1							0
C2							0
C3							0
C4							0
C5							0
C6							0
C7	1.042			0.814	0.942		2.798
C8	2.883		0.497	2.322			5.702
C9		1.855		5.176	5.474		12.505
C10	0.669	4.68	4.547	0.755	4.299		14.95
C11	0.526	2.148	0.479		2.654		5.807
C12	3.531	0.688		0.466	8.227		12.912
C13	2.883						2.883
C14	0.692						0.692
Total	12.226	9.371	5.523	9.533	21.596	0	58.249
						Total Unknowns	41.751
						Grand Total	100

Table 23: 18-35 mesh Şırnak Asphaltite Hydrogenation Liquid Product Sample Detailed Hydrocarbon Analysis

	n-Paraffins	**i-Paraffins**	**Olefins**	**Naphtenes**	**Aromatics**	**Oxygenates**	**Total**
C1							0
C2							0
C3							0
C4							0
C5							0
C6							0
C7	1.41			0.995	1.197		3.602
C8	3.474		0.655	2.705			6.834
C9		2.588		5.724	6.047		14.359
C10	0.712	4.914	4.686	0.804	3.463		14.579
C11	0.557	1.724			3.318		5.599
C12	3.662	0.702			7.924		12.288
C13	3.011						3.011
C14	0.627						0.627
Total	13.453	9.928	5.341	10.228	21.949	0	60.899
						Total Unknowns	39.101
						Grand Total	100

Table 24: >40 mesh Şırnak Asphaltite Pyrolysis Liquid Product Sample Detailed Hydrocarbon Analysis

	n-Paraffins	**i-Paraffins**	**Olefins**	**Naphtenes**	**Aromatics**	**Oxygenates**	**Total**
C1							0
C2							0
C3							0
C4							0
C5							0
C6							0
C7							0
C8							0
C9				2.392	4.107		6.499
C10		1.813	3.809		4.998		10.62
C11	0.603	1.233	0.628		4.416		6.88
C12	4.641	0.846			10.315		15.802
C13	3.909						3.909
C14	1.037						1.037
Total	10.19	3.892	4.437	2.392	23.836	0	44.747
						Total Unknowns	55.253
						Grand Total	100

G. TGA and Elemental Analysis

a. Unprocessed Sample

TGA of unprocessed Şırnak asphaltite under air and nitrogen atmosphere can be found in Figure 79 and DrTGA of unprocessed Şırnak asphaltite under air and nitrogen atmosphere can be found in Figure 80.

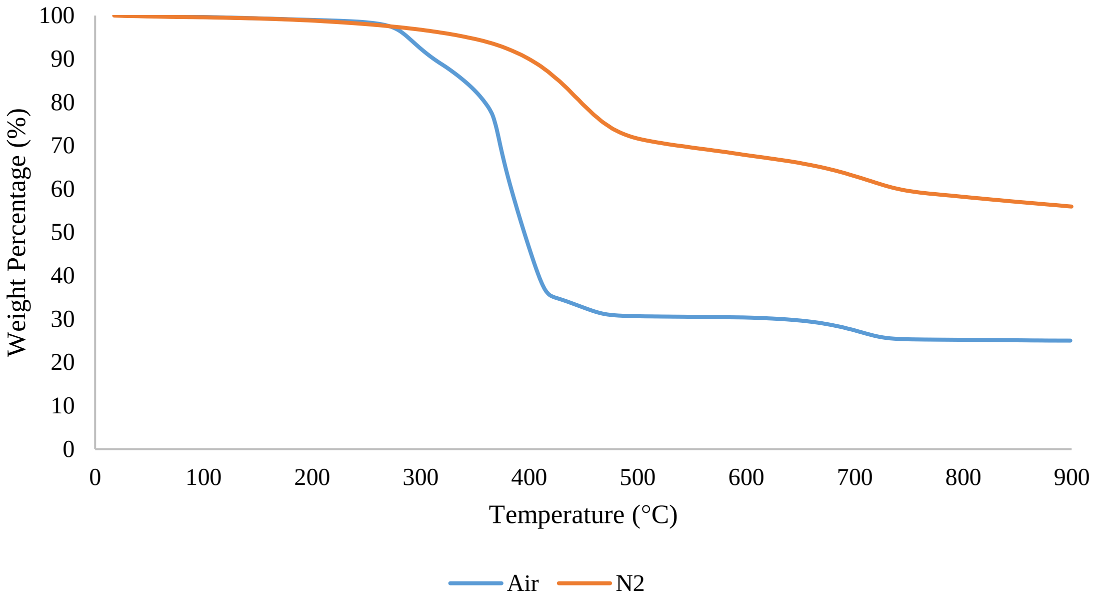

Figure 79: TGA of Pure Şırnak Asphaltite Sample Under Air and Nitrogen Atmosphere up to 900°C

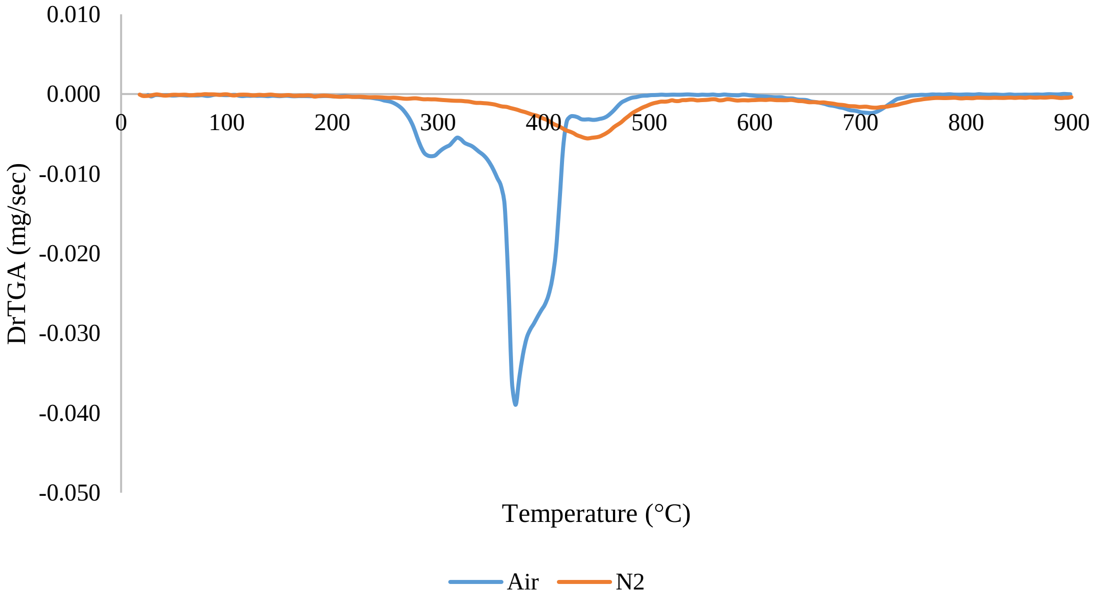

Figure 80: DrTGA of Pure Şırnak Asphaltite Sample Under Air and Nitrogen Atmosphere up to 900°C

b. Pyrolyzed Sample

TGA of pyrolyzed Şırnak asphaltite under air and nitrogen atmosphere can be found in Figure 81 and DrTGA of pyrolyzed Şırnak asphaltite under nitrogen atmosphere can be found in Figure 82.

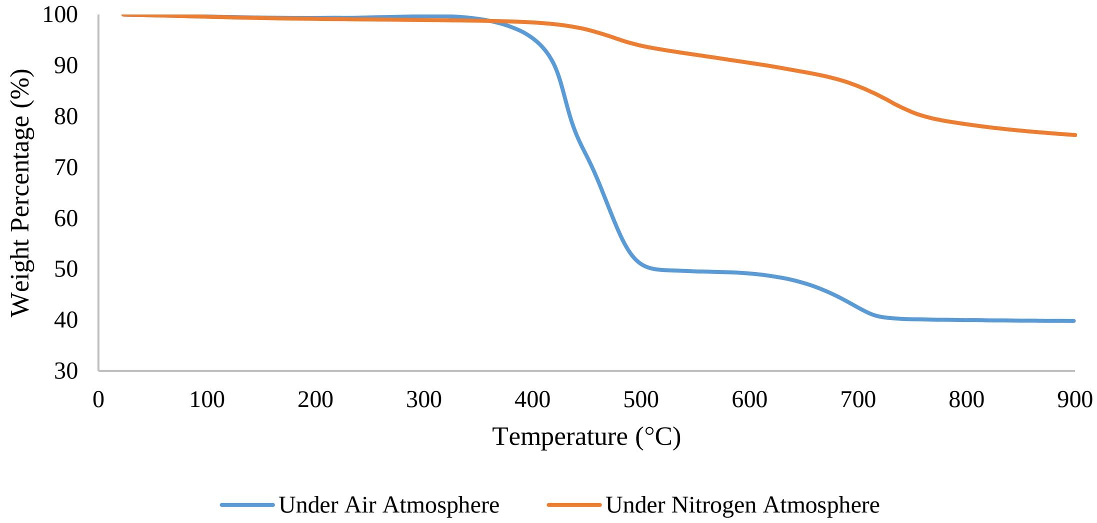

Figure 81: TGA of Pyrolyzed Şırnak Asphaltite Sample Under Air and Nitrogen Atmosphere up to 900°C

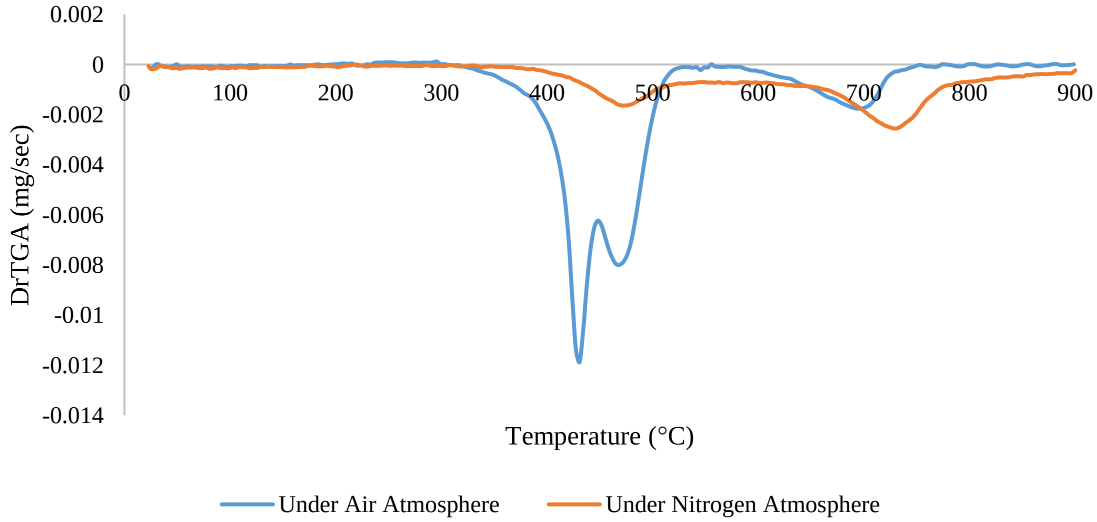

Figure 82: TGA of Pyrolyzed up to 450°C Şırnak Asphaltite Sample Under Air and Nitrogen Atmosphere up to 900°C

c. Hydrogenated Sample

TGA of hydrogenated Şırnak asphaltite under air and nitrogen atmosphere can be found in Figure 83 and DrTGA of hydrogenated Şırnak asphaltite under air and nitrogen atmosphere can be found in Figure 84.

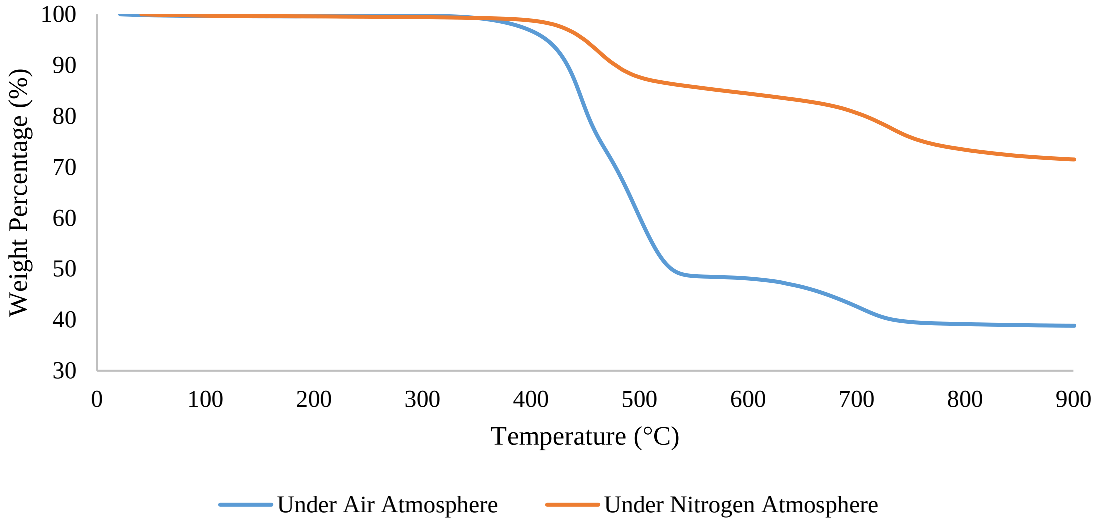

Figure 83: TGA of Hydrogenated up to 450°C Şırnak Asphaltite Sample Under Air and Nitrogen Atmosphere up to 900°C

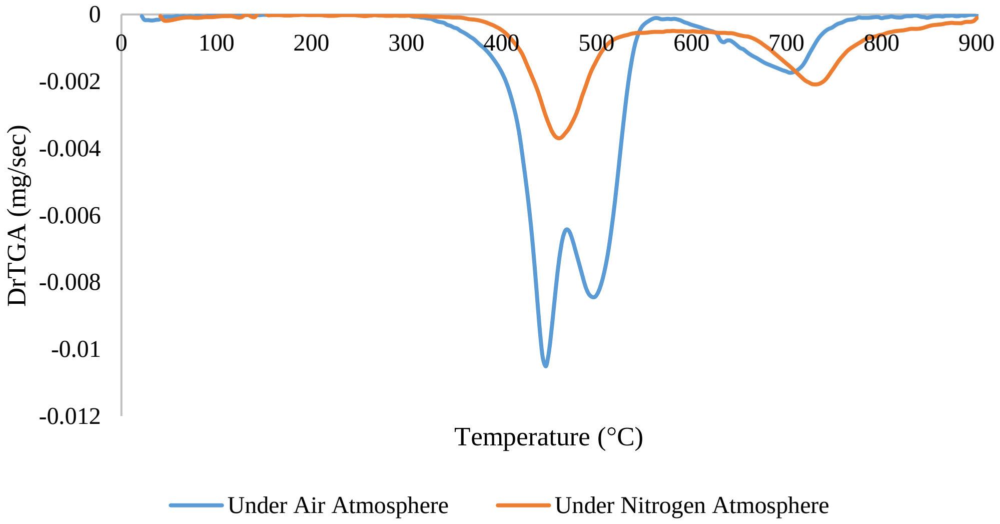

Figure 84: DrTGA of Hydrogenated up to 450°C Şırnak Asphaltite Sample Under Air and Nitrogen Atmosphere up to 900°C

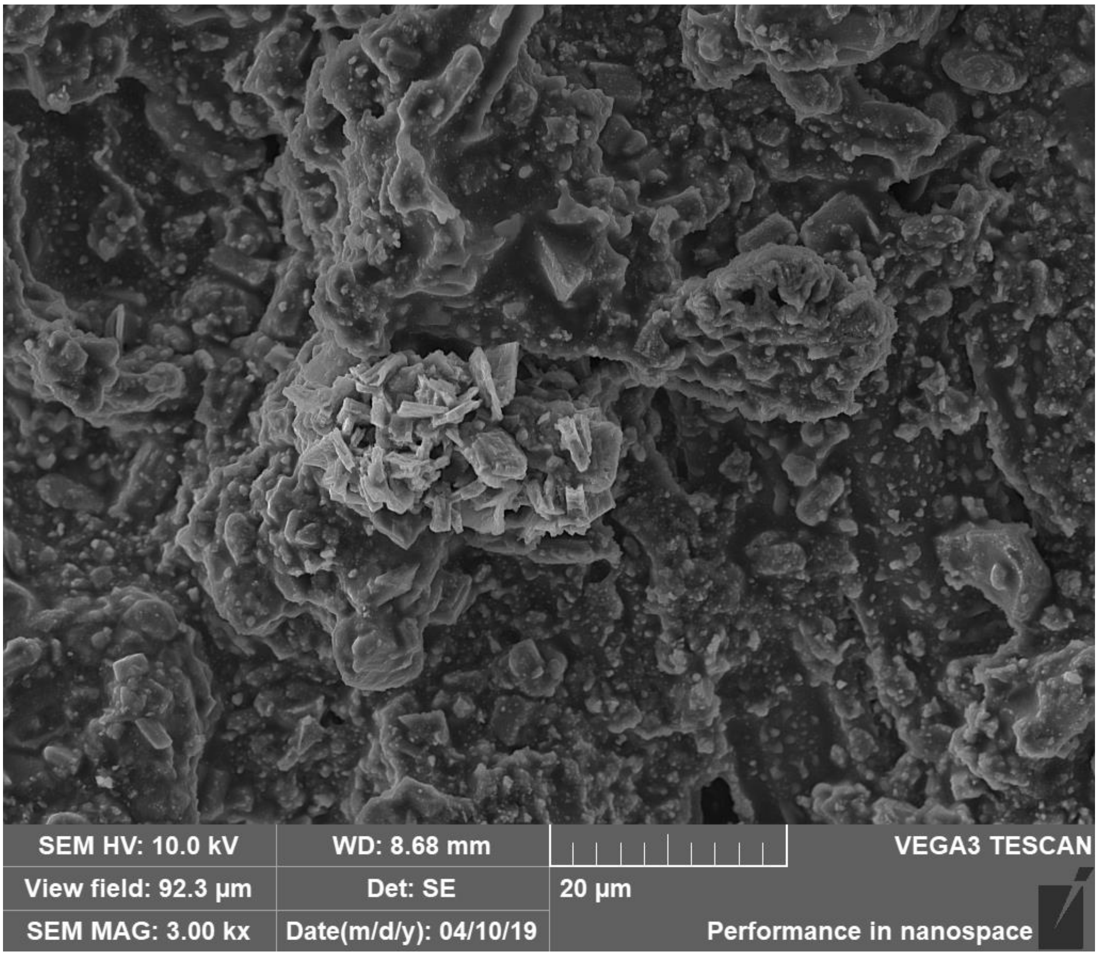

Figure 85: 3.00 kx SEM Image of Pepper Plant Biomass Steam Distillation Residue

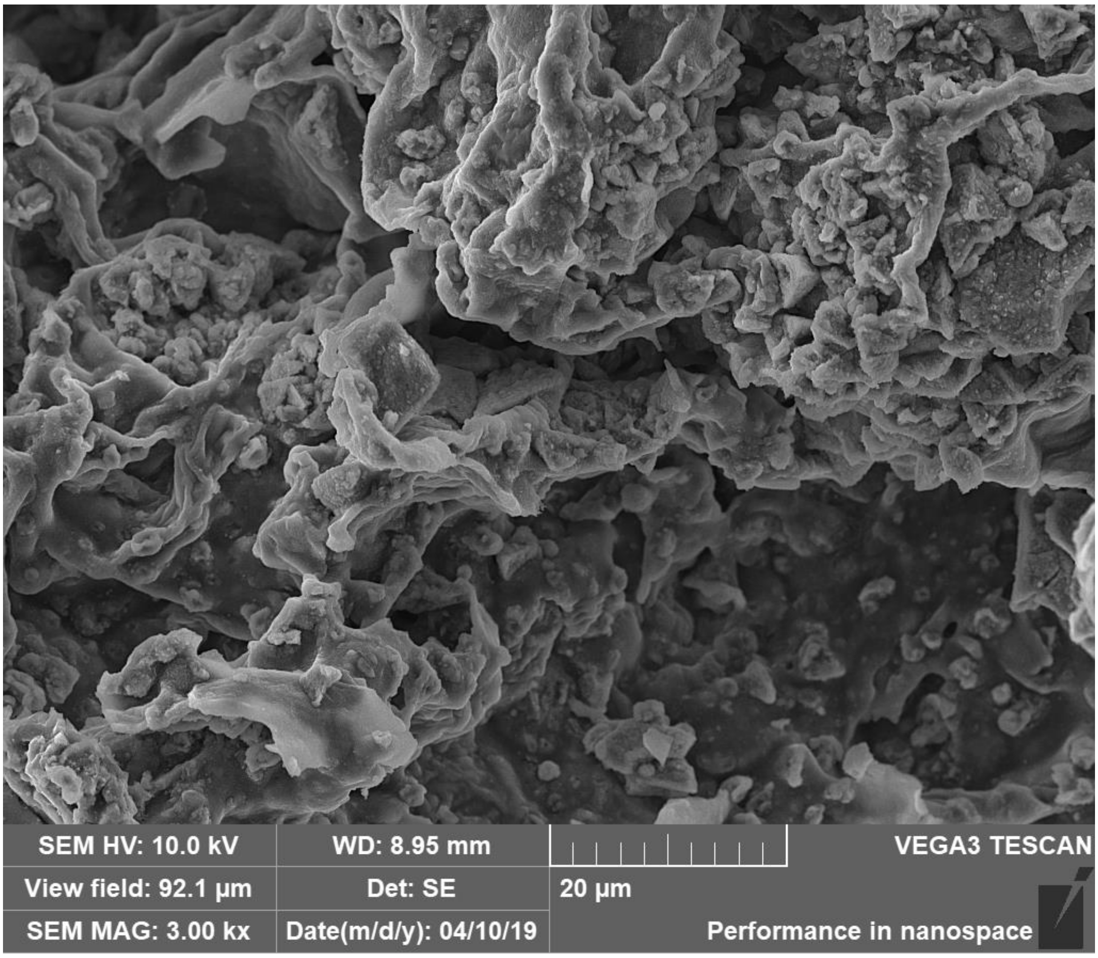

Figure 86: 3.00 kx SEM Image of 50:50 Şırnak Asphaltite and Biomass Mixture Steam Distillation Residue

H. Mesh Size Table

Inches	Milimeters	Mesh
0.1	2.54	5
0.062	1.575	8
0.05	1.27	10
0.416	1.057	12
0.312	0.792	16
0.025	0.635	20
0.02	0.508	25
0.0166	0.422	30
0.0142	0.361	35
0.0125	0.318	40
0.01	0.254	50
0.0083	0.211	60
0.0071	0.18	70
0.0062	0.157	80
0.005	0.127	100
0.0033	0.084	150
0.0025	0.064	200